The Role of Wettability, Surface Roughness, and Rock-Fluid Interactions on Multiphase Flow Dynamics in Geologic Carbon Storage

---

A Dissertation

Presented to

the faculty of the School of Engineering and Applied Science

University of Virginia

In Partial Fulfillment

of the requirements for the Degree

Doctor of Philosophy (Civil and Environmental Engineering)

by

Bo Liang

September 2018

Abstract

Geologic carbon storage (GCS) is a process where CO_2 emissions from power plants and other point source emitters are injected deep into the subsurface to avoid their release into the atmosphere, where they contribute to climate change. Within the porous rock formations of the deep subsurface, CO_2 will displace connate brines creating complex multiphase flow conditions that are impacted by rock characteristics. The connections between the interfacial characteristics of rock surfaces and fluid flow are poorly understood. Using a combination of experimental and modeling approaches, this work explores these connections at the pore (mm) to core (m) scale to provide new insight about fluid trapping and migration at the reservoir (km) scale where the security and efficacy of these injections will be determined.

Small scale micromodel experiments were carried out to study the effect of nanoscale textures on multiphase flow relative to other factors such as interfacial tension and the wettability of the solid. Glass capillaries were used with their surface wettability or roughness modified. Micromodel experiments were conducted at ambient pressure using to fluid pairs (water/Fluorinert and water/Dodecane) to represent a variety of fluid properties. A modified 2k factorial experimental design was used to test the effect of independent variables on interfacial dynamics and flow. The results suggest that surface roughness and ionic strength have an important impact on multiphase flow and that together they impact flow dynamics more significantly than any other factor. Analysis over interface velocity deviation suggest that surface roughness, wettability and the presence of a water film contribute to over 70% of the variation, which in a more complex porous media, could alter flow directions and capillary pressure.

Intermediate scale column experiments were carried out using a 1-meter-tall high-pressure column packed with layered sand with different properties (e.g., grain size, wettability), to represent a low-contrast stratigraphic horizon. CO_2 in supercritical or liquid phase was injected into the bottom of the column at a range of temperatures, pressures, and capillary numbers and the transport of the resulting plume was recorded using electrical resistivity. The effects were measured by the saturation profile at steady state and the relationship between residual and initial saturations. The results show that stratigraphic and residual trapping of CO_2 were most strongly impacted by shifting the wettability balance to mixed wet conditions, with lasting impacts on saturation. A 16% increase in the cosine of the contact angle for a mixed wet sand resulted in nearly twice as much residual trapping. Permeability contrast, pressure, and temperature also impacted the residual saturation but to a lesser extent. Flow rate affected the dynamics of saturation profile development, but the effect is transient, suggesting that the other effects observed here could apply to a broad range of leakage conditions.

To understand the impacts of these studies at the largest scales, the results were combined with new data on wettability and pore structure to inform a model of fluid transport. High-pressure experiments were carried out, to investigate a variety of specific wettability and roughness trends that we observed in experiments supporting previous work and considers the aggregate impact they would have on fluid fate and transport in heterogeneous porous media. Capillary pressure and residual saturation curves were synthesized using a combination of previously published results and new experimental data to input into two-phase flow simulations using the TOUGH2 suite of codes to understand how these interfacial phenomena influence fate and transport at the largest scales.

Acknowledgements

First, I would like to express my deepest appreciation to my advisor, Dr. Andres Clarens. This dissertation is not possible without your guidance, support and encouragement over the course of my Ph.D. journey.

Next, I'd like to thank my committee members:

Dr. Terasa Culver

Dr. James Smith

Dr. David Green

Dr. Stephen Macko

I enjoyed learning from your classes, discussion sessions, comments and suggestions that helped this dissertation work. Words cannot fully express my gratitude, and I will always cherish this going into the future.

I would also like to acknowledge the support that I have received from all faculty and staff members, my fellow graduate students, friends at UVa. Also to my colleagues and collaborators, undergraduate assistants, past and current, near and far, I appreciate being able to know and work with all of you.

Finally, for the unconditional love and support of my parents; for the commitment and selflessness of my better part, Shanshan; for growing up with an extended family filled with

happiness and encouragement, thank you all for making me a better person. I feel blessed to have you, and owe you the rest of my life.

Table of Contents

Chapter 1

Introduction

1.1 Background

Geologic carbon storage (GCS) is a technology that involves capturing CO_2 emission from stationary sources and injecting it into geologic formations. It is considered the only approach, if taken in large scale in the near to mid-term, that can bridge fossil fuel burning economy to the future of renewable energies, to achieve the goal of controlling global warming below the 2 ˚C threshold. Over 60% of the worldwide CO_2 emissions comes from point sources, such as power plants and cement factories. It is estimated that up to 10k Gigatons of CO_2 could be stored globally in geological formations [*White et al.*, 2003; *Michael et al.*, 2010]. Technical and economic estimates suggest that up to 20% of the CO_2 emission reductions could be achieved by GCS [*METZ*, 2007; *Benson and Cole*, 2008].

In a typical GCS operation, compressed CO_2 is injected to geologic formations kilometers below the ground, where the pressure and temperature is beyond the supercritical point of CO_2

(7.2 MPa and 37 ˚C). The typical candidates for injection operations include depleted oil and gas reservoirs, saline reservoirs and depleted coal seams, as shown in Figure 1.1.

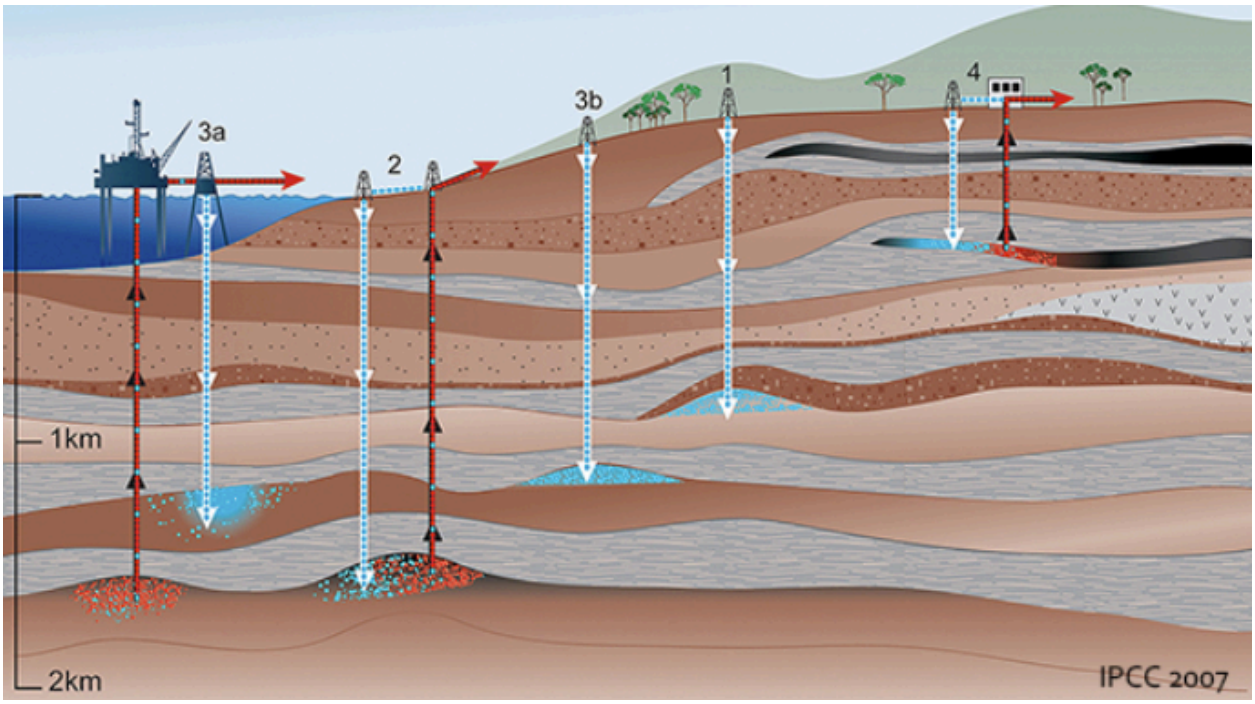

Figure 1.1. Overview of CO_2 storage options: 1. Depleted oil and gas reservoirs; 2. Producing oil and gas reservoirs; 3. Deep saline aquifers; 4. Enhanced coal bed methane recovery. Adopted from IPCC Special Report: Carbon Dioxide Capture and Storage [*METZ*, 2007].

There are a few important trapping mechanisms for CO_2 storage, with different time scale associated with each of them, as shown in Figure 1.2. The first mechanism is called structural, or stratigraphic, trapping. After injection, supercritical/liquid CO_2 will stay above connate brine as a discrete phase due to buoyancy but beneath low-permeability caprocks. Normally, an ideal carbon storage reservoir of this kind requires a caprock, performing as a boundary and sealing layer aiming to prevent the leakage of CO_2 caused by buoyancy. When CO_2 moves to dead-end pores in porous

media or in very narrow fractures or pore structures, it may be trapped in the limited space because of fluid surface attractive forces, such as capillary forces. This is another trapping mechanism called residual/capillary trapping.

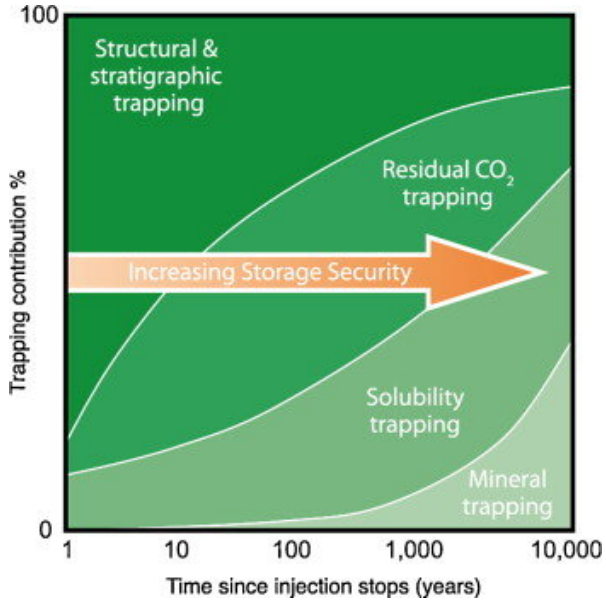

Figure 1.2. CO_2 trapping mechanisms associated with different time scales and storage securities. Over time, the physical process of residual CO_2 trapping and geochemical processes of solubility trapping and mineral trapping increase [*METZ*, 2007].

Solubility trapping is the mechanism by which CO_2 dissolves into the pore water, and therefore can become more securely immobilized [*Kent*, 2011]. CO_2 is reactive with water and will dissolve into the pore water, creating carbonic acid and other dissolved carbonate species at concentrations that are a function of temperature, pressure, and pore water composition. This CO_2 will remain in the aqueous phase, which usually has migration rates on the order of centimeters to meters per year. Residual trapping and dissolution trapping are the primary mechanisms for storage in these pilot programs. When dissolved carbonates react with various ionic species in the fluid, such as Ca^{2+} and Mg^{2+}, to form metal carbonates which could precipitate out of solution and form

carbonate solids, another mechanism called mineralization occurs [*Luhmann et al.*, 2013]. Since the liquid phase CO_2 is converted to more stable solid phase mineral, this mechanism is considered to be the safest among the different mechanisms.

1.2 Research Statement

In GCS, the flue gas from power plants and other point sources is captured, separated, compressed, transported and injected into porous geologic formations at depths typically greater than one kilometer below the earth surface. In these formations, CO_2 exists in the liquid or supercritical phase because of large hydrostatic pressures and geothermal temperatures. Buoyancy driven rise of the CO_2 is prevented by overlying impermeable "caprock" layers and also by secondary processes including capillary trapping and mineral precipitation of CO_2.

Despite its promise, a number of concerns exist about the safety and economic viability of GCS and most of these concerns are related to leakage of CO_2 from target formations. CO_2 injected into the subsurface could leak via a number of pathways including porous media, abandoned well bores, fractures in the bounding formation, and geologic faults. The processes that lead to leakage are difficult to study in the field because the heterogeneity of the subsurface, complex phase behavior, trapping and transport at multiple scales, and chemical reactions make cause-and-effect relationships difficult to establish.

This dissertation aims to address these questions at a fundamental level, by conducting experimental and modeling at different scales, as shown in Figure1.3. Small scale micromodel experiments were carried out to study the effect of a series of solid-fluid interaction factors, such

as nanoscale roughness, solution chemistry, and wetting history. Intermediate scale column experiments were carried out using a 1-meter-tall high-pressure column to evaluate the response of CO_2 trapping. These findings were then combined with large scale simulation, to understand how the interfacial phenomena could influence fate and transport in GCS sites.

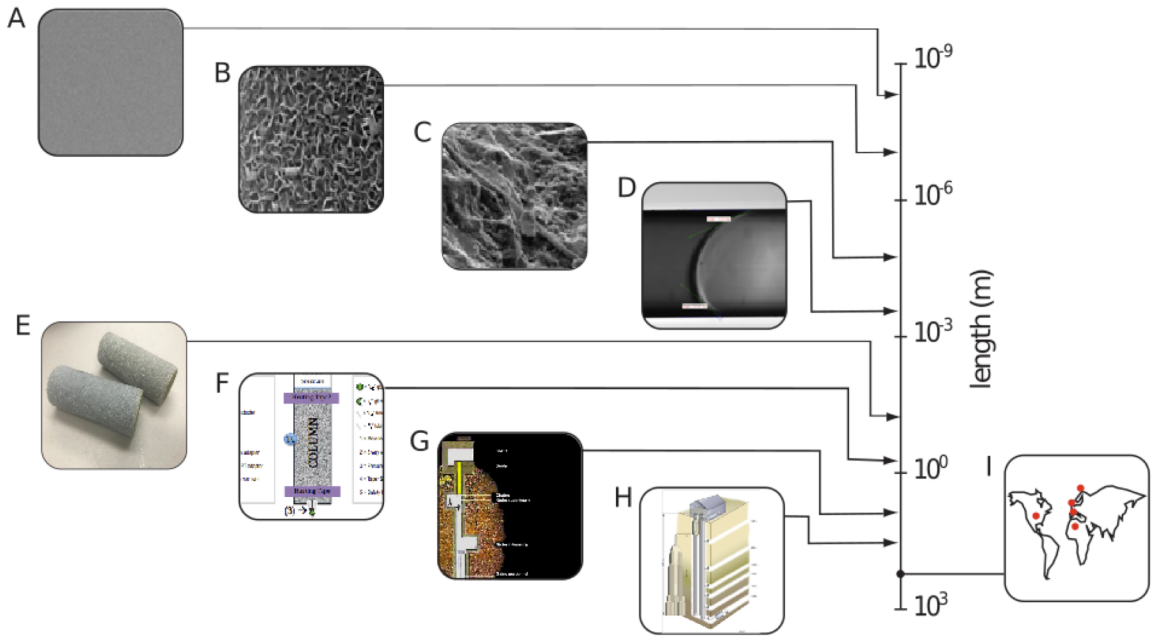

Figure 1.3. A graphical summary of the multi-scale experiments proposed in this study. A & B – Nano to micron scale smooth or rough surface features; C – micron scale textures on sandstone surface; D – mm-scale capillary sample, in which an interfacial meniscus is moving to the left; E – cm-scale sintered glass cores; F – m-scale high pressure column experiments; G & H – Column studies that this research leads to, in large underground labs, at the scales of tens and hundreds of meters; and I – Field-scale GCS demonstration projects.

The overarching goal of this work is to develop a fundamental understanding of the ways in which fluid-rock interfacial properties impact the transport and trapping of CO_2 in porous media. *To achieve this goal, three fundamental research objectives will be pursued:*

1. *To understand the interactions of micro-scale surface roughness and wettability on CO_2 movement on pore scale.*
2. *To reveal the factors that drives CO_2 vertically through sedimentary media with heterogeneities of petro-physical and fluid properties.*
3. *To explore the magnitude of the effects that these interfacial properties have on large scale phenomenon by scaling capillary pressure - saturation functions.*

Chapter 2

Literature Review

2.1 Properties controlling multiphase flow of CO_2 in carbon sequestration

In GCS, CO_2 is injected into target repositories which are typically high-permeability deep saline aquifers located beneath a low-permeability formation (e.g., caprock) to provide mechanical stabilization of the CO_2 plume. Figure 2.1 presents a conceptual representation of a CO_2 sequestration well and the subsurface overlaying the target repository. CO_2 has the potential to escape to overlaying formations via a variety of pathways including faults or fractures in cap rocks or abandoned well bores [*Lewicki et al.*, 2007; *Pruess*, 2008]. Once it reaches overlying formations, it will rise in response to buoyant forces until it reaches a capillary barrier where it will spread beneath the interface until the capillary entry pressure of the overlying low-permeability layer is overcome [*Bryant et al.*, 2008; *Saadatpoor et al.*, 2010]. This phenomenon shares some characteristics with the trapping provided by cap rock with a few important differences: (1) the contrast between the layers is subtle and so only small amounts of CO_2 will accumulate before the

capillary entry pressure of the overlying layer is overcome; (2) the number of these intra-reservoir barriers that a particular parcel of CO_2 will encounter on its path to the surface is great; and (3) the CO_2 ganglion will be far from the injection site and so gravity-driven buoyant forces will dominate [*Krevor et al., 2011; Zhang et al., 2011*].

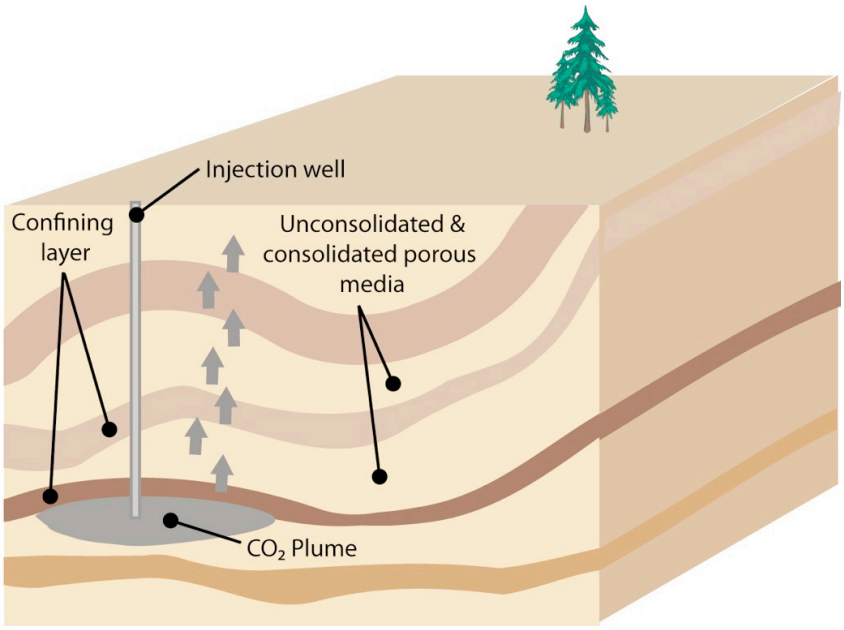

Figure 2.1. Schematic of Geologic Carbon Sequestration (GCS), including the target repository, impermeable caprock, and the overlying layered formations. CO_2 is subject to buoyant force, and has the leakage potential through faults or fractures in the caprock, into the shallow formations.

At the depths considered for CO_2 injection and storage (below ~1 km) hydrostatic forces produce pressures greater than 100 bar, and thermal gradients result in temperatures greater than 35°C. CO_2 would exist in the supercritical state, having a density close to that of liquid CO_2 and compressibility close to that of gaseous CO_2. The migration of CO_2 as a distinct phase (e.g., not dissolved) is driven by three forces: (1) convective forces created by over-pressurization; (2) the capillary force created by the surface tension between the fluids and the pore walls, and (3),

buoyant forces that result from the lower density of CO_2 relative to the connate brine [*Bryant et al.*, 2008; *Mouche et al.*, 2010; *Plampin et al.*, 2014b]. When a CO_2 bubble or ganglion encounters a horizontal capillary barrier, CO_2 will accumulate beneath the interface and spread forming a tapered saturation profile [*Zhang et al.*, 2011; *Niu et al.*, 2015; *Prather et al.*, 2016]. The CO_2 will percolate into the overlying formation once enough CO_2 accumulates beneath the interface to overcome the capillary entry pressure (P_E). In steady state, this entry pressure can be set equal to the capillary pressure(P_c) of the leading edge of the CO_2 ganglion or bubble as follows:

$$P_E = \frac{2\sigma cos\theta}{r_n} = \Delta\rho g L + \frac{2\sigma cos\theta}{r_p} \qquad \text{(Equation 1)}$$

where σ is the surface tension between CO_2 and brine, θ is the contact angle at the CO_2-brine-mineral interface, r_n and r_p are the radius of pore throat and pore body, respectively, $\Delta\rho$ is the density difference, g is the gravity constant, and L is the entry height of the CO_2 plume. This form of the equation suggests that there are three major factors that will impact the amount of CO_2 that becomes trapped at the interface. The first is the sand grain size contrast between the two layers in the column as this will impact r_n and r_p. The temperature and pressure conditions will impact fluid density and viscosity, while the wettability appears directly in equation 1.

2.2 Wettability in CO_2/brine/rock system

Wettability at the CO_2-brine-mineral interface is a fundamental parameter that has significant effects on a number of parameters and processes relevant to GCS, such as capillary pressure, relative permeability and residual saturation [*Chiquet et al.*, 2007]. Contact angle

directly measures the balance between three sets of interfacial tensions in this system (as shown in Equation 2), and has direct impact on capillarity [*Quéré*, 2008a] (as shown in Equation 1). Of the three interfacial tension values in Young's equation, γ_{SL} (between solid and liquid) and γ_{SG} (between solid and CO_2) are not directly measurable, which is the reason that contact angle has to be measured experimentally.

$$\cos(\theta) = \frac{\gamma_{SL} - \gamma_{SG}}{\gamma_{LG}} \qquad \text{(Equation 2)}$$

Over the past decade, a large amount of research has been devoted to contact angle measurement of CO_2 sequestration conditions, as noted in the review by Iglauer [*Iglauer et al.*, 2015b]. However, notable uncertainties still remain [*Al-Yaseri et al.*, 2016], which could be caused by a number of different factors such surface contamination, roughness and heterogeneity, drop size and equilibration with the aqueous phase [*Kaveh and Delft*, 2015]. The underlying mechanisms accounted for these differences and their impact on flow and sealing properties have yet to be fully established [*Wang et al.*, 2013b; *Iglauer et al.*, 2015a].

It is generally accepted that contact angle depends on three classes of factors: those related to rock material, those caused by CO_2-brine phase interaction, and the thermo-physical conditions (such as pressure and temperature). The various types of rock materials further amplify the discrepancies between studies, and it's been noted that predicting reservoir wettability should be on a mineral-specific basis. The underlying reasons behind this is that different rock or mineral surfaces have different charged functional groups. The literature to date generally agree that contact angle has a positive correlation with pressure (especially across the critical point where

phase change happens) and a slight negative or no correlation with temperature. It should be noted these effects could also be linked with other parameters depending on P and T conditions, such as pH of the brine phase, solubility and partial pressure of CO_2. The wettability at the solid surface is also strongly impacted by interfacial force between the two fluids. This is generally quantified in terms of the interfacial tension between fluid pairs [*Burant et al.*, 2013]. Interfacial tension has been shown to be inversely proportional to spontaneous imbibition [*Zhang et al.*, 2011]. For aqueous systems, the ionic strength and composition play an important role in driving interfacial tension, and ultimately capillary pressure. Ionic composition can also impact the charged functional groups both on the solid surface or in the fluids [*Farokhpoor et al.*, 2013].

2.3 Surface roughness and its relationship to wettability and flow

Wettability has long been known to impact flow through porous media [*Wang et al.*, 2013b] but recent work using new imaging techniques suggests that small-scale (e.g., nanoscale) roughness or texturing on the mineral surface strongly impacts wettability [*Bikkina*, 2011], which can in turn impact fluid flow processes [*Iglauer et al.*, 2015b; *Al-menhali and Krevor*, 2016]. These findings are consistent with much of the recent work focused on designing superhydrophobic or superhydrophilic surfaces which rely in large part on nanoscale structure at the surface [*Steefel et al.*, 2013]. But the impact that these types of features would have on flow in a complex heterogeneous rock formation are difficult to know *a priori*.

The role that roughness might play, on the interfacial forces of a static tertiary contact line (Figure 2.2), has been considered extensively in the literature starting with the work of Wenzel and Cassie-Baxter [*Quéré*, 2008a; *Murakami et al.*, 2014]. Wenzel's model predicts that roughness

enhances wettability, and Cassie modeled interfacial energy depending on structure of the solid surface. Like most models of wettability, these are based on the notion that the motion of the interface between the two fluids and the solid will impact the dynamics of fluid flow. One of the fundamental difference between the Cassie and Wenzel models is the presence/absence of a continuous wetting film as depicted in Figure 2.2. Wetting films have been shown to play an important role in multiphase flow on rough surfaces [*Quéré*, 2008a]. In the context of groundwater remediation, for example, the thickness of the water film is proportional to the underlying solid surface roughness [*Girardo et al.*, 2012a]. In CO_2 storage, water films have been shown to exist during CO_2 injection and these become thinner as pressure increases and the surface becomes more negatively charged as CO_2 dissolves into the film [*Broseta et al.*, 2012]. The film enables changes in solution chemistry. During imbibition of the wetting phase, a thin surface film can play an important role in making the effective surface roughness of solid much less pronounced.

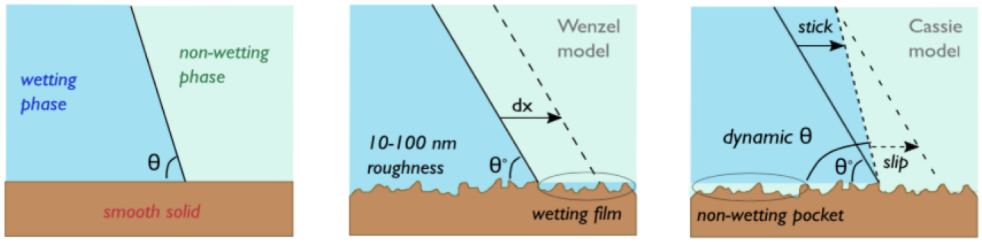

Figure 2.2. Illustration of sample surface features including rough and smooth surface. (a) Smooth surface; (b) pre-wetted rough surface with wetting phase filled in the pores – Wenzel model; (c) rough surface with non-wetting phase filled in the pores that leads to stick-slip flow – Cassie model.

Anecdotally, macroscale observations such as contact line pinning or adhesion are often attributed to these microscale characteristics related to surface textures and wetting [*Kim et al.*, 2012; *Wang et al.*, 2013a]. The mechanisms that govern this upscaling are not fully developed, although recent insight supports the notion that roughness and the presence of a wetting film impacts flow dynamics [*Lamert et al.*, 2012; *Kunz et al.*, 2015]. While much fundamental work had been carried out in recent years to catalog and describe the impact of mineral chemical heterogeneities on wettability, less work has focused on how textures in different rock types that originated via diagenetic processes might impact multiphase flow.

Efforts to numerically simulate these complex dynamics are often based on the original Washburn equation [*Washburn, 1921*], written as:

$$\Delta P + \frac{2\gamma \cos\theta}{r} = \frac{8\mu l}{r^2}\left(\frac{dl}{dt}\right) \qquad \text{(Equation 4)}$$

where μ is the fluid viscosity, r is the radius of the capillary, l is the length of the capillary, and γ is the interfacial tension. An important assumption in the Washburn equation is that the static contact angle and the dynamic contact angle are the same. Fluids in motion often have a different contact angle than they do at equilibrium [*Quéré*, 2008a], so a dynamic contact angle is a more appropriate measure. The relationship between equilibrium (θ_e) and dynamic (θ_d) contact angles is a function of fluid velocity:

$$\theta_d = f\left(\frac{dl}{dt}, \theta_e\right) \qquad \text{(Equation 5)}$$

Both analytical and empirical methods have been used to explore this relationship [*Heshmati and Piri*, 2014; *Sheng*, 2014], which are often times good predictors of experimental observations in a gas-liquid system but do not effectively capture the behavior of liquid-liquid systems [*Girardo et al.*, 2012a] that prevails in GCS applications. This could be because both the hydrodynamic and molecular kinetic analysis are based on the assumption that one phase dominates the flow momentum, as would be the case for fluid pairs with a large viscosity ratio.

Empirical relationships proposed by [*Joos et al.*, 1990] and [*Cox et al.,* 1986] matched experimental data for various systems (liquid-gas and liquid-liquid). Joos conducted capillary rise experiments and used the Washburn equation with modified dynamic contact angle to match experimental data, proposing the following correlation:

$$\cos\theta_d = \cos\theta_e - 2\,(1 + \cos\theta_e)Ca^{1/2} \qquad \text{(Equation 6)}$$

where the interface velocity ($v = \frac{dl}{dt}$) is incorporated in capillary number ($Ca = \frac{\mu v}{\sigma}$).

While the literature effectively captures some aspects of the impact of contact line dynamics and roughness, less work has been focused on exploring dynamic wettability on mineral surfaces where a number of different factors might be changing at once. In particular, little effort has been focused on understanding the relative contributions and interactions between ionic strength, flow conditions and presence/absence of a water film on wettability and multiphase flow.

2.4 Capillary pressure and saturation (Pc-S) relationship in multiphase flow

Capillary pressure (P_c) refers to the pressure difference between two immiscible fluids in porous media, resulting from the different capillary forces that solid surface has on the two fluids, given by $P_c = P_n - P_w$, where P_n and P_w refer to the pressure in non-wetting and wetting phase, respectively. In multiphase flow, capillary pressure depends on the relative saturation of the two fluids, increasing as the saturation of non-wetting fluids increases. This relationship is crucial to modeling multiphase flow, and has been studied extensively in various applications and particularly in the context of CO_2/water flow in geologic carbon storage [*Zhou et al.*, 2013]. There have been a number of experimental studies measured capillary pressure – saturation (Pc-S) curves using a variety of techniques [*Plug and Bruning,* 2007]. Pini [*Pini et al.*, 2012] conducted core flooding experiments using sandstone and limestone, found out that rock heterogeneity, in terms of pore connectivity and shape, has an effect on Pc-S curve. Wang [*Wang et al.*, 2016] found that exposure of CO_2 to rock surface has wettability hysteresis effect that shift Pc-S curves down, and this effect also varies between different rock types.

The Leverett J-function has been developed to describe a normalized capillary pressure curve as a function of water saturation, which serves as the foundation for predicting capillary behavior of all immiscible fluids in porous media [*Plug and Bruining*, 2007; *Krevor et al.*, 2011]. The mathematical formula of Leverett J-function is written as:

$$J(S_w) = \frac{1}{\sigma cos\theta}\sqrt{\frac{K}{\emptyset}}P_c(S_w)$$

where S_w is the saturation of the wetting phase; k and ϕ are intrinsic permeability and porosity of the porous media. This function allows a characteristic Pc-S curve for a given rock material and fluid type to be scaled for a different fluid by the contact angle and interfacial tension measures, allowing creation of a Pc-S curve for each new fluid. An example of comparing high pressure experimental measurements (Berea sandstone, ε = 22%, k = 466 mD, θ = 0° and γ = 36 mN/m) and mercury intrusion porosimetry (MIP) experiments ($\theta = 40°$ and $\gamma = 485$ mN/m) is provided in Figure 2.3.

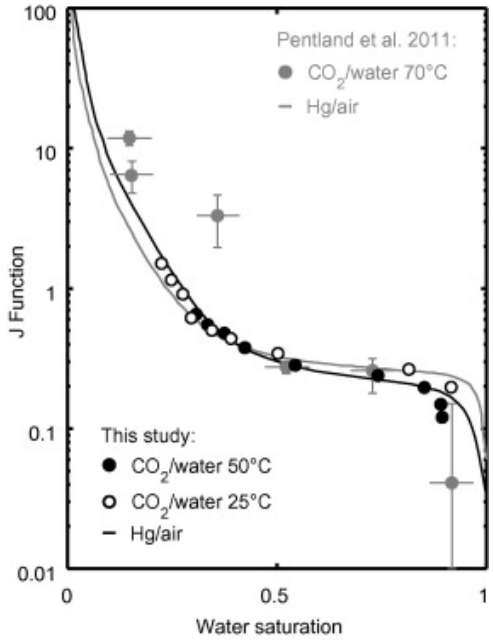

Figure 2.3. J-Function for Berea sandstone between real high-pressure experiment, and mercury intrusion porosimetry (MIP) experiments [*Pentland et al.*, 2011].

For various systems, the applicability of this framework has been studied and debated extensively in the literature. Some researchers have been able to successfully scale the Pc-S data with cos(θ) [*Morrow*, 1976, *Wang et al.,* 2016], some researchers claim that other factors such as

roughness could complicate this system, and having an operative contact angle that is different than the intrinsic contact angle. Therefore, a fundamental gap exists in our understanding of the relationship between characteristic Pc-S curves and changes in interfacial properties. This could have significant implications in the real world, where behaviors such as mixed wetting are observed. At the core scale, experiments need to be carried out to explore questions of wettability alteration in the CO_2-brine-mineral system and its effect on flow through porous media. Based on the limited core-flooding data available, some show lower Sr values and non-monotonic dependence on Si, and some report lower Pc than calculated from pore throat sizes, both of which suggest that the rocks might be mixed-wet, or intermediate-wet with regard to CO_2.

2.5 Modeling of CO_2/brine multiphase flow

Most of the efforts of modeling CO_2/brine multiphase flow start from the mass balance and conservation equations [*Juanes et al.*, 2006; *Oldenburg and Lewicki*, 2006; *Celia et al.*, 2015]. In a multiphase system, the mass balance equation is usually written as a summation of the mass components in each phase [*Celia et al.*, 2015]. Here, phase α could represent CO_2 or brine, and the mass balance equation could be written as:

$$\sum_{\alpha}[\frac{\partial}{\partial t}(\rho_\alpha \varphi\, s_\alpha\, m_\alpha) + \nabla(\rho_\alpha\, u_\alpha\, m_\alpha + j_\alpha)] = \sum_{\alpha}\psi_\alpha$$

where ρ_α is the density of phase α, φ is porosity, s_α is the saturation of fluid phase α, m_α is the mass fraction, u_α is the volumetric flux vector for phase a, j_α is the non-advective flux vector in phase α, ψ_α represents external sources or sinks of mass in phase α. The flux (u_α) is

determined by the constitution equations, which, in this system, is a multiphase Darcy equation, written as follows,

$$u_\alpha = -\frac{k_{r,\alpha}\, k}{\mu_\alpha} \left(\nabla p_\alpha - \rho_\alpha\, g\right)$$

where k is the intrinsic permeability, $k_{r,\alpha}$ is the relative permeability, which is a function of the saturation, and is impacted by physical and interfacial properties. p_α is the phase pressure, and g is the gravitational acceleration constant.

Other factors that are usually included in the non-advective flux (j_α)term of the governing equations are diffusion and partitioning. Diffusion is governed by Fick's law, where the flux is driven by the component concentration gradient. Partitioning is driven primarily by the dissolution of a fluid into the other. In GCS conditions, CO_2 dissolution in brine could be up to 5% by mass fraction, where brine dissolution into CO_2 phase is minimal [*Kent*, 2011; *Burant et al.*, 2013].

To date, the non-linear dependency of capillary pressure and relative permeability on saturation is not captured in most of the flow models. Part of the reason is a lack of experimental data to define the underlying processes, and these parameters also relate to each other by various underlying mechanisms that haven't been fully understood [*Celia et al.*, 2015]. Most models use a capillary pressure-saturation curve derived from one experimental measurement, sometimes from analogue fluid, and some scaling factors. This greatly overlooked the possible spatial heterogeneity of the field, in terms of both rock physical properties, and the fluid properties.

Also, despite the aforementioned complexity in interfacial processes, contact angle is often assumed to be zero for the wetting phase, which could also introduce a significant source of error [*Cavanagh and Haszeldine*, 2014; *Bandilla et al.*, 2015].

Chapter 3

Evaluating the Role of Wettability and Roughness on Flow Dynamics Using Capillary Experiments

Multiphase flow through porous media is important in a wide range of environmental applications such as enhanced oil recovery and geologic storage of CO_2. Recent *in situ* observations of the tertiary contact line between immiscible fluid phases and the solid surface suggest that existing models may not fully capture the effects of nanoscale textures on the solid surfaces relative to other factors such as the interfacial tension between fluids and the wettability of the solid. To better characterize these processes, spontaneous and forced imbibition experiments were carried out using glass micromodels with modified surface roughness and/or wettability. Two fluid pairs were tested with contrasting viscosities and interfacial tensions: water/Fluorinert and water/Dodecane. A modified 2^k factorial experimental design was used to test the effect of independent variables on interfacial dynamics and flow. Four variables were evaluated: surface treatment (e.g. wettability, roughness), ionic strength in the aqueous phase, non-aqueous fluid type, and the presence/absence of a wetting film. Analysis of variance was used to test the statistical significance of each factor and the interactions between them. The results suggest that surface

roughness and ionic strength have an important impact on multiphase flow and that together they impact flow dynamics more significantly than any other factor. Analysis over interface velocity deviation suggest that surface roughness, wettability and the presence of a water film contribute to over 70% of the normalized interface velocity variation, which, in a more complex porous media, could alter flow directions and capillary pressure. These experimental results are used to propose an empirical extension of the Joos and Wenzel equations relating static and dynamic contact angles as a function of roughness, presence of a water film, and water chemistry.

3.1 Introduction

A number of naturally occurring and engineered processes in the environment involve the flow of multiple phases through porous media [*Pinder and Gray*, 2008]. Processes such as groundwater remediation, geologic carbon storage, enhanced geothermal energy production, and enhanced oil recovery are impacted by the porosity, pore geometry [*Deng et al.*, 2015], viscosity ratio of fluids [*Wang et al.*, 2013c], flow conditions [*Yadali Jamaloei et al.*, 2011], interfacial tension [*Yadali Jamaloei and Kharrat*, 2009], fluid topology [*Schnaar and Brusseau*, 2006; *Oughanem et al.*, 2015] and wettability of the host rock [*Yadali Jamaloei et al.*, 2011; *Geistlinger and Ataei-dadavi*, 2015; *Iglauer et al.*, 2015a]. Wettability in particular has long been known to impact these flow processes [*Anderson*, 1987a] but recent work using new *in situ* imaging techniques suggests that small-scale (e.g., nanoscale) roughness or texturing on the mineral surface strongly impacts wettability [*Wang et al.*, 2013a; *Botto et al.*, 2017] which can in turn impact fluid flow processes [*Al-Menhali et al.*, 2015; *Al-yaseri et al.*, 2016]. These findings are consistent with much of the recent work focused on designing super-hydrophobic or super-hydrophilic surfaces which rely in large part on nanoscale structure at the surface [*Li et al.*, 2013; *Raeesi et al.*, 2013].

The impact that these types of features would have on flow in a complex heterogeneous rock formation are difficult to quantify.

The role of roughness on the interfacial forces of a static tertiary contact line has been considered extensively in the literature starting with the work of Wenzel and Cassie-Baxter [*Wenzel*, 1936; *Cassie and Baxter*, 1945]. Wenzel's model predicts that roughness enhances wettability. Cassie modeled interfacial energy as a function of the structure of the solid surface. Like most models of wettability, these are based on the notion that the motion of the interface between the two fluids and the solid will impact the dynamics of fluid flow. One of the fundamental difference between the Cassie and Wenzel models is the presence/absence of a continuous wetting film, which has important implication in contact line dynamics [*Berg et al.*, 2013].

The presence or absence of a wetting film has been shown to play an important role in multiphase flow on rough surfaces [*Quéré*, 2008a]. In the context of groundwater remediation, for example, the thickness of water film is proportional to the underlying solid surface roughness[*Kibbey*, 2013]. In CO_2 storage, water films have been shown to exist during CO_2 injection and these become thinner as pressure increases and the surface becomes more negatively charged as CO_2 dissolves into the film[*Tokunaga*, 2012], which enables changes in solution chemistry[*Kim et al.*, 2012]. During imbibition of the wetting phase, a thin surface film can play an important role in making the effective surface roughness of solid much less pronounced. In both applications, the existence and swelling of the wetting film could also lead to snap-off of the non-wetting phase [*Zhou et al.*, 1994]. which is a critical part of the displacement processes.

Macroscale observations such as contact line pinning or adhesion are often attributed to these microscale characteristics related to surface textures and wetting [*Kim et al.*, 2013; *Wang et al.*, 2013a]. This roughness contributes, at least in part, to the development of stick-slip flow behavior at the interface [*Girardo et al.*, 2012b; *Geistlinger et al.*, 2016]. In the context of environmental porous media, stick-slip flow can have complex impacts on multiphase flow in media, especially at low Capillary Numbers [*Kunz et al.*, 2015]. Irregular movement of the interface at microscales at low velocity can impact the stability of the system at macroscales. For example, in two-phase flow where residual saturation has been reached, the instability of the interface between the continuous wetting phase and a non-wetting phase ganglion could result in the mobilization or break-up of that ganglion [*Singh et al.*, 2017].

The wettability at the solid surface is directly impacted by interfacial forces between fluids. This is generally quantified in terms of the interfacial tension between fluid pairs [*Karadimitriou et al.*, 2012]. Interfacial tension is inversely proportional to ratio of spontaneous imbibition [*Mirchi et al.*, 2015]. In aqueous systems, the ionic composition and strength play an important role in driving interfacial tension, and ultimately capillary pressure. But the ionic composition of water can also impact the charged functional groups on the solid surface [*Farokhpoor et al.*, 2013]. And while much fundamental work has been carried out in recent years to catalog and describe the impact of mineral chemical heterogeneities on wettability, less work has focused on how textures in different rock types that originated via diagenetic processes, might impact multiphase flow [*Girardo et al.*, 2012a].

The physical processes underlying these complex systems were first modeling by Washburn [*Washburn*, 1921]. The Washburn equation is a dynamic energy balance on idealized (incompressible and Newtonian) fluid flow through a single capillary with a uniform circular cross section under the laminar (Poiseuille) flow conditions that are common in subsurface flow environments:

$$\sum P = \frac{8\mu l Q}{\pi r^4} \qquad (1)$$

where $\sum P$ is the total pressure difference between two phases (the sum of the external pressure, ΔP, and capillary pressure, $P_c = \frac{2\gamma \cos\theta}{r}$, where θ is the contact angle and γ is the interfacial tension), i.e., $\sum P = \Delta P + P_c$. μ is the fluid viscosity, l is the length of the capillary, Q is the volumetric flow rate, and r is the radius of the capillary.

Substituting these two pressure expressions into the Poiseuille equation, the Washburn equation can be written as:

$$\Delta P + \frac{2\gamma \cos\theta}{r} = \frac{8\mu l}{r^2}\left(\frac{dl}{dt}\right) \qquad (2)$$

where $\frac{dl}{dt}$ is the interfacial velocity. An important assumption in the Washburn equation is that the static contact angle and the dynamic contact angle are the same. Fluids in motion often have a different contact angle than they do at equilibrium [*Quéré*, 2008a] and so a dynamic contact

angle is a more appropriate measure in the flow system. The relationship between equilibrium (θ_e) and dynamic (θ_d) contact angles is a function of fluid velocity:

$$\theta_d = f\left(\frac{dl}{dt}, \theta_e\right) \qquad (3)$$

Both analytical and empirical methods have been used to explore this relationship. Sheng [*Sheng and Zhou*, 1992] and Popescu [*Popescu et al.*, 2008] developed analytical hydrodynamic relationships based on viscosity energy dissipation. Brochard-Wyart [*Brochard-Wyart and De Gennes*, 1992] used a molecular dynamic approach, based on the relationship between displacement of fluid molecules and the movement of contact line. These approaches have been used by Blake [*Blake*, 2006] to develop a hydrodynamic and molecular kinetic model. The resulting equations are good predictors of experimental observations in a gas-liquid system, but do not capture the behavior of liquid-liquid systems effectively. This could be because both the hydrodynamic and molecular kinetic analysis are based on the assumption that one phase dominates the flow momentum, as would be the case for fluid pairs with a large viscosity ratio.

In an effort to develop empirical relationships that work for a broader range of fluid pairs, Joos [*Bracke et al.*, 1989; *Joos et al.*, 1990] conducted capillary rise experiments and used the Washburn equation with modified dynamic contact angle to match experimental data, proposing the following correlation:

$$\cos\theta_d = \cos\theta_e - 2\,(1 + \cos\theta_e)Ca^{1/2} \qquad (4)$$

where the interface velocity ($\frac{dl}{dt}$) is incorporated in the capillary number (Ca). Cox[Cox, 1986] and other have expanded this correlation more recently over a wider range of geometries, capillary numbers and fluid pairs. Despite these advances in fundamental wettability theory and more recent applied characterization under reservoir conditions [*Chaudhary et al.*, 2013; *Andrew et al.*, 2014; *Zhao et al.*, 2016], the role that surface textures have on wettability has not been explored in a way that enables easy comparison with other factors understood to impact multiphase flow.

To build on the understanding developed by Joos and Wenzel, we carried out a set of controlled micromodel experiments to test a number of hypothesis related to the impact of nano-scale surface textures on multiphase flow. The first hypothesis was that textures would have as great of an impact on fluid flow as wettability. The second hypothesis is that nano-scale textures would have interaction effects with ionic strength in the aqueous phase, flow rate and the presence/absence of a wetting film to influence flow dynamics in more complex ways. 1-D capillary micromodels were used to enable easy visualization and control of flow properties. Both spontaneous and forced imbibition experiments were conducted to collect data over a wide range of capillary numbers. The experimental results were then interpreted in the context of modeling frameworks to extend predictive capabilities.

3.2 Materials and Methods

3.2.1 Micromodel fabrication

Soda lime glass capillaries (Hilgenberg GmbH) with an external diameter 0.82 mm and internal diameter 0.64 mm were modified to generate either a nano-textured surface roughness or to make them more water wetting. Alkali etching was used to generate sub-micron surface features on the glass surface [*Mazurczyk et al.*, 2008; *Karadimitriou et al.*, 2012]. Compared to other dry etching techniques and HF-based etchants, alkali etching is safer and simpler, and capable of achieving extreme wettability (super-hydrophilicity and super-hydrophobicity) and associated properties such as antireflection [*Xiong et al.*, 2010] and low-dielectricity [*Yao and He*, 2014]. The dimension and morphology of surface texture were controlled by changing the etching time, temperature and glass chemical composition [*Xiong et al.*, 2010; *Du and He*, 2012]. The glass capillaries were first cleaned in demineralized water and then with a 1:1:1 volume mixture of acetone, methanol and trichloroethylene under sonication. The cleaned capillaries were placed in a sealed container containing an aqueous solution of 0.2 mol/L KOH and then heated at 95^{o}C for 24 hours to enable chemical etching. Following etching, the capillaries were rinsed with demineralized water, and then again with the acetone, methanol and trichloroethylene solution under sonication, and finally with demineralized water. The capillaries were dried using compressed air between each treatment.

The validation and quantification of the etching was carried out using scanning electron microscopy (SEM) observations and energy dispersive X-ray spectrometry (EDS) (FEI-650). The effect of the etching process on the glass surface is shown in Figure 3.2. The size of the surface asperities created in this etching process are on the order of 10-100 nm. The etching process also changes the ionic surface composition of the underlying glass itself, as ions are lost to the aqueous

phase (R = Na, Ca, etc.) due to hydrolysis and ion-exchange during the treatment,[*Xiong et al.*, 2010]

$$Si–O–Si + H_2O = 2\ Si–OH$$

$$Si–O–Si(OH)_3 + OH \rightarrow Si–O–Si(OH)_4 \rightarrow Si–O + Si(OH)_4$$

$$Si–OR + H_3O+ \rightarrow Si–OH + R^+ + H_2O$$

$$Si–OR + H_3O \rightarrow Si–OH + R^+ + OH$$

The net effect of these physical and chemical alternations is that the glass surface became considerably more hydrophilic, which was observable as the capillaries exhibited smaller contact angles and more pronounced capillary action, as expected based on Wenzel theory.

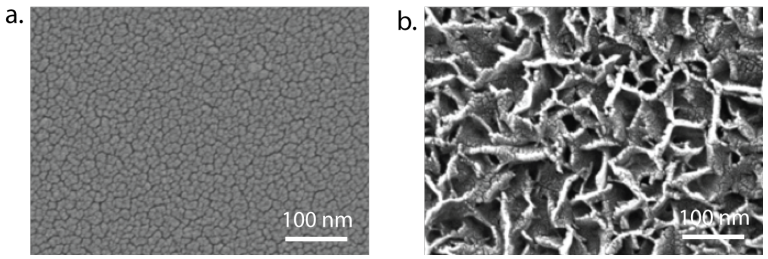

Figure 3.2. Surface micrograph of an (a) untreated and (b) etched glass capillary.

To create wettability modified samples, a separate group of capillaries were treated using oxygen plasma to make the surfaces more water wetting without changing the surface roughness. Plasma treatment works by enabling electron transfer between ions in solution and the glass surface, neutralizing the dissolved ions and creating a more positively charged surface layer on the glass. Oxygen plasma treatments was carried out using a South Bay Plasma System (PC 2000) for 10 minutes. Cleaned capillaries were put into the plasma chamber and aligned with the two discharge ends. After treatment, the wetting properties of the treated capillaries were measured

using contact angle and capillarity experiments. The surface structure was examined using SEM to confirm that no additional roughness had been introduced.

3.2.2 Experimental setup

Imbibition experiments were carried out in capillary samples, where the non-wetting phase is displaced by the wetting phase. Both spontaneous and forced imbibition experiments was carried out to cover as wide a range of capillary numbers as possible. The capillary was initially saturated with the non-wetting phase. To ensure the absence of water film on the walls of the capillary, the capillary was oven dried prior to the initial saturation. After the initial saturation, the wetting phase was imbibed. The same protocol was followed for every set of experiments.

Fluorinert and dodecane were used as the two non-wetting fluids in the experiments. Fluorinert is a colorless, fluorine based, and inert liquid (refraction index, n = 1.291). It is 4.7 times more viscous, and 1.86 times heavier, than water ($\mu = 4.7 \times 10^{-3}$ Pa*s, $\rho = 1860$ kg/m^3). Dodecane, on the other hand, is less viscous and lighter than water ($\mu = 1.36 \times 10^{-3}$ Pa*s, $\rho = 749$ kg/m^3). This design is aimed to test the findings of this study across different fluid properties. The selection of these two fluids enables high quality and reproducible images of multiphase flow properties and so they are used often in micromodel work. The water had Ecoline 578 ink added to improve visualization by the microscope. In order to investigate the combined effect of roughness and different interfacial tension the chemistry of the wetting phase was modified by the addition of NaCl into the solution. When the dye was formulated using deionized water its interfacial tension with Fluorinert was 58mN/m [*Karadimitriou et al.*, 2012]. When NaCl was added to the water-based dye to increase its ionic strength, the interfacial tension dropped to 35mN/m.

Spontaneous imbibition experiments: Capillaries were filled with the non-wetting phase and positioned vertically in a stand above a petri-dish containing the wetting phase. At the start of each experiment the capillary was lowered into the container so that the bottom edge came in contact with the wetting phase in the petri-dish and rose through the capillary as a result of capillary forces. A high-velocity camera (Memrecam GX-1, NAC) equipped with a micro-lens (AF Micro-NIKKOR 200mm, Nikon) was used to capture images of the interface. A frame rate of 10,000fps was used to capture images in our experiments at a resolution of 512*384. A pair of LED lights (uLite 2-Light Octabox 200W Fluorescent Kit, Westcott) were used to provide optimal contrast between fluids. Contact angle for the images was measured using ImageJ with Drop Analysis plugin. The static contact angles for each combination of solids and fluid pairs was measured before the experiments using glass microscope slides. For each experiment at least 9 pairs of contact angles were measured and data were compiled for statistical analysis.

Forced imbibition experiments: Capillaries were aligned horizontally in the field of view of a Nikon A1R confocal microscope. The fluid input was controlled with the use of Harvard Picoplus syringe pump using a Hamilton 7000 series glass syringe. Two syringes containing the wetting and the non-wetting phase fluids were connected together at a T-section type connection. The syringe with the wetting phase was placed on the syringe pump, while the other was controlled by the user. A valve located between the t-section and the non-wetting phase syringe was closed during imbibition, to ensure not back-flow towards non-wetting phase syringe. The capillary was placed and secured under the microscope and finally the outflow was connected to a drain. The whole set-up was installed on a vibration-free table. The field of view was monitored optically

with a DS-Ri2 camera with a resolution of 16.25 megapixels (resolution 2.46μm/pix, at 10x magnification) which can record high resolution images, at a stable frame rate of 20fps. We used confocal laser scanning microscopy to identify the presence or absence of water film, and also investigate its thickness and structure. In this application we used a LU-N3 laser unit, set up at 488nm, an A1-DU4, set-up to 525nm, and a high resolution Galvano scanner, set-up at 1.24μm/pix. The image tracking data were used to calculate the velocity of the center of the interface between wetting and non-wetting fluids as a function of time under constant flow conditions. Acceleration was calculated from these velocity data and the standard deviation of the velocity data was used to calculate a measure of the overall jumpiness of the interface.

3.2.3 Experimental Design

Four independent variables were included in a modified 2^k factorial design of experiments: surface treatment (3 levels: untreated, roughened, or wettability modified), presence of a water film (2 levels), aqueous chemistry (DI water and 1 M NaCl solution) and non-aqueous fluid type (Fluorinert and dodecane), as shown in Table 3.1. This approach allowed us to investigate the contribution of each independent variable and the interaction effects between these on the dependent variables. Setting up the experiments in this way enabled us to run analysis of variance (ANOVA) on the results. Replicates of each experiment were carried out and normal distributions for the results were visually examined and quantified using Tukey test with quantile-quantile plot; homogeneous variance is checked using Levene's method and there is no statistically significant difference in variance across experimental conditions.

Table 3.1. Factorial design of experiments used to develop the experimental matrix presented here.

Exp. #	Surface treatment	Presence of wetting film	Aqueous chemistry	Non-aqueous fluid
1	Untreated	-	DI water	Fluorinert
2	Untreated	+	DI water	Fluorinert
3	Roughened	-	DI water	Fluorinert
4	Roughened	+	DI water	Fluorinert
5	Wet Modified	-	DI water	Fluorinert
6	Wet Modified	+	DI water	Fluorinert
7	Untreated	-	1 M NaCl	Fluorinert
8	Untreated	+	1 M NaCl	Fluorinert
9	Roughened	-	1 M NaCl	Fluorinert
10	Roughened	+	1 M NaCl	Fluorinert
11	Wet Modified	-	1 M NaCl	Fluorinert
12	Wet Modified	+	1 M NaCl	Fluorinert
13	Untreated	-	DI water	dodecane
14	Untreated	+	DI water	dodecane
15	Roughened	-	DI water	dodecane
16	Roughened	+	DI water	dodecane
17	Wet Modified	-	DI water	dodecane
18	Wet Modified	+	DI water	dodecane
19	Untreated	-	1 M NaCl	dodecane
20	Untreated	+	1 M NaCl	dodecane
21	Roughened	-	1 M NaCl	dodecane
22	Roughened	+	1 M NaCl	dodecane
23	Wet Modified	-	1 M NaCl	dodecane
24	Wet Modified	+	1 M NaCl	dodecane

3.3 Results and Discussion

Idealized capillary experiments were used to measure the microscopic characteristics of the interface under a range of capillary numbers. As a fluid pair moves through the capillary, the shape of the interface changes. These so-called quasi-static movements are characterized by short-term (i.e., on the order of milliseconds) accelerations and decelerations. The resulting stick-slip flow would influence macroscale flow dynamics of interest in more complex porous media such as residual saturation and capillary pressure.

3.3.1 Spontaneous imbibition experiments

Dynamic contact angle was measured for the conditions listed in Table 3.1 and the results are presented in Figure 3.3. The dashed line is the least square root fit of the data with Joos equation modified using Wenzel theory. The Wenzel model defines an apparent contact angle for rough surfaces as:

$$\cos\theta^* = r * \cos\theta \qquad (6)$$

where θ^* is apparent contact angle on a rough surface, θ is the Young contact angle on an ideal flat surface, and r is roughness ratio, defined as the ratio of true area of solid surface to apparent area. Combining this with the Joos equation (Eqn. 4) to account for surface roughness yields:

$$\cos(\theta_d) = \mathrm{r} * \cos(\theta_e) - \alpha * (1 + \mathrm{r} * \cos(\theta_e))Ca^{1/2} \qquad (7)$$

where θ_d is the dynamic contact angle and θ_e is the contact angle at equilibrium, r is the roughness coefficient defined as total area over apparent area, and Ca = $(\mu v)/\gamma$ is the capillary number, in which μ is the fluid viscosity, γ is the interfacial tension, and v the velocity of contact line.

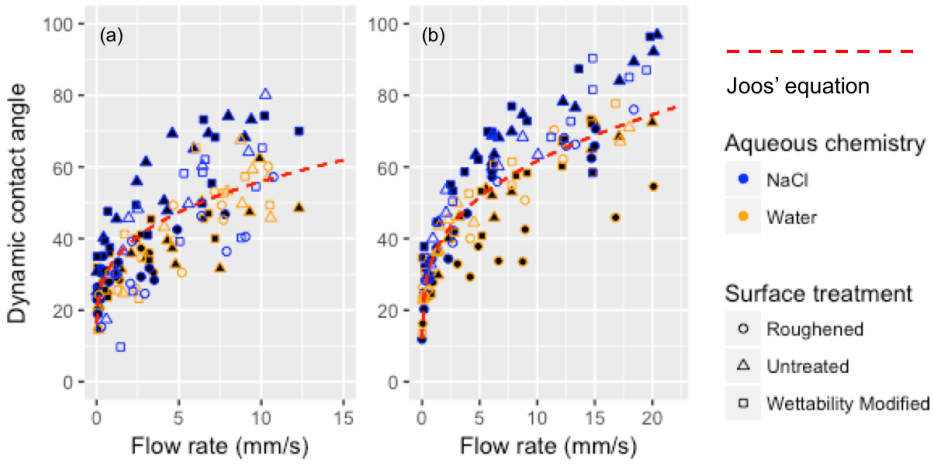

Figure 3.3. Dynamic contact angle of (a) Fluorinert and (b) dodecane interface as a function of flow rate, surface treatment, and aqueous chemistry.

The model results in Figure 3.3 were obtained by fitting the dynamic contact angle data under two flow rate conditions, in which the parameter $\alpha$is derived by least square fit. This combination of Joos model and Wenzel's law effectively predicts the general correlation between dynamic contact angle and flow rate, but it is evident that there is a great deal of scatter in the data. This suggests there must be factors other than flow velocity that affect dynamic contact angle.

3.3.2 The impact of surface features, water film and solution chemistry

To develop a more complete understanding of the factors controlling this system, the effect of independent variables and their interactions on dynamic contact angle was analyzed in the form of ANOVA. The results presented in Table 3.2 are interpreted as follows. Degrees of freedom (Df) is the level of factors minus 1. Sum of squares represents the variability in the response data that could be attributed to each independent variable. Mean squares are sum of squares divided by degree of freedom, and F value is the ratio between factor mean squares and the residual mean

squares. For each independent variable, the null hypothesis of ANOVA is that there is no difference in the response variable between different groups. And the P value is the probability of the finding the observed results when the null hypothesis is true. In this context, the smaller P value indicates stronger effect of the factor, or combination of factors. Usually we define statistical significance when P value is less than 0.05.

Table 3.2 suggests that surface treatment and aqueous chemistry have a statistically significant impact on dynamic contact angle, while water film alone does not. For two-way factors, surface and water film have an effect, and the interaction between aqueous chemistry and water film has a stronger effect. Water film does not show any significant effect by itself, but accounts for a large portion of the variance when combined with surface or aqueous chemistry. The non-aqueous fluid (Fluorinert or dodecane) shows an effect, but no interaction with any other factor. This suggests that the trends observed could be applied to other fluid system in a more generalized form. None of the three-way interactions here had a statistically significant effect.

Table 3.2. Analysis of Variance (ANOVA) table for dynamic contact angle collected in spontaneous imbibition experiments as a function of various independent variables.

Independent variable and interactions	Df	Mean Sq	F value	p-value
Surface	2	6207	27.13	2.89E-11
Aqueous chemistry	1	7953	34.76	1.38E-08
Water film	1	223	0.98	0.32
Non-aqueous fluid	1	4031	17.62	3.91E-05
Surface + Aqueous chemistry	2	541	2.37	0.10
Surface + Water film	2	1575	6.89	1.34E-05
Aqueous chemistry + Water film	1	1025	4.48	0.04
Surface + Non-aqueous fluid	2	194	0.85	0.43
Aqueous chemistry + Non-aqueous fluid	1	483	2.11	0.15
Water film + Non-aqueous fluid	1	6	0.03	0.86

As the ANOVA results presented in Table 3.2 suggest, the most important single factors influencing dynamic contact angle are surface treatment and aqueous chemistry. The interaction between aqueous chemistry and water film combined has a stronger effect than any other factor alone. To better illustrate this interaction effect, results are plotted in Figure 3.4 as two separate panels with and without water film. When no water film is present, water and NaCl results are distributed in the same cluster, however, when a water film exists, dynamic contact angles are considerably larger when NaCl is in the solution.

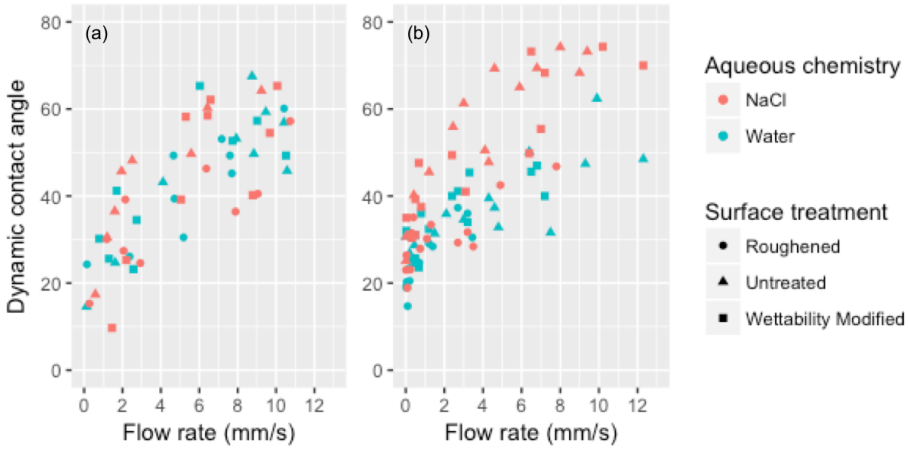

Figure 3.4. Dynamic contact angle for different surfaces and solution chemistry at (a) with wetting film and (b) with no wetting film.

Ionic strength impacts this system by changing the interfacial tension (IFT) between the fluids and by impacting the energy of glass surface. For the Fluorinert/water system, for example, the addition of 1 M NaCl lowers the IFT from 58mN/m to 35mN/m, which would in effect make the capillary more water wetting. This effect would be even more pronounced for more complex ionic solutions. Aggelopulos[*Aggelopoulos et al.*, 2010] showed that divalent cations influence wettability even more strongly than the mono-valent ions tested here. These ions also interact with

the charged silica surface including the electrical double layer[*Kang*, 2002; *Kim et al.*, 2013] near the surface. Higher concentrations of ions provide additional electrostatic force[*Kang*, 2002], which can offset some of the increased contact angle due to changes in the IFT.[*Steitz et al.*, 2001; *Jones et al.*, 2002]

3.3.3 Derivation of an improved modeling framework

As shown in Figure 3.3, fitting using a combination of the Joos and Wenzel equations (Equation 7) , where α is the only fitting parameter (α = 0.472), does not provide a particularly good fit for our experimental results. To incorporate some of the qualitative findings from the ANOVA we extend equation 7, adding an additional fitting parameter:

$$\cos(\theta_d) = \mathrm{r} * \cos(\theta_e) - \alpha * [(\beta + \mathrm{r} * \cos(\theta_e))]\mathrm{Ca}^{1/2} \qquad (8)$$

where β is a second fitting parameter obtained empirically from our data. While both α and β could be used as fitting parameter to get a best fit for each experimental conditions, we propose to treat them as empirical constants that are tied to a physical characteristic of the system. α is related to the presence of a water film and β is related to the ionic strength of the aqueous phase:

$$\cos(\theta_d) = \mathrm{r} * \cos(\theta_e) - \alpha(\mathrm{wf}) * [(\beta(\mathrm{ac}) + \mathrm{r} * \cos(\theta_e))]\mathrm{Ca}^{1/2} \qquad (9)$$

where $\alpha(\text{Water film [wf]}) = \begin{cases} 0.415, when\ wf = 1 \\ 0.640, when\ wf = 0 \end{cases}$, and

$$\beta(Aqueous\ chemistry\ [ac]) = \begin{cases} 1.21, when\ \text{ac} = NaCl \\ 0.903, when\ \text{ac} = DI\ Water \end{cases}.$$

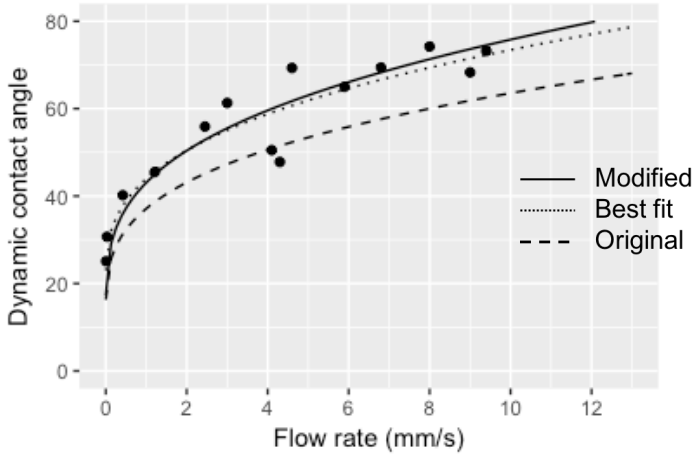

Figure 3.5. Comparison of models on experimentally measured dynamic contact angle data for Fluorinert/ NaCl solution on untreted wet surface.

Figure 3.5 presents the relationship between flow rate and dynamic contact angle for a representative experiment along with the different fitting equations. Four equations are used to fit the data. The goodness-of-fit is evaluated by a modified root mean square error (RMSE) to adjust for the number of fitting parameters used, which is defined as:

$$RMSE = \left(\frac{RSS}{m-p}\right)^{1/2} \qquad (10)$$

where RSS is the residual sum of squares, m is the number of observations and p is th number of adjustable parameters. The original Joos/Wenzel (Equation 7) is shown as a dashed line. In this case, it underestimates the increase of dynamic contact angle, resulting a root mean square error (RMSE) of 14.3 degrees. The best fit (Equation 8) is the least square fitting for a

specific condition with $\alpha$and β as fitting parameters, representing the lowest possible RMSE of 4.3. Modified (Equation 9) is using the global constants $\alpha$and β and compares well with the best fit (RMSE of 4.4 degrees in this case).

Equation 9 was used to fit the all experimental data collected in this study, and the results are presented in Figure 3.6. Here, we compare the fitting performance of the newly proposed Equation 9, and the roughness modified Joos' (Equation 7), on Fluorinert contact angle with water film. On average, the average RMSE between the data and model fit is reduced from 9.5 degrees using Equation 7, to 5.1 degrees using the newly proposed Equation 9. This improvement is especially significant when ionic strength is higher, where it interacts with surface features, and therefore have co-effects that are not captured by the original model. The single set MSE for Figure 4.9b (untreated surface) and Figure 3.9d (roughened surface) are both reduced by more than 65% from the original model. The comparison between the improved model and the original model on the full 24 experimental conditions demonstrate the improved prediction compared with the original model on Fluorinert/water fluid pair with water film.

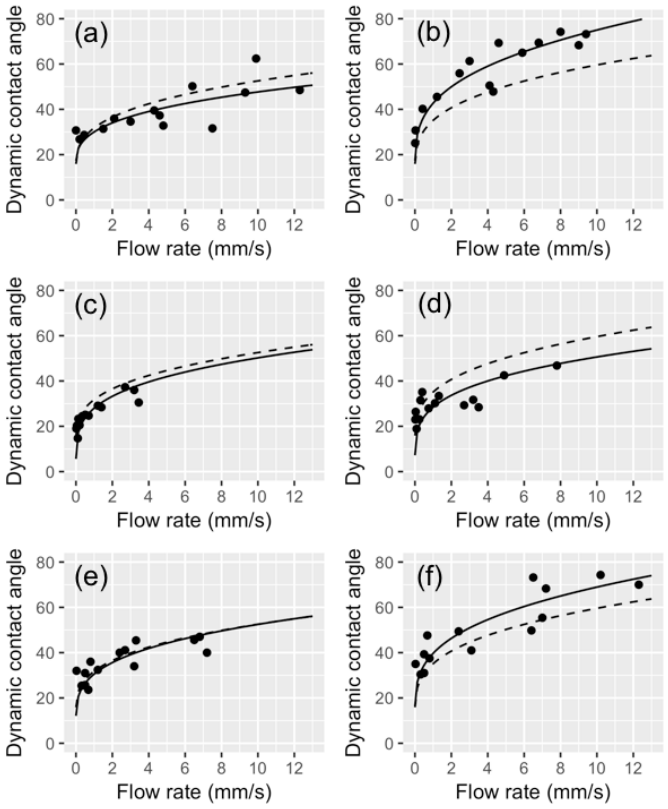

Figure 3.6. Fitting of Fluorinert/water dynamic contact angle with water film for (a) Fluorinert/water on untreated surface; (b) Fluorinert/NaCl solution on untreated surface; (c) Fluorinert/water on roughened surface; (d) Fluorinert/NaCl solution on roughened surface; (e) Fluorinert/water on wettability modified surface; (f) Fluorinert/NaCl solution on wettability modified surface. Dashed line and solid line represents the best fit using the original Joos equation, and the newly proposed equation 9, respectively.

4.3.4 Forced Imbibition experiments

To better characterize flow dynamics mechanistically, two-phase flow dynamics were conducted under forced imbibition conditions for a range of lower capillary numbers. Interaction between fluid interface and solid surface becomes more pronounced in capillary dominant flow

regimes, as suggested by previous experimental studies [*Blake and Shikhmurzaev*, 2002; *Blake*, 2006]. Having a wide range of capillary numbers, by accurately controlling flow rate, could reveal the flow dynamics, and test the applicability of the findings for both viscous and capillary dominant flow. Also, the integrated high speed microscope imaging system allows the geometry of the two-phase interface to be closely monitored along with its velocity over time. The detailed statistical analysis and image comparisons could significantly improve the mechanistic understanding of these processes.

In forced imbibition experiments, the normalized deviation of interface velocity is used as a measure of the irregularity of flow. It is quantified as the standard deviation of horizontal velocity of the moving interface through a capillary, divided by the average velocity value. Table 3.3 presents the ANOVA results using normalized velocity deviation as the response, roughened surface and wettability modified surface are both compared to untreated surface. Significant (>8% of SoS contribution) parameters and their interactions are highlighted in the tables.

The results reported in Table 3.3 suggest that surface roughness contributors to the response variability for all cases. For the roughened case, flow rate, surface property and the surface – water film interaction (as highlighted in the table) have large effects that together account for over 60 percent of the variability in velocity deviation. For the wettability modified case, effects are more uniform across the four factors, with water film being the second strongest model term. Surface treatment (untreated, roughened, or wettability modified) shows a significant contribution to the response variation, as well as flow rate. Water film is a large contributor for untreated and

wettability modified samples, but not for roughened samples. However, the co-effect of water film and surface treatment shows up as a major factor for the roughened case.

Table 3.3. Analysis of variance for velocity deviation (i.e., the instantaneous acceleration of the fluid contact line) collected using forced imbibition experiments. Top 3 factors that contribute to the variation are shaded.

	Roughened			Wettability Modified		
Independent variable and interactions	Effect	SoS	% Cont.	Effect	SoS	% Cont.
Flow rate	-0.31	0.75	19.82	-0.77	4.79	38.69
Water film	-0.05	0.02	0.462	0.52	2.2	17.78
Surface	0.34	0.91	24.15	-0.36	1.05	8.466
Aqueous chemistry	0.18	0.27	7.13	0.31	0.77	6.21
Flow rate + Water film	0.01	0	0.031	-0.23	0.42	3.421
Flow rate + Surface	-0.19	0.28	7.51	0.28	0.63	5.053
Water film + Surface	0.28	0.65	17.16	-0.29	0.66	5.306
Flow rate + Aqueous chemistry	0.04	0.02	0.412	0.03	0.01	0.075
Water film + Aqueous chemistry	-0.03	0.01	0.168	0.28	0.62	4.987
Surface + Aqueous chemistry	0.01	0	0.027	-0.12	0.11	0.858
Flow rate + Water film + Surface	-0.07	0.04	1.165	0.17	0.23	1.823
Flow rate + Water film + Aqueous chemistry	-0.13	0.14	3.693	-0.22	0.38	3.089
Flow rate + Surface + Aqueous chemistry	0.01	0	0.04	0.02	0	0.037
Water film + Surface + Aqueous chemistry	0.19	0.28	7.344	-0.12	0.11	0.927
Flow rate + Water film + Surface + Aqueous chemistry	-0.07	0.04	1.046	0.02	4.79	0.017
Residuals	0	0.37	9.839	0	2.2	3.263

From the Analysis of Variance (ANOVA) results presented in Table 3.3, the interplay between surface treatment (wettability modified, roughened) and water film accounts for significant variance of the response variable. The detailed normalized velocity deviation data over the three surfaces with and without water film are shown in the box and whisker plots in Figure 3.7. Normalized velocity deviation values across the three surfaces are very similar when a water film is absent, but vary significantly when a water film is present. This suggests that the Wenzel

regimes qualitatively capture the behavior of our system, i.e., that the presence of a water film dramatically enlarges the differences of displacement pattern between surfaces [*Quéré*, 2008b].

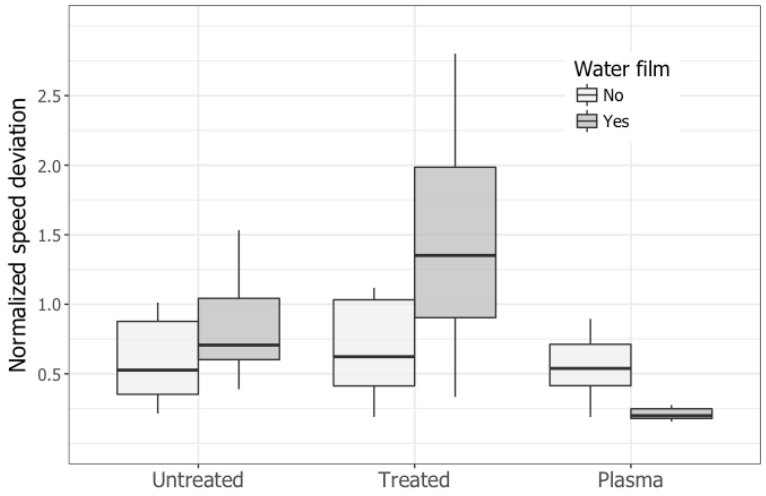

Figure 3.7. Normalized velocity deviation for different surfaces and water film.

3.3.5 Water film analysis

To understand the interaction of surface feature and water film, we imaged the water film using the confocal microscope on difference surfaces. The results, shown in Figure 8, reveal that the untreated surface generally has a thin and isolated water residual after drainage; wettability modified surface has more uniform water film due to enhanced wetting; and roughened surface has a thick, but broken, water film. The smoothest flow was observed for wettability modified surfaces with a pre-existing wetting film, which is consistent with literature suggesting that the presence of a wetting film enhances stable displacement. This velocity deviation can be explained by the thickness and the geometry of the water film. Figure 8b indicates that the low velocity deviation, in the case of the wettability modified surface, is linked to the uniformity of the water

film. In addition to that the lower average velocity deviation, in this case, recorded by the tracking algorithm can be explained by the thickness of the water film.

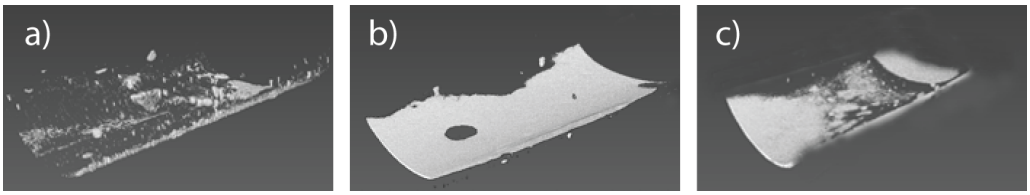

Figure 3.8. 3D reconstruction of wetting phase film, under the non-wetting phase, after imbibition at no flow conditions. (a) untreated surface; (b) wettability modified surface; and (c) roughened surface.

In the case of the rough capillary, Figure 8c indicates the presence of a water film that may be masking the roughness in places. However, the velocity deviation is the highest when the roughness is combined with the presence of water film. Qualitative observations of the experimental videos reveals vibrations at the interface suggesting that repeated instances of fluid pinning were taking place as the fluids moved through the capillary. This pinning can only be linked to the areas of the water film where the thickens varies significantly.

3.4 Conclusions

The combination of extensive experimental set and statistical analysis presented in this study evaluates the effect of surface roughness on multiphase flow, compared with other factors such as wettability, solution chemistry, and water film. Analysis of variance (ANOVA) was used to analyze the relative contribution from the different independent variables following a modified

2^k factorial design. To the best of our knowledge, this is the first time that a statistical analysis comparing the effect of these factors is reported. The results suggest that surface texturing, wettability and the presence of a water film contribute to over 70% of the variation in the interface velocity deviation, which in a more complex porous media, could alter flow directions and capillary pressure.

A new empirical equation was proposed for predicting dynamic contact angle, using a modified empirical framework based on Joos equation, with the incorporation of Wenzel's law to account for surface roughness. It takes into account the important factors identified by the ANOVA analysis, where the interaction between surface roughness and solution chemistry change dynamic contact angle much more significantly than either of the two alone. A modified Joos equation is proposed to include both surface features and the solution chemistry as two terms. This equation is tested against two different fluid pairs and show generally good predictability, and showed significant reduction in the average RMSE (9.5 degrees to 5.1 degrees) when compared with the original empirical equation.

Overall, this study bridges the knowledge gap between mechanistic understanding of the relative importance of the factors controlling contact angle dynamics, from a statistical stand point. Based on the factors that are identified in ANOVA, one-way and two-way effects were modelled using this mathematical relationship, which improves the general applicability of this modeling frame work to more complex and realistic conditions. These results highlight the importance of incorporating a comprehensive set of factors in pore scale modeling when predicting macroscopic multi-phase flow behaviors.

Chapter 4

Study of Stratigraphic and Capillary Trapping in Column Experiments

Gas leakage from geologic carbon storage sites could undermine the long-term goal of reducing emissions to the atmosphere and negatively impact groundwater resources. Despite this, there remain uncertainties associated with the transport processes that would govern this leakage. These stem from the complex interaction between governing forces (e.g., gravitational, viscous and capillary), the heterogeneous nature of the porous media, and the characteristic length scales of these leakage events, all of which impact the CO_2 fluid flow processes. This work assessed how sub-basin-scale horizons in porous media could impact the migration and trapping of a CO_2 plume. A high-pressure column packed with two layers of sand with different properties (e.g., grain size, wettability) was used to create a low-contrast stratigraphic horizon. CO_2 in supercritical or liquid phase was injected into the bottom of the column under various conditions (e.g., temperature, pressure, capillary number) and the transport of the resulting plume was recorded using electrical resistivity. The results show that CO_2 trapping were most strongly impacted by shifting the wettability balance to mixed wet conditions, particularly for residual saturation. A 16% increase

in the cosine of the contact angle for a mixed wet sand resulted in nearly twice as much residual trapping. Permeability contrast, pressure, and temperature also impacted the residual saturation but to a lesser extent. Flow rate affected the dynamics of saturation profile development, but the effect is transient, suggesting that the other effects observed here could apply to a broad range of leakage conditions.

4.1 Introduction

Geologic carbon storage (GCS) is being widely explored as a strategy for reducing atmospheric emissions of carbon dioxide (CO_2) [*White et al.*, 2003]. In GCS, CO_2 captured from fossil power plants and other stationary sources is injected into porous formations in the deep subsurface to keep the CO_2 out of the atmosphere where it contributes to climate change [*Michael et al.*, 2010]. Target geologic repositories are typically high-permeability deep saline aquifers located beneath a low-permeability formation (e.g., caprock), which provides mechanical stabilization of the CO_2 plume, resulting in stratigraphic trapping. Over longer time scales, other trapping mechanisms, such as capillary trapping, solubility trapping, and mineral trapping, also help sequester the CO_2. The potential for leakage exists because CO_2 is less dense than the surrounding brine and is thus subject to buoyant forces [*Oldenburg and Lewicki*, 2006; *Trevisan et al.*, 2015]. Leakage can occur when fractures or heterogeneities in caprocks, failed wellbore casing, seismic activity or other events and/or features in the subsurface create pathways for transport into overlying formations [*Nicot et al.*, 2009; *Strandli and Benson*, 2013].

Stratigraphic trapping impacts storage potential and leakage concerns, and has been studied extensively [*Nordbotten et al.*, 2005, 2009; *Oruganti and Bryant*, 2009]. In contrast, the

comparatively more abundant sub-basin scale horizons with subtle differences in permeability or wettability, have received less attention. Most effort have been focused on modeling their impact at basin scales [*Gershenzon et al.,* 2015; 2016a; 2016b]. These horizons are the result of changes in depositional environments over geologic time during which diagenetic processes produce inter-bed layers with distinct properties [*Strandli and Benson*, 2013]. In the context of CO_2 leakage, this layered stratigraphic heterogeneity could impact capillary trapping that might attenuate leakage events and represent an important safety mechanism should the primary cap rock fail.

Figure 4.1 presents a conceptual representation of a CO_2 sequestration well and the subsurface overlaying the target repository. CO_2 could escape the formation into which it is injected via faults or fractures in cap rocks or abandoned well bores [*Lewicki et al.*, 2007; *Pruess*, 2008]. Once it reaches overlying formations, it will rise in response to buoyant forces until it reaches a capillary barrier where it will spread beneath the interface until the capillary entry pressure of the overlying low-permeability layer is overcome [*Bryant et al.*, 2008; *Saadatpoor et al.*, 2010]. This phenomenon shares some characteristics with the stratigraphic trapping provided by caprock with a few important differences: (1) the contrast between the layers is subtle and so only small amounts of CO_2 will accumulate before the capillary entry pressure of the overlying layer is overcome; (2) the number of these intra-reservoir barriers that a particular parcel of CO_2 will encounter on its path to the surface is great [*Gershenzon et al.,* 2014, 2017a, 2017b]; and (3) the CO_2 ganglion will be far from the injection site and so buoyant forces will dominate [*Krevor et al.*, 2011; *Zhang et al.*, 2011].

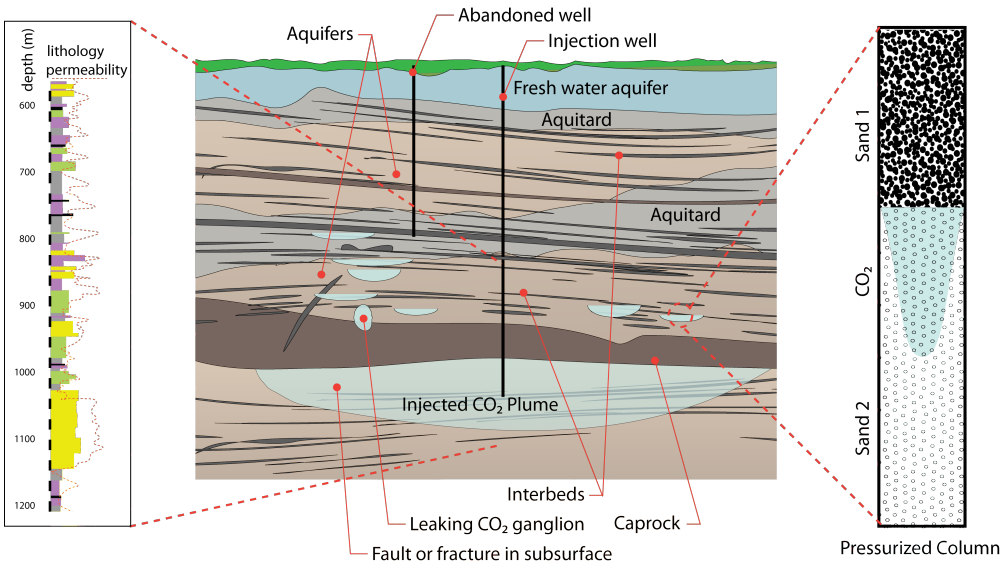

Figure 4.1. Schematic of CO_2 leakage in GCS illustrate how local heterogeneities in the subsurface could influence overall leakage rates and residual trapping by overlying formations. The schematic on the left is a wellbore log that shows how much permeability and rock composition varies in formations overlying the target reservoir. The schematic on the right is for an individual horizon between two strata, which were explored experimentally here using packed column experiments.

The trapping and migration of CO_2 as a distinct phase (e.g., not dissolved) is driven by three forces: (1) advective forces created by over-pressurization; (2) the capillary force created by the surface tension between the fluids and the pore walls, and (3) buoyant forces that result from the lower density of CO_2 relative to the connate brine [*Bryant et al.*, 2008; *Mouche et al.*, 2010; *Plampin et al.*, 2014b]. Influencing these driving forces are three physicochemical characteristics of the system: (1) pore size and permeability contrast between the two layers in the column as it determines capillary pressure contrast; (2) temperature and pressure conditions and the subsequent fluid density and surface tension; and (3) interfacial properties between solid and fluid phase, such as surface wettability.

The relationship between capillary pressure and saturation in a multiphase flow has been studied extensively in various applications and recently in the context of CO_2/water flow in geologic carbon storage [*Zhou et al.*, 2013]. Leverett J-function has been used to describe a normalized capillary pressure curve as a function of water saturation, which serves as the foundation for predicting capillary behavior of all immiscible fluids in porous media [*Plug and Bruining*, 2007; *Krevor et al.*, 2011]. The two-phase vertical displacement process that would characterize CO_2 leakage events is unstable and may fall into three patterns in porous media: capillary, gravitational, and viscous regimes, which are dominant by each of these three governing forces [*Lenormand et al., 1988; Bandara et al., 2011; Holtzman et al., 2012]*. These regimes have been identified analytically and through bench-scale experiments [*Zhang et al.*, 2011; *Holtzman et al.*, 2012; *Wang et al.*, 2013c], based on non-dimensional numbers: the Capillary number, Bond number and Gravity number [*Zhou et al.*, 1994; *Lovoll et al.*, 2005; *Cottin et al.*, 2010; *Levine et al.*, 2011; *Mikami et al.*, 2014]. However, there is still a gap in the understanding of how this trapping behavior takes place under reservoir pressures and temperature subject to realistic fluid phase and interfacial conditions.

A great deal of research has been carried out using high-pressure core flooding experiments [*Krevor et al.*, 2011; *Pentland et al.*, 2011; *Andrew et al.*, 2014; *Manceau et al.*, 2015]. These studies have reported on the relationships between capillary pressure and saturation, initial and residual saturation, and the impact of different pore structure and wetting conditions [*Al-Menhali et al.*, 2015; *Niu et al.*, 2015]. Most of these experiments have been conducted in rock cores that are either homogeneous or contain randomly distributed heterogeneity. Pini et al. demonstrated

that sub-core-scale heterogeneities at the pore scale could impact the flow paths, creating different saturations of non-wetting phase fluids over time [*Pini et al.*, 2012]. The use of real rocks in these experiments, however, makes it difficult to systematically control for horizons within the rock and establish causal relationships that would lead to a first-principle understanding of these displacement processes [*Tokunaga et al.*, 2013; *Skurtveit et al.*, 2015].

To understand how CO_2 moves through formations at larger scales, several groups have studied CO_2 transport in the subsurface using experimental observations in analogous fluid systems, such as oil-water or gas-water systems using low pressure packed sand testbeds [*Pentland et al.*, 2011; *Breen et al.*, 2012; *Tokunaga et al.*, 2013]. Sand-packed test-beds are often used in the study of flow through porous media and these experimental configurations offer many advantages for studying the role of permeability relative to other factors [*Camarasa et al.*, 1999; *Fagerlund et al.*, 2008; *Zhao et al.*, 2010]. Over the years, researchers have managed to find proper analogue fluids to make the invading phase non-wetting such that the displacement falls into a capillary-dominant unstable flow regime [*Mori et al.*, 2015]. For example, *Trevisan et al.* [2014,2015] conducted two-dimensional experiments at ambient condition using analogous fluids and found a spatial correlation with heterogeneity and the dominance of gravitational force on fluid transport. While these experiments help better explain the transport processes at intermediate length scales, there are important aspects of the CO_2 leakage problem that these experiments cannot capture. Notably, CO_2 has a viscosity that is significantly lower than the surrogate fluids, it has a higher solubility in brine and the surface chemistry and wettability aspects of analogue systems are difficult to reproduce in these model systems [*Bourg et al.*, 2015; *Manceau et al.*, 2015; *Wang et al.*, 2016].

Wettability in particular is a key parameter influencing multiphase flow properties, such as capillary pressure, relative permeability, and residual trapping [*Bachu and Brant Bennion*, 2009; *Wang et al.*, 2013b]. Most rocks are water-wet and have a low contact angle (by convention, contact angle is referred to as the angle through the denser phase, in this case, the water phase). A large body of literature has focused on characterizing wettability for GCS relevant conditions. The relationship between wettability and reservoir conditions such as pressure, temperature, salinity and the exposure history of the rock surface has been recently reviewed [*Iglauer et al.*, 2015; *Palamara et al.*, 2015]. On the other hand, the impact of wettability on trapping and migration is a relatively open question. Earlier research showed that contact angle and residual saturation at the core-scale are inversely proportional. As contact angle increases, the residual trapping of non-wetting phase in the rock decreases [*Jadhunandan and Morrow*, 1995; *Spiteri et al.*, 2008]. Recent experiments, however, suggest the relationship may be somewhat more complex [*El-Maghraby and Blunt*, 2013; *Wang and Tokunaga*, 2015]. In depleted oil reservoirs, aging of oil-bearing rocks tends to shift the wettability towards more mixed-wet or oil-wet properties. The wettability of CO_2 storage reservoirs could also change over time when exposed to CO_2 and other species occurring naturally in the subsurface [*Chiquet et al.*, 2007; *Tanino and Blunt*, 2012].

The understanding of displacement processes in bench-scale studies has been used to inform simulations of these processes at the basin scale [*Oldenburg and Lewicki*, 2006; *Bryant et al.*, 2008; *Silin et al.*, 2008; *Oldenburg*, 2011; *Lassen et al.*, 2015]. These basin-scale models typically rely on the empirical relationship between capillary pressure, phase saturation and relative permeability [*Juanes et al.*, 2006]. In order to cross spatial scales and understand CO_2

transport over long distances, a number of groups have adapted techniques from the geophysics domain to monitor CO_2 injection and migration processes during field trials. Examples include seismic wave analysis and real-time monitoring [*Bateman et al.*, 2005, 2011; *Wigand et al.*, 2008; *Pentland et al.*, 2011]. In some of these modeling and field studies, the impact of bedding planes and horizons on vertical transport has been explicitly considered [*Nordbotten et al.*, 2009; *Saadatpoor et al.*, 2010]. There remains, however, a disconnect between our bench-scale understanding of these processes under well-controlled conditions and the impact of stratigraphy on vertical transport in the subsurface that is observed in the field and in basin scale models [*Plampin et al.*, 2014a].

The goal of this work is to explore how heterogeneity that is perpendicular to the direction of flow impacts vertical transport of CO_2. In particular, this work will explore the role that reservoir conditions could have on these flow processes, particularly fluid phase (e.g., viscosity, density) and interfacial properties (e.g., surface tension, wettability). Drainage and imbibition experiments were carried out using a high-pressure column test-bed to study both initial capillary trapping and residual trapping of CO_2. Three primary hypotheses are studied: (1) the accumulation of CO_2 under the stratigraphic horizons could influence capillary and residual trapping; (2) these effects would be more or less pronounced depending on how deep in the subsurface the horizon existed because of the influences on pressure and temperature conditions; (3) CO_2 flow rate, phase equilibrium, and wettability would influence the way in which the interactions between the stratigraphy and residual trapping developed.

4.2 Methods and Materials

4.2.1 Experimental system and data processing

A high-pressure vertical column test-bed was assembled using a commercially available vessel made of 316 stainless steel (OC-11, High Pressure Equipment Company) (inside length of 53 cm and diameter of 5.2 cm). The vessel was modified by adding a port to the bottom and a custom-made seal to the top to enable access to the electrical resistivity connections at high pressure (PLPTM4/-20-B8-G,12/30, Conax Technologies). A separate high-pressure vessel (Model 4764, Parr Instruments) was used to equilibrate the brine with CO_2 before injecting it into the column. In this work, electrical resistivity was used to measure the migration of supercritical CO_2 through the brine-phase saturated porous media system in a pseudo-one-dimensional configuration. An insulating sleeve made of poly-methyl methacrylate was machined to hold the nickel electrodes in place and also to prevent interference from conductive stainless steel walls. The current was applied through the top and bottom electrodes, as a rectangular alternating wave starting at 10mA. The drop in the electrical potential between adjacent probes was recorded in real time using a National Instruments data acquisition system (NI cDAQ-9178). The dense-phase CO_2 and brine were delivered to the vessel at reservoir pressures using a syringe pump (Teledyne HP500D), and an HPLC pump (Model VG310PFT01, LabAlliance), respectively. The high-pressure column was also wrapped in heating tape to control the temperature in the column (Model B00051020, XtremeFLEX). A schematic of the system is provided in Figure 4.2.

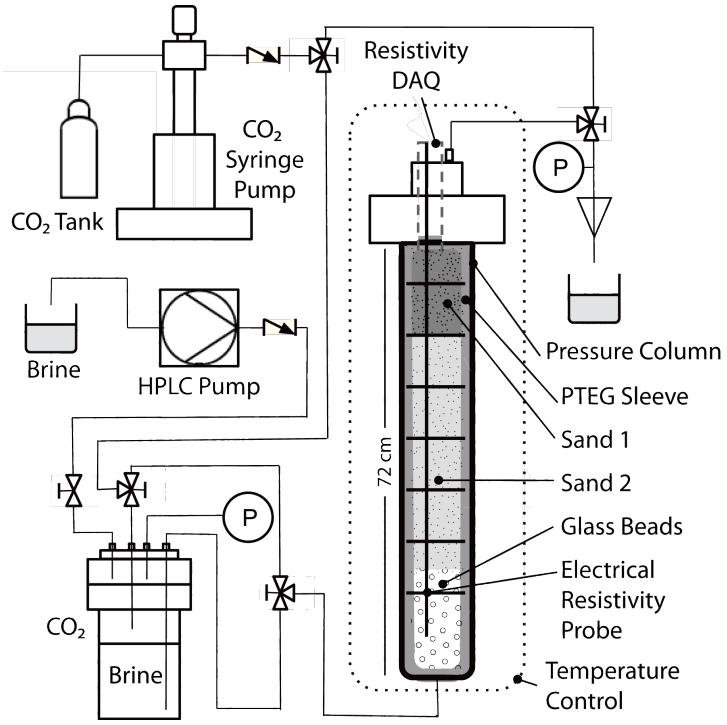

Figure 4.2. Experimental setup using electrical resistivity to track CO_2 plume migration through a sand packed column.

Columns were packed with sand and saturated with brine before the electrical resistivity readings were given time to stabilize across the entire column (usually within a few hours). Then CO_2 was introduced into column from the bottom port at a controlled flow rate, until the evolution of CO_2 saturation profile in each section reached a steady state. This typically occurred shortly after the CO_2 plume broke through the capillary barrier, which usually takes ~0.2 pore volumes of injection. Brine was then injected into the bottom port at the same rate to perform an imbibition cycle. The saturation profile after >10 pore volume of brine injection was generally stabilized and treated as the residual saturation for the system. After each experiment, sand and glass beads were recovered from the column and all components were rinsed in deionized water to limit corrosion.

The resistivity data were converted to gas saturation data using a modified version of Archie's law, which relates the resistivity ratio of the porous media partially saturated with air over that fully saturated with brine [*Nakatsuka et al.*, 2009] via:

$$\frac{\rho}{\rho_o} = I = (S_w)^{-n}$$

where ρ_0 is the initial resistivity ($\Omega \cdot m$); I is the resistivity index [*Guéguen and Palciauskas*, 1994]; S_w is the water saturation; $S_w=1 - S_{air}$ where S_{air} is air saturation; and n, which is the empirical saturation exponent that varies based on the types of porous media. Here we use a value of n=2 based on the work of Nakatsuka et al. [*Nakatsuka et al.*, 2010]. The raw electrical resistivity data were collected every second, then averaged over 30-second periods, in order to reduce the noise. Some of the fluctuations in the results could be attributed to the non-linear correlation of the CO_2 saturation and resistivity in the column. Within a section, CO_2 that is closer to the probes will have a disproportionately stronger impact on measurements. However, over the scale of a whole column, this did not impact the accuracy of the results. The electrical resistivity data was found to be accurate to ± 2% after calibration, based on detected volume compared to that injected by the pump.

4.2.2 Sand preparation

The column was packed with well-sorted Ottawa sand (US silica) and glass beads (Mo-Sci Corp). Sands were sorted following *ASTM C136-06 Standard Test Method for Sieve Analysis of Fine and Coarse Aggregates*. All sands were washed using 0.5 M sodium acetate solution with pH adjusted to 4.0 to remove the surface organic matter. The glass beads packed under the sands, used

to provide a region in which to inject the CO_2 without fracturing the packed sand at the beginning of the experiment, are round spheres with a larger size than the sands. Both glass beads and sand were wet-packed and pre-saturated with the brine to remove air bubbles, and to eliminate any possible sorting effect in this process.

Mercury intrusion experiments were carried out to obtain the pore throat size distribution of the three sand samples. Mercury Intrusion Porosimetry (MIP) is widely used to characterize the pore throat size and microstructures of porous materials, which controls the capillary pressure of fluids [*Clarkson et al.*, 2013]. As shown in Figure 4.3, the results from MIP confirmed that these sands had some nominal overlap in size distributions following the sieving process but were generally distinct.

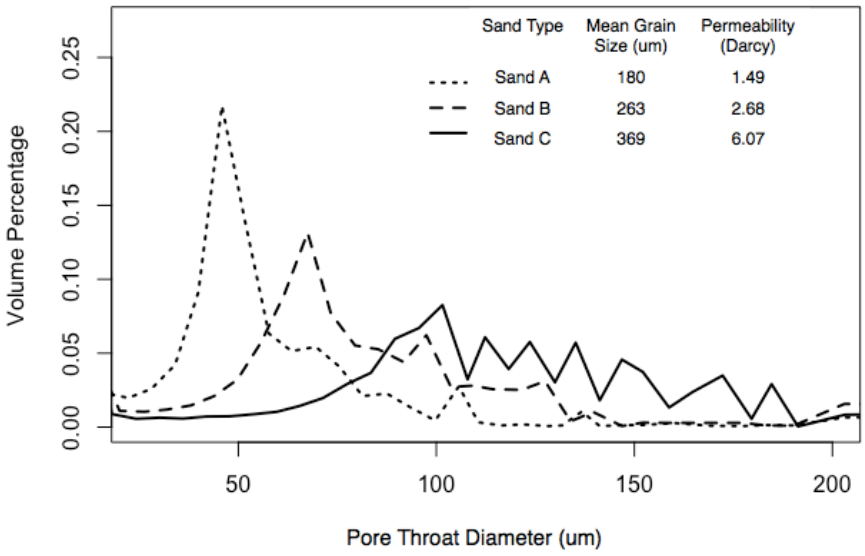

Figure 4.3. Pore throat size distribution of the three sand used in this study. While the absolute magnitude of the pore size is much larger than sandstones or carbonates that would

typically be target repositories in GCS, the relative difference provides a good model system for exploring the role of stratigraphic trapping.

Cleaned sand was treated using benzoic acid to modify the wettability using a method reported previously [*Legens et al.*, 1999]. Briefly here, clean sand was soaked in toluene containing 0.05M benzoic acid at 105℃ for 24 hours and then rinsed using DI water. The contact angle (air-brine-mineral) for solid samples with flat and smooth surfaces of silica treated in this way was measured under ambient pressure conditions. A quartz thin section, and a sample of Berea sandstone with a similar chemical composition of Ottawa sand, were used as surrogate to sand to carry out the contact angle measurements. These two surfaces were found to have nearly identical wettability characteristics comparable to the values for high pressure CO_2/brine system obtained by our group [*Wang et al., 2013b*]. After treatment, both changing from strong water wet to intermediate wetting range, with the average contact angle shifting from 17.7˚before treatment to 77.5˚after treatment. In the wettability alteration experiments, treated sands were thoroughly mixed with untreated sand at different ratios. For example, in Exp.#5, 20% of the treated sand was mixed with untreated sand. Since contact angle affects capillary pressure via the term cos (θ), the change of weighted cos (θ) of the mixed sand to [0.8 cos (17.7˚) + 0.2 cos (77.5˚)] is equivalent to a ~16% decrease from the original untreated sand. While the behavior of fluids moving through porous media with mixed wet surfaces can be different than fluids moving through a more heterogeneous porous media, this mixed wet configuration enabled us to control the wettability in our experiments.

4.2.3 Design of experiments

Table 4.1 presents the experimental conditions tested in this study. Two replicate experiments were conducted for each of these conditions. A base condition (Exp.#1) was selected as a reference for the other experiments. The pressure/temperature conditions (10 MPa, 40ºC) are representative of a typical geological sequestration site [*Lu and Lichtner*, 2007]. Exp.#2 was designed to measure the effect of permeability contrast and the resulting capillary pressure contrast between the layers, by selecting a smaller grain size in the overlying formation. Exp.#3 and #4 were carried out under different temperature and pressure conditions to influence the CO_2 density and viscosity values of the CO_2. While the changes in temperature and pressure would also impact the properties of the water phase including the two-phase solubility and interfacial properties these effects are minor relative to the impacts on the CO_2 phase. In Exp.#5 the wettability of the sand surface was altered while all other conditions were left the same to study the role of CO_2 wetting on trapping. In Exp.#6 we increased the flow rate of CO_2 and in Exp.#7 we injected non-equilibrated CO_2 to see if the dissolution of two fluids could impact the results. Exp.#8 and #9 were added after the initial set of 7 experiments was complete to further characterize the pronounced role that wettability played in this system.

Table 4.1. Experimental conditions used here. The brine in the dissolution experiments (Exp.#7) was not saturated with CO_2. Capillary number was defined as the product of viscosity and velocity divided by interfacial tension.

Exp. #	Experimental condition	Sand 1 (□)	Sand 2 (□)	Pressure (MPa)	Temp. (ºC)	Flow (ml/min)	Density (kg/m^3)	Viscosity (10^{-6} Pa*s)	IFT (10^{-3} N/m)	Capillary Number
1	Reference	A(17.7°)	B(17.7°)	10	40	1	628.7	47.8	25.8	3.6E-08
2	Permeability	A(17.7°)	C(17.7°)	10	40	1	628.7	47.8	25.8	3.6E-08
3	Temperature	A(17.7°)	B(17.7°)	10	20	1	827.7	22.3	29	1.5E-08
4	Pressure	A(17.7°)	B(17.7°)	8	40	1	277.9	78.3	30	5.1E-08
5	Wettability	A(17.7°)	B (36.6°)	10	40	1	628.7	47.8	25.8	3.6E-08
6	Flow rate	A(17.7°)	B(17.7°)	10	40	5	628.7	47.8	25.8	1.8E-07

7	Dissolution	A(17.7°)	B(17.7°)	10	40	1	628.7	47.8	25.8	3.6E-08
8	Wettability	A(17.7°)	B (23.8°)	10	40	1	628.7	47.8	25.8	3.6E-08
9	Wettability	A(17.7°)	B (54.2°)	10	40	1	628.7	47.8	25.8	3.6E-08

4.3 Results

4.3.1 Fluid saturation results via electrical resistivity tomography

Figure 4.4 presents the experimental result of CO_2 saturation evolution in the column as a function of time for one experiment (Exp.#4) using the electrical resistivity tomography system. For simplicity, only the drainage stage is shown here but the imbibition stage follows a similar progression. The six curves correspond to CO_2 saturation in each segment of the column, presented in order from bottom to top of the column. The vertical distance labels associated with each line correspond to the distance between the interface and the midpoint of each segment. The gray circles denote saturation points, which are identified as the point that the CO_2 phase reaches a steady state in a given segment and the saturation is stabilized.

At the start of each experiment, saturation values for all sections were close to zero. After approximately 5 minutes, the CO_2 plume entered the lower sand section from the glass beads. Then CO_2 percolated into the next sections at a rate faster than the injection rate as a result of both advective and buoyant forces. This suggested that fingers and preferential flow pathways were forming, as previously reported in studies of CO_2 flow through rock cores [*Pini et al.*, 2012; *Plampin et al.*, 2014a]. The CO_2 plume entered the top of the lower sand segments after approximately 10 minutes. Here, the CO_2 plume was stopped by the stratigraphic heterogeneity where it began to accumulate in the section beneath the interface. The CO_2 plume then started to accumulate downward through the lower sand sections. This effect was clearly visible in the 3 sections closest to the interface. As this occurred, CO_2 became a more connected phase and

therefore its vertical extension grew from the top down when the upper sections are near their maximum saturation. Eventually, the capillary entry pressure into the overlying formation was overcome and the CO_2 entered the overlying segment. In the experiment presented in Figure 4.4, this occurred after approximately 40 minutes.

After steady state saturation was established, imbibition was carried out in each experiment. Brine was injected from the same port at the same flow rate used in the drainage stage. This process typically took 2-4 hours (more than 10 pore volumes) before a steady state residual saturation was achieved. The raw saturation data of imbibition were processed in the same manner as those of drainage, and steady state saturations were identified and used in the next sections, to analyze low-contrast stratigraphic and residual trapping.

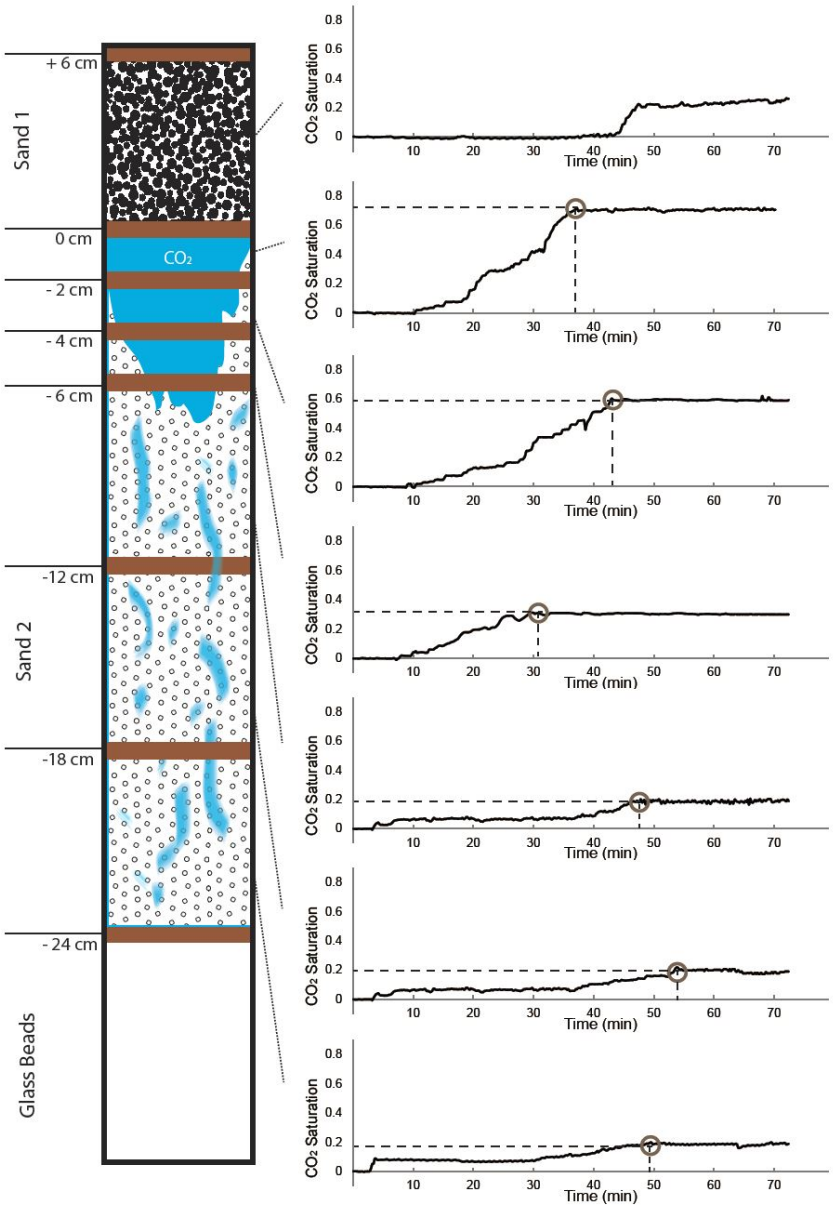

Figure 4.4. Schematic of electrical resistivity probes with a qualitative representation of CO_2 phase distribution in the column (left), and the time-lapse CO_2-saturation data for the drainage stage in Exp.#4 (right). Saturation point (in gray circle) are identified as the plume reaches steady state saturation in a given section.

4.3.2 Permeability, pressure, and temperature effects

Figure 4.5 presents the saturation profiles of low-contrast stratigraphic trapping (left) and residual trapping (right) for all experiments. Saturation data is plotted on the x-axis and the vertical distance from the interface is plotted on the y-axis. Physically this distance extends downward into the lower sand-pack that the CO_2 plume moves through as it approaches the capillary boundary. The error bars represent 95% confidence interval calculated from two replicate experiments of each condition. The stratigraphic trapping was taken as the initial saturation measurements during the CO_2 injection (drainage) stage when saturation reaches steady state, and residual saturation measurements are taken after brine injection (imbibition) reaches equilibrium. The results from the reference condition (Exp.#1) are presented on the top row (4.5.1.1 and 4.5.1.2) and then also (without error bars) in the other plots for comparison.

All experiments show that the interface between sand layers results in a capillary dominant region where higher initial and residual saturation of CO_2 is observed [*Silin et al.*, 2008]. After imbibition, the CO_2 saturation in this region is still significantly higher than in those regions far from the interface. This is consistent with recent work reported by Pini et al. [2012] and *Trevisan et al.* [2015], and highlights the importance of understanding the role that heterogeneities on the millimeter to centimeter scale can have on predicting transport and storage on much larger scales (meters and kilometers).

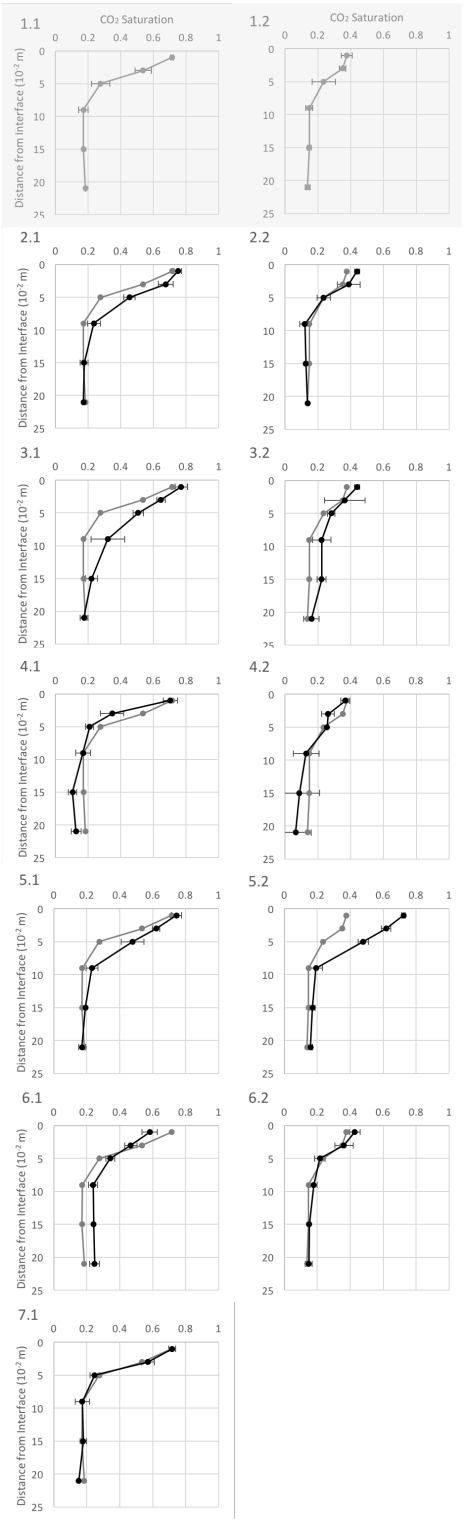

Figure 4.5. Initial (left) and residual (right) saturation profiles for (Exp.#1) reference condition (in gray); (Exp.#2) permeability; (Exp.#3) temperature; (Exp.#4) pressure; (Exp.#5)

wettability alteration; (Exp.#6) flow rate; and (Exp.#7) dissolution. The row numbers in this plot correspond to the experiment numbers. The curves from Exp.#1 (reference case) are also presented in all other plots for comparison.

The results in Figure 4.5.2.1 and 4.5.2.2 (Exp.#2) show that the permeability contrast between the sands does influence the extent of stratigraphic and residual trapping. This increase in the permeability contrast between Exp.#1 and #2 increases in the degree of CO_2 saturation beneath the interface. It affects stratigraphic trapping (24.4% increase) more so than residual trapping (6.4% increase), and most of the difference is concentrated immediately below the interface. Higher contrasts in permeability, and the resulting heterogeneity of capillary pressure, play an important role in stabilizing injected CO_2 plumes in target repositories. The permeability contrast between a sandstone and a shaley caprock, for example, can exceed 5 orders of magnitude [*Nordbotten et al.*, 2009]. These results suggest that much more modest contrasts could play some role in mechanical stabilization of a CO_2 plume [*Plampin et al.*, 2014b]. Even though the percent of CO_2 that is trapped following imbibition is <10%, this effect could be significant given that a rising plume of CO_2 is likely to encounter a large number of these types of horizons as it rises to the surface.

The results in Figure 4.5.3 and 4.5.4 (Exp.#3 and #4) reveal the role of fluid phase properties on CO_2 transport. CO_2 fluid properties vary significantly with geothermal and hydrostatic pressure gradients, impacting fluid density and interfacial tension, which influences the force balance between the two fluids. Figure 4.5.3 shows how lower temperatures impact saturation. Lower temperatures result in a phase change from supercritical CO_2 to liquid CO_2 and a corresponding increase in density from 628 kg/m^3 to 856 kg/m^3. This leads to a decrease in the

difference between CO_2 and brine density, which lowers the buoyancy force. This, in turn, will increase CO_2 trapping two ways: first, it requires a larger plume of CO_2 to overcome the capillary pressure and second, buoyant forces are overcome by capillary force which enhances capillary fingering [*Rostami et al., 2010; Suekane et al., 2015*]. Some of the CO_2 remains trapped in the higher permeability region beneath the interface even after the column is flushed with brine, suggesting that the rate of residual trapping would increase initially as CO_2 migrates toward the surface.

Pressure and temperature are coupled and increase monotonically in the subsurface but their effect on CO_2 fluid properties is nonlinear. Figure 4.5.4 presents the effect of pressure on trapping beneath the capillary interface. In these experiments, a decrease in pressure from 10 to 8 MPa elicited a density decrease from 628 kg/m^3 to 278 kg/m^3. At both pressures, the CO_2 is a supercritical fluid but the density contrast between the CO_2 and brine in Exp.#4 is nearly double to that of Exp.#1. This results in less CO_2 capillary trapping at the interface as represented by the modest but statistically significant difference between the results in Exp.#1 and #4. This trend is most pronounced after the imbibition phase wherein the low-pressure experimental case has higher residual saturation than in the reference case. Given that geothermal and hydrostatic pressure profiles vary from site to site, weighing these effects in conjunction with the sub-basins scale structure of overlying formations will be an important process in assessing the relative risk of leakage from different target repositories.

4.3.3 Wettability effects and residual trapping

Figure 4.5.5 shows the results of mixed wet experiments (Exp.#5), in which 20% of the sand in the lower section of the column is treated with benzoic acid to mimic more hydrophobic, mixed wet conditions. The contact angle between water and CO_2 on the treated sand was measured to be 77.5˚, and at a mix ratio of 20/80, it is equivalent to a ~16% change in cos (θ) from the original untreated sand. This increase in contact angle resulted in a substantial increase in the total initial saturation though the most dramatic effect associated with wettability alteration was on residual saturation. After brine imbibition, the residual trapping was considerably higher (93% higher in the first three sections) in Exp.#5 than that in Exp.#1.

Figure 4.6 helps illustrate the impact that these wettability shifts have on initial non-wetting phase saturation ($S_{nw,i}$) vs. residual saturation ($S_{nw,r}$) results for CO_2 and brine. These type of data have been reported for a range of rock types under different conditions [*Pentland et al.*, 2011; *Iglauer et al.*, 2012; *Tanino and Blunt*, 2012; *El-Maghraby and Blunt*, 2013; *Al-menhali et al.*, 2015]. *Pentland et al.* [2011] collected data for CO_2 flooding experiments using Berea sandstone, and these results are included as a benchmark. The no production line, which corresponds to the 100% trapping unit slope ($S_{nw,i} = S_{nw,r}$) is also plotted as a dashed line in these figures. Because the saturation decreases with distance from the interface and in order to compare our results to those of other published studies we averaged the initial and residual saturation values in the first three sections (6 cm) from the capillary interface. Below that, the interface had a less pronounced impact on CO_2 saturation under the conditions tested here.

The results for Exp.#1-4 are shown in Figure 4.6a. These results fall between the no production line and the results of *Pentland et al.* [2011]. The higher residual saturation for our results could be attributed to the presence of the heterogeneity in the sand pack or to the larger pore size in our sands, which leads to a smaller capillary pressure. Much of the high initial saturation in our experiments is created by the entry pressure of the overlying capillary barrier, so there is a less pronounced effect of advection-driven flow during the imbibition stage, which leads to the formation of preferential flow pathway. This is consistent with the findings in core scale imaging experiments that residual saturation tends to increase at high flow rates, where preferential water flow pathways are more predominant [*Chaudhary et al.*, 2013, *Herring et al.,* 2016].

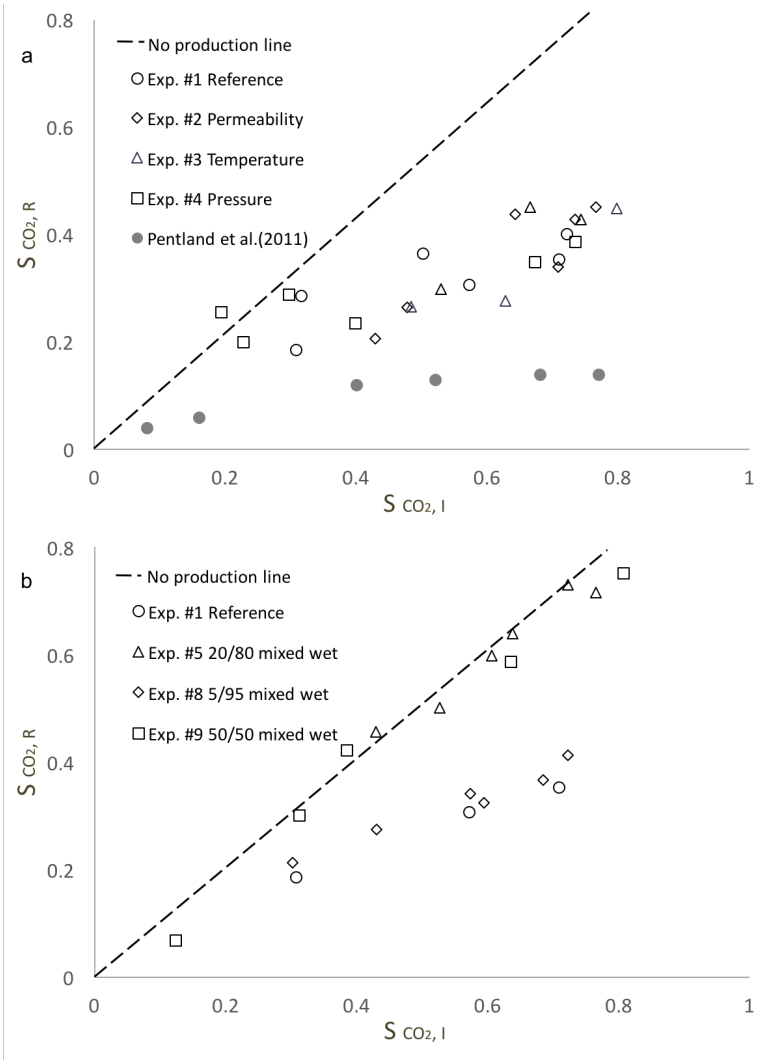

Figure 4.6. Residual vs initial saturation data in this study compared to previous results and empirical models. (a) Data from this study (Exp.#1 to Exp #5) compared with data obtained by Pentland [*Pentland et al.*, 2011], (b) Results from Exp.#1 (water wet), Exp.#5 (20/80 mixed wet), and two additional wettability experiments: Exp.#8 (5/95 mixed wet) and Exp.#9 (50/50 mixed wet). The dotted line presents the no production line, which corresponds to the 100% trapping unit slope ($S_{nw,i} = S_{nw,r}$).

Figure 4.6b shows that even a small amount of wettability contrast results in a large increase in residual trapping. This plot shows three blends of treated and untreated sand formulated to simulate increasing degrees of mixed wet conditions. A 5% by volume blend of treated sand, results in a residual saturation curve that was slightly higher than the baseline untreated sand. A blend that includes 20% by volume of treated sand produces dramatic increases in residual saturation, approaching the no production line. A 50% blend did not incite further increases in residual saturation. This suggests that the impact of wettability increases dramatically between 5-20% treated sand and that the maximum amount it will affect trapping exists within that range as well. These results reveal a non-linear effect of different mix ratio on residual trapping, which could be a significant factor in thinking about how mixed wet reservoir conditions would impact CO_2 trapping [*Al-menhali and Krevor*, 2016].

3.3.4 Flow rate and dissolution effects

The results presented in Figure 4.5.6 and Figure 4.5.7 suggest that flow rate and dissolution do not have a clear effect on steady state saturation relative to the reference condition (Exp.#1). During leakage events, a wide range of CO_2 flow rates could develop, with the corresponding capillary number varying eight orders of magnitude (from 10^{-10} to 10^{-2}) [*Cottin et al.*, 2010; *Zhang et al.*, 2011]. In addition, mass transfer is likely to occur across the phase boundary between CO_2 and brine. These parameters have been shown previously to have an impact on wettability hysteresis and contact line pinning, among other factors [*Wang et al.*, 2013a]. Even though at the temporal and spatial scales assessed here this mass transfer between phases did not have a pronounced impact on CO_2 transport, there was a time transient relationship between these

parameters and CO_2 saturation indicating that under some leakage regimes these parameters could be important.

The dynamics of the CO_2 pooling beneath the capillary boundary are explored in more detail in Figure 4.7, which shows the evolution of CO_2 saturation profile for Exp.#1 (1 ml/min, corresponding to a capillary number of 3.6×10^{-8}) and Exp.#6 (5 ml/min, corresponding to a capillary number of 1.8×10^{-7}). The lines represent the CO_2 saturation within the column at different time steps in the experiment quantified in terms of pore volumes (pv) of CO_2 injected into the column. Pore volume is calculated in terms of the overall pore space in the lower region of the column. The profile before breakthrough are shown in solid lines in gray scale. The black lines represent the saturation curve at CO_2 breakthrough. The colored lines represent the saturation after breakthrough. In general, the results show that higher flow rates lead to faster break through. Under the conditions tested here, it takes 0.16 pore volumes to achieve break through as compared to 0.28 pore volume for the low flow condition. In addition, the relative time required to reach steady saturation is also dependent on flow rate. In Exp.#1, the CO_2 plume reaches steady state saturation after approximately 0.3 pore volumes of injection, whereas it takes 0.8 pore volumes in the high flow rate case.

When CO_2 flow rate is low, the saturation in the lower region of the column reaches steady state at approximately the same time that the CO_2 plume breaks into the overlying fine layer. At higher flow rates, the saturation of the underlying sections occurs after the CO_2 has broken through into the overlying sand layer. This behavior suggests that the balance between capillary, gravity and viscous forces is very sensitive to advective forces in the fluid flow. As shown in previous

experiments [*Ennis-King and Paterson*, 2005; *Polak et al.*, 2011], advection forces (viscous forces) would be more pronounced under the high flow rate conditions, and consequently there is less opportunity for lateral mixing of the CO_2 across the width of the column. After breakthrough, it took longer for the sand beneath the interface to become saturated because of preferential flow paths into the overlying layer of sand. This behavior can also be interpreted by a dynamic capillary pressure behavior [*Hassanzadeh et al.*, 2007] wherein the advective force is the dominant driving force over buoyancy and capillary force. In the real world situation, this characteristic indicates that under some transient high flow conditions, where capillary numbers would be expected to be very high, these sub-basin scale heterogeneities may not reach their full potential for capillary trapping.

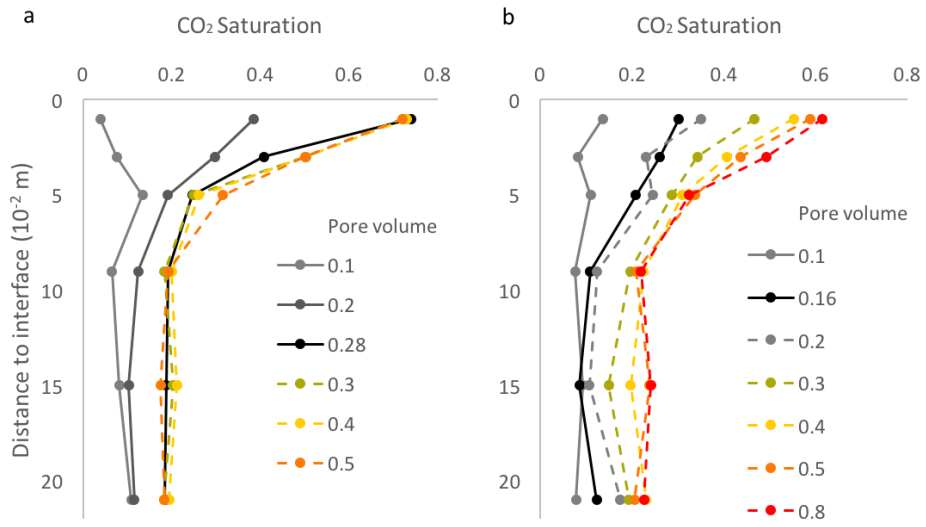

Figure 4.7. The CO_2 saturation profile during drainage at different pore volumes for (a) Exp.#1 and (b) Exp.#6.

4.4 Discussion

4.4.1 Comparison between factors and field relevance

Table 4.2 presents the different parameters evaluated here along with the ratio that was tested in our experiments and a comparison between our experiment values and those expected in the field. Data of permeability contrast was from core-logs of the Mount Simon in Michigan, USA, which has been identified as an attractive target formation for GCS. Pressure and temperature ranges reported here cover the range of geothermal and pressure gradients that can be expected in target formation [*Benson and Cole*, 2008]. The flow rate range was adopted from the literature [*Ross and Bustin*, 2009; *Pollak et al.*, 2013] to represent the values that would be expected during leakage events. Contact angle values were collected from recent studies reporting on the wettability of minerals representative of rocks in carbon sequestration reservoirs [*Iglauer et al.*, 2015]. The last two columns, quantify the results shown in Figure 4.5.

While some parameters tested here cover a wide range of the contrasts that could be expected in the field (e.g., temperature and wettability), others do not (e.g., permeability). Efforts to provide a more uniform comparison were limited by experimental conditions in the column, but the results do nevertheless fill experimental gaps in the literature where pressure/temperature and interfacial effects are concerned, and provide side-by-side comparisons that could support mechanistic interpretation of these transport processes. Notably, this framing puts into perspective the important role wettability contrast could have on attenuating CO_2 leakage.

Table 4.2. Summary of experimental results and conditions relative to the realistic range it covers.

Experimental factor	Independent variable change	Expected range in subsurface	Coverage percentage	% change in trapping * (initial)	% change in trapping * (residual)
Permeability contrast	Sieve #80-60 Sieve #80-35	1 1×10^5	0.0018%	+ 23% ± 7%	+ 10% ± 8%
Pressure	10 MPa 8 MPa	10 MPa 0.1MPa	0.25%	- 18% ± 9%	- 27% ± 35%
Temperature	313 K 293 K	350 K 280 K	28%	+ 26% ± 6%	+ 12% ± 13%
Capillary Number	3.6×10^{-8} 1.8×10^{-7}	1×10^{-9} 1×10^{-6}	0.5%	+ 2% ± 2%	+ 21% ± 12%
Wettability cos (θ)	0.95 0.81	1 -0.26	12%	+ 21% ± 8%	+ 93% ±7%

* relative to the reference condition.

4.4.2 Empirical models for residual trapping

Figure 4.8 shows the relationship between residual and initial saturation from the experimental data and two empirical models developed by Spiteri et al. and Land et al. [*Land*, 1968; *Spiteri et al.*, 2008]. Both of them were originally developed for an oil/water system but have also been applied to CO_2/brine systems [*Krevor et al.*, 2012; *Wang and Tokunaga*, 2015]. The Spiteri equation expresses the residual non-wetting phase saturation, $S_{nw,r}$ as a second order polynomial function of the initial non-wetting phase saturation, $S_{nw,i}$; whereas Land expresses the relationship as a multiplicative inverse function between the two. The equations are shown below:

$$S_{nw,r} = A \cdot S_{nw,i} - B \cdot S_{nw,i}^2$$

$$S_{nw,r} = \frac{S_{nw,i}}{1 + C \cdot S_{nw,i}}$$

where A, B and C are empirical coefficients.

To fit data from Exp.# 1-4 and #5, coefficients were calculated and included in Figure 4.8. When compared to other database [*Pentland et al.*, 2011; *Al-Menhali et al.*, 2015; *Trevisan et al.*, 2015], the fitting curve for our data from Exp.#1-4 produces a smaller coefficient C in Land's model, and a larger coefficient B in the Spiteri model. This means that our system has slightly higher residual trapping, which could be influenced by the high permeability in the sand pack. The capillary entry pressures in these two systems differ by two orders of magnitude, with values usually greater than 10,000 Pa for typical sandstones [*Plug and Bruining*, 2007] versus 100s of Pa for sand packs with pore diameters on the scale of 10s of um [*Tokunaga et al.*, 2013]. As previously noted by *Krevor et al.* [2011], the fitting coefficient C in Land's model decreases (e.g., trapping efficiency increases) as the permeability of the porous medium increases in core-flooding experiments. It should be noted that the data reported by *Trevisan et al.* [2015] could be influenced by the large number of data points that are clustered in the low saturation region.

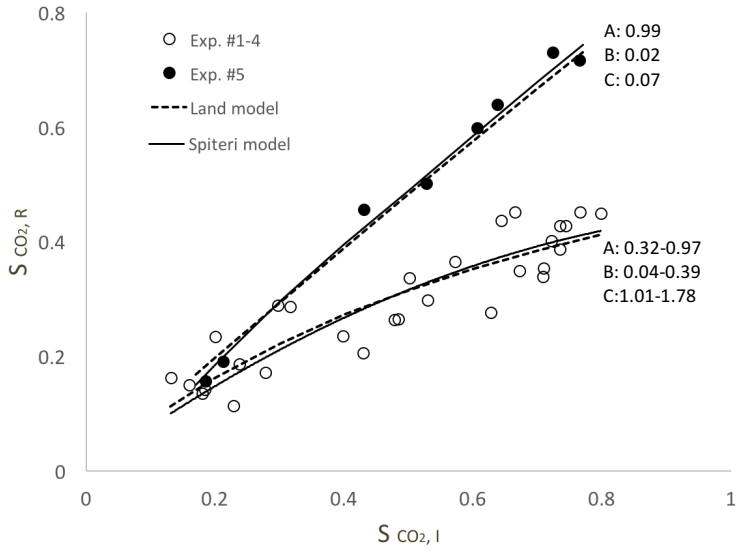

Figure 4.8. The correlation between residual and initial saturation for Exp.#5 and Exp.#1-4, fitted by Land and Spiteri models [*Spiteri et al.*, 2008].

The results for Exp.#5 are plotted separately in Figure 4.8, to highlight how different the behavior was in this experiment. The strong effect that mixed wet conditions had on residual trapping is likely caused by the increase in affinity on a molecular level between CO_2 and the treated sand surface, which could contribute to adhesion that traps CO_2 during the imbibition process. A few data points from the mixed wet condition are higher than the no production line, suggesting that CO_2 was being redistributed in the sand pack rather than being displaced by the imbibing brine. The mobile CO_2 was able to connect with more stable or larger CO_2 ganglion in regions of the sand pack with a more CO_2-philic surface [*Wang et al.*, 2013d; *Zhao et al.*, 2013]. This same process would likely work in reverse, creating preferential flow paths for water through the mixed wet porous medium [*Hu et al.*, 2014], to by-pass the CO_2 ganglia and leave a high residual trapping.

4.4.3 Underlying mechanisms for wettability effect

Even though the role of wettability on capillary phenomenon and residual trapping has been the subject of considerable experimental attention, there is still a great deal of uncertainty surrounding the topic [*Agbalaka et al.*, 2008; *Mohammed and Babadagli*, 2015; Krevor et al., 2015]. This problem has been studied for many years in the context of oil recovery [*Anderson*, 1987a, 1987b], where a larger wettability contrast is generally thought to increase the influence of capillary forces, and therefore leads to more residual trapping. For the CO_2/brine system, efforts on pore-scale observations and core scale measurements have reported that more water-wet media leads to more residual trapping, due to the prevalence of snap-off mechanism [*Pentland et al.*, 2011; *Tanino and Blunt*, 2012; Krevor et al., 2015; Herring et al., 2016].

Recent work on the CO_2/brine system [Wang and Tokunaga, 2015; Wang et al., 2016], however, suggests that residual trapping is enhanced when the porous medium turns more CO_2-wet. The authors suggested a hysteretic effect caused by exposure to CO_2 under reservoir conditions. These are analogous to the "aging" processes observed in oil and gas reservoirs, where amphiphilic species within the hydrocarbons change the wettability of hydrophilic mineral species over time. The mechanisms of rock aging in contact with CO_2 are still poorly understood and the effect on contact angles to elicit the significant impacts seen in hydrocarbon reservoirs need to be explored on a molecular level in more detail.

The significant role that modest wettability contrasts had on residual saturation in this study extend our understanding of these processes in a few important ways. First, our results generally support the recent conclusions that more mixed wet media will have a higher residual trapping of

CO_2. Second, it is the first time to report that this effect starts to show at a low mix wet conditions and reaches a high degree at an intermediate mixed wet condition. In rocks with mixed wet horizons and lenses through it, even subtle contrasts can elicit big effects on residual trapping. Third, this effect is not liner and has a upper limit, e.g. a threshold after which more mixed-wetting does not impact residual trapping much. These new findings could be important for modeling reservoirs with varying degrees of wettability contrasts, such as depleted oil and gas fields.

4.5 Conclusions

Sand-packed column experiments were carried out to understand the role that low-contrast stratigraphic horizons might have on the transport of dense phase CO_2 under GCS reservoir conditions. The experiments were intended to help provide a new experimental perspective on the role that sub-basin scale heterogeneities in porous formations could have on mitigating vertical transport of CO_2 and to complement recent studies carried out in rock cores [*Al-Menhali et al.*, 2015] or using surrogate fluids [*Trevisan et al.*, 2014, 2015]. The intermediate scale of these experiments is crucial to upscale the fundamental understanding of conditions influencing trapping.

Our results corroborate previous findings that these horizons result in low-contrast stratigraphic trapping and increase in residual saturation of the porous media beneath the interface. As a CO_2 plume rises through the lower sand pack it accumulates under the capillary barrier and becomes a connected phase that grows vertically into the lower portions of the column until the capillary entry pressure of the overlying layer is overcome. Of the experimental conditions tested here, the residual saturation is most sensitive to contrasts in wettability. Even though wettability has been studied extensively in the GCS context over the past five years, its impact on mesoscale

fluid dynamics has not been fully explored and these experiments help provide a better understanding of these processes. The wettability contrast has a particularly pronounced effect on residual trapping, suggesting that mixed-wet horizons, even with high permeability, could play an important role in attenuating vertical transport of CO_2. Temperature and pressure conditions in the column were also found to have an important effect as they impact the fluid phase properties of the dense CO_2. These results were consistent across a range of flow rates, though the effect was most pronounced under the lower flow rate conditions that would characterize most leakage events from target repositories in a geologic carbon sequestration context.

Chapter 5

Upscaling Can Provide Insight into the Role of Interfacial Processes on CO_2 Fate and Transport in Geologic Storage

To understand the effect that wettability, roughness, and interaction effects could have on the basin scale, where they will impact the technological viability of geologic carbon storage, it is necessary to scale the work reported in capillaries or columns in the previous two chapters to larger spatial and temporal scales. This chapter performs that upscaling by looking at a variety of specific wettability and roughness trends that we observed in experiments supporting previous work and considers the aggregate impact they would have on fluid fate and transport in heterogeneous porous media. Additional experiments are carried out using mercury intrusion porosimetry (MIP) to characterize the pore structure in synthetic porous media and the interplay that interfaces might have on residual trapping and capillary entry pressure in these 'rocks'. These experimental results collected at the bench scale (microns to meters) were then used to predict behavior at the meso-scale (meters to kilometers) using the TOUGH2 code.

5.1 Introduction

Interfacial properties at the CO_2-brine-rock interface directly impact large-scale flow characteristics in porous media such as capillary pressure, relative permeability and residual saturation [*Bachu and Brant Bennion*, 2009]. The connection between these micro-scale chemical characteristics of a fluid-rock system and this large scale behavior are generally described only in the broadest terms in the literature. For example, there is evidence that CO_2-wet rocks would have lower stratigraphic [*Chiquet et al.*, 2007; *Iglauer et al.*, 2015a, 2015b] and capillary trapping [*Chaudhary et al.*, 2013; *Al-Menhali et al.*, 2015; *Rahman et al.*, 2016] capacities and would therefore be less suitable for GCS but more nuanced connections are difficult to establish. The purpose of this chapter is to help elucidate that connection. The following section provides a review of the existing literature.

5.1.1 Contact angle in CO_2/water/rock system – knowledge and uncertainties

Over the past decade, a number of studies have reported on the contact angle measurement of CO_2 sequestration conditions [*Bikkina*, 2011; *Kim et al.*, 2012; *Saraji et al.*, 2013, 2014]. Contact angle is a measure of the balance between the interfacial tension between the fluid-solid and the two fluids in the system. These interfacial tensions are sensitive to pressure and temperature conditions as well as the chemistry of the solid surface, which generally contains different functional groups and is therefore subject to changes in the adjacent fluid phase [*Quéré*, 2008b].

Most experimental studies to date suggest that contact angle is positively correlated with pressure especially across the critical point where CO_2 changes phase [*Saraji et al.*, 2013; *Wang*

et al., 2013b]. These studies also suggest that contact angle has a slightly negative or no correlation with temperature [*Broseta et al.*, 2012; *Shojai Kaveh et al.*, 2012]. The impact of pressure and temperature is likely indirect as the pH of the brine phase, solubility and partial pressure of CO_2 are all impacted by these state variables and these could be driving the impact on wettability [*Saraji et al.*, 2014; *Iglauer et al.*, 2015b].

The literature is inconclusive on the role that dissolved species in the aqueous phase play in controlling wettability [*Palamara et al.*, 2015]. A number of studies report that dissolved ions impact the interfacial tension between fluids [*Espinoza and Santamarina*, 2010; *Farokhpoor et al.*, 2013; *Saraji et al.*, 2014] while others report little to no effect in higher ionic strength solutions [*Broseta et al.*, 2012]. Recent work suggests a positive linear correlation between the concentration of amorphous silica on a surface and contact angle, though there are both acid/base aspects and roughness aspects to that report [*Jung and Wan*, 2012] that are a function of the underlying mineral surface chemistry. Separate work showed that surfaces with charged functional groups are sensitive to the pH of the solution and so contact angle will vary as a function of the pH point of zero charge for a given mineral surface [*Wang et al.*, 2013b].

The previous work points to the sensitivity that these systems could have to ionic strength in solution and this matters because there is growing evidence [*Kharaka et al.*, 2009; *Allred et al.*, 2017] that salinity at existing GCS sites is higher than previously expected. For example, estimates suggest that in the Frio formation, a regional aquifer in the US Gulf Coast that is of interest for GCS, salt concentrations ranges from 7g/L to 340 g/L [*Doughty et al.*, 2008; *Kharaka et al.*, 2009], which corresponds to an NaCl concentration up to 5.8 mol/L. Most of the experimental studies to

date only cover the range up to 1 mol/L, with a few papers reporting concentrations up to 2 mol/L [*Jung and Wan*, 2012; *Saraji et al.*, 2014]. The composition of dissolved species in the connate brines of these reservoirs is complex and varies from site to site. Up to 30% of the cations could be Ca^{2+} or other divalent ions, most studies use NaCl solution as surrogate brine solution. One of the few papers to consider more complex mixtures of ionic species showed that wettability was strongly correlated with both the concentration and the composition of the salt [*Wang et al.*, 2013b]. To date, few studies have looked at interaction effects between ions and the effect this could have on wettability.

As discussed in earlier chapters, the concentration and composition of the salt matrix in GCS brines impacts interfacial properties in a few ways. Of the three interfacial tension values in Young's equation, γ_{SL} (between solid and liquid) and γ_{SG} (between solid and CO_2) are not directly measurable, which is why contact angle has to be experimentally determined, but the brine-CO_2 interfacial tension, γ_{LG}, has been extensively studied experimentally [*Chalbaud et al.*, 2009; *Georgiadis et al.*, 2010] and using simulations [*Nielsen et al.*, 2012; *McCaughan et al.*, 2013].

$$\cos(\theta) = \frac{\gamma_{SL} - \gamma_{SG}}{\gamma_{LG}}$$

Available data revealed that, γ_{LG} is within the range of 25 to 40 mN/m in most conditions relevant to GCS, and increases around 2~3 mN/m per unit of molar charge on average [*Bachu and Brant Bennion*, 2009; *Chalbaud et al.*, 2009; *Li et al.*, 2012]. This behavior is attributed to the decrease in CO_2 solubility in brine at higher salinities [*Saraji et al.*, 2013], and to the hydration of ions that leads to an ion-free layer at the water interface [*Bachu and Brant Bennion*, 2009]. A

comprehensive study also compared the effect that ion chemistry on impacting interfacial energy, with divalent cations generally having a larger impact than monovalent ions with common ions impacting interfacial tension in the order Mg^{2+}>Ca^{2+}>Na^{+}>K^{+} [*Aggelopoulos et al.*, 2010]. In many GCS contexts, where precipitation/dissolution conditions prevail, this relationship between aqueous phase composition and wettability can be important for understanding the effect that chemical reactions could have on physical transport.

5.1.2 The role of organic materials

Recent studies have begun to explore the role that organics could play on wettability in a GCS context. A number of solid organic species such as kerogen or bitumen can exist on the rock surface in certain types of formations (e.g., depleted oil and gas fields, shales) and dissolved organic species such as carboxylic acids can exist in a wider range of formations. The range of concentrations that might be observed in connate brines varies considerably ranging from 5-10,000mg/L in different GCS target reservoirs [*Survey et al.*, 2006; *Kharaka et al.*, 2009]. These organics have the potential to impact the wettability of the of CO_2-water-rock system in three ways. First, dissolved organic ions could influence the interfacial tension between CO_2 and the aqueous phase [*Sutjiadi-Sia et al.*, 2008]. Second, these species could buffer changes in the pH that occur at high partial pressures of CO_2 or they could impact the electrical double layer balance of the water film [*Scherf et al.*, 2011]. Third, ligand functional groups in these organic species could lead to complexation reactions with other dissolved ions or charges on mineral surfaces [*Lewicki et al.*, 2007; *Miller et al.*, 2014].

The presence of solid organic species on the rock surface, such as the residual oil phases in an oil-bearing reservoir, will have important impacts on wettability. Adsorbed organic species are well known to impact wettability of solid surfaces [*Graue et al.*, 1999; *Kowalewski et al.*, 2003]. In the rock-brine-CO_2 system, there is also the potential for some of these non-polar organic molecules to partition into the CO_2 phase [*Andrew et al.*, 2014]. This opens up the potential for aging of the mineral surface in the presence of CO_2, which could have significant impacts on the potential for a rock to store CO_2 over longer time scales.

Much of what we know about the role of solid organics on CO_2 storage comes from studies of caprock chemistry. Caprocks are typically low-permeability shales, which contain 2-20% organic material by mass [*Wang et al.*, 2013d; *Iglauer et al.*, 2015b]. Several studies have confirmed that as fractures and other flow paths in shale, which are naturally CO_2-wetting, could age when exposed to CO_2, which would create leakage pathways with lower capillary entry pressures. This wettability shift is similar to the aging mechanisms that were explored in the petroleum engineering literature several decades ago [*Buckley,* 1999] where a combination of factors were reported: (1) polar interactions that predominate in the absence of a water film between oil and solid, (2) surface precipitation, dependent mainly on crude oil solvent properties with respect to the asphaltenes, (3) acid/base interactions that control surface charge at oil/water and solid/water interfaces, and (4) ion-binding or specific interactions between charged sites and higher valency ions. More recently, much of this understanding has been applied to by those seeking to use CO_2 in enhanced oil recovery operations [*Gozalpour et al.*, 2005; *Alvarado and Manrique*, 2010], and found that the impact on CO_2 as a non-wetting phase is more complex.

5.1.3 The impact on flow behavior

Despite the large amount of work that has gone into characterizing CO_2 wettability under GCS conditions, its impact on flow and sealing properties has yet to be clearly established [*Iglauer et al.*, 2015b]. Inconsistency in reported values is generally attributed to surface contamination, roughness and heterogeneity, drop size and equilibration with the aqueous phase [*Shojai Kaveh et al.*, 2012; *Ameri et al.*, 2013; *Wan et al.*, 2014; *Botto et al.*, 2017]. Efforts to measure wettability shifts [*Bikkina*, 2011; *Farokhpoor et al.*, 2013; *Mirchi et al.*, 2015] using time-steps and pressure-steps, have failed to conclude whether the alteration is due to pressure or other time-related changes. [*Bikkina*, 2011] observed a contact angle change over repeated bubbles, but the sample they used may not be representative of the typical water-wet samples, as the static contact angle range are already much higher than most observations. Also, it was found that wettability alteration could be more pronounced on mica than quartz [*Chiquet et al.*, 2007; *Wan et al.*, 2014] which makes comparing across studies a challenge.

Most real rocks exhibit some form of mixed wettability state where the pore surfaces exhibit heterogeneous wettability. Core studies of these kinds of rocks reveal lower Sr values and non-monotone dependence on Si [*Pini et al.*, 2012; *Tanino and Blunt*, 2012], and some report lower Pc than calculated from pore throat sizes [*Plug and Bruining*, 2007; *Tokunaga et al.*, 2013; *Wang and Tokunaga*, 2015], both of which suggest that the rocks might be mixed-wet, or intermediate-wet with regard to CO_2. These observations are consistent with work carried out in micro-models where initially strong water-wet surfaces becoming less water-wet after exposure to CO_2 [*Iglauer et al.*, 2012; *Kim et al.*, 2013].

To date, the non-linear dependency of capillary pressure and relative permeability on saturation is not captured in most of the flow models. Part of the reason is a lack of experimental data to define the underlying processes, and these parameters also relate to each other by various underlying mechanisms that haven't been fully understood [*Celia et al.*, 2015]. Most models use a capillary pressure-saturation curve derived from one experimental measurement, sometimes from analogue fluid, and some scaling factors. This greatly overlooked the possible spatial heterogeneity of the field, in terms of both rock physical properties, and the fluid properties. Also, despite the aforementioned complexity in interfacial processes, contact angle is often assumed to be zero for the wetting phase, which could also introduce a significant source of error.

To fill in these knowledge gaps, integrated experimental and modeling work is carried out, to understand the complexities of interfacial processes and their impact the technological viability of geologic carbon storage. We start with investigating a variety of specific wettability and roughness trends in real pressure and temperature conditions, including the effects of solution chemistry, organic partitioning, and coupling with surface roughness. Then, experiments are carried out using mercury intrusion porosimetry (MIP) to characterize the capillary pressure-saturation relationship in synthetic porous media, and the interplay that interfaces might have on. These experimental results collected at the bench scale (microns to meters) were then used to predict behavior at the meso-scale (meters to kilometers) using the TOUGH2 code.

5.2 Methods and materials

5.2.1 Contact angle measurement on surfaces with different composition and roughness

The contact angle between CO_2-brine-mineral was measured in a custom-built high-pressure chamber, with two sapphire windows on both sides. A sample is placed on a Teflon holder, which sits inside the chamber. CO_2 is delivered from the bottom of the cell via a high-pressure tubing from a HPLC pump. Both pressure and temperature measurements were recorded using a National Instruments DAQ and LabView software. Pressure was collected using a Honeywell TJE 1240891 pressure transducer with in-line amplifier and controlled using a Teledyne ISCO 500HP syringe pump. Temperature was collected using an Omega K-type thermocouple and controlled using heating tape.

The following hypotheses are tested:

1. Static contact angle could change just by over long time exposure to CO_2 (with all other conditions remain unchanged), and different rock materials behave differently.
2. The ionic strength and valence of dissolved salts have an effect on static contact angle.
3. Contact angle could be further complicated by the presence of dissolved organic species.
4. Fluid dynamics (by diffusion and advection) can impact contact angle, and time is a critical factor.

5.2.2 Capillary pressure-saturation relationship from mercury intrusion porosimetry

Mercury intrusion porosimetry (MIP) measurements were carried out in which sintered glass beads with different treatment methods applied was used as analogue porous medium. Soda-lime glass beads are selected for the simplicity to modify wettability and roughness. A sintering

process with temperature increase to 650 C followed by slow annealing was adopted from a previous study [*Wang et al.*, 2012].

Wettability alteration was achieved by oxidation with O_2 plasma, and silanization with OTS coating, and two scales of shape modification will be provided by grinding glass, to create granular particles, and etching, to create nano-textured surface. The five core samples are defined in Table 4.2 (1 reference, and 4 experiment). Mercury intrusion porosimetry (MIP) measurements are carried out on small sintered samples (~0.5 cm^3) in a Micromeritics Autopore IV (Norcorss, GA, USA). MIP is a fast and easy way to get Pc-S curves. To convert to the capillary pressure data obtained for CO_2-water system, the MIP Pc-S data will be scaled to appropriate experimental conditions based on contact angle and interfacial tension data (Leverett J function).

5.2.3 Upscaling these effects using TOUGH model

To upscale these important microscopic findings, we used TOUGH ("Transport Of Unsaturated Groundwater and Heat"), a suite of numerical codes developed at Lawrence Berkeley National Laboratory that has been widely used in simulations for CO_2 sequestration application. It contains multi-dimensional numerical models for simulating the coupled transport of water, vapor, non-condensible gas, and heat in porous and fractured media.

TOUGH was used to simulate CO_2 transport across heterogeneous layers, to compare with the experimental findings in Chapter 3. Capillary pressure-saturation curves obtained from the previous task will be used as input variables to represent physical layers of porous media with different properties. There is no analytical determination of the capillary pressure-saturation

relation, because of the irregular pore size, geometry and connectivity. Therefore, a number of empirical relationships have been derived to provide a correlation between capillary pressure and saturation, with the most well-known models developed by Brook and Corey (1964) and Van Genuchten (1980). The Van Genuchten method is used to match Pc-S curves obtained in task 4.2 and used as input for TOUGH simulation. The equations of Van Genuchten method are written as the follows:

$$P_c = P_0({S_e}^{-1/\lambda} - 1)^{1-\lambda}$$

where P_0 and λ are Van Genuchten parameters, and S_e is the effective water saturation,

$$S_e = \frac{S_w - S_{wr}}{S_{ws} - S_{wr}}$$

where S_w is water saturation, S_{ws} is the saturated water saturation (in most cases considered here, $S_{ws} = 1$), and S_{wr} is the residual water saturation.

5.3 Results and discussion

5.3.1 Static contact angle measurements

To test the hypothesis that salt solutions can impact the wettability of mineral surfaces, we measured contact angle change on a quartz surface in NaCl or $CaCl_2$ solution at various salt concentration. Those results are presented on the left hand side of Figure 5.1. The static contact angle exhibits an increase with concentration for both of the aqueous solutions, which is consistent

with most of the previously published contact angle results [*Jung and Wan*, 2012; *Saraji et al.*, 2014]. The valence of the chemical species, thought to have an important impact on wettability has a small effect if any. Higher concentrations of salt have a statistically significant impact on the contact angle of mineral surface. The effect of concentration on wettability shifts cannot be explained solely by the interfacial tension effects and does suggest that the divalent salt has a more significant relative impact on wettability. Recent work suggests that salinities in connate brines are in some instances higher than 2 M.

The right hand side of Figure 5.1 shows that dissolved organic species have a stronger impact than inorganic species at the same concentration on increasing contact angle. Interestingly, these results also suggest that there is a connection between valence in organic species and wettability as was observed for the inorganic species. Oxalate, which is a divalent anion, had a stronger impact on wettability than formate or acetate at low concentrations. Higher concentrations of oxalate could not be tested because it was solubility limited.

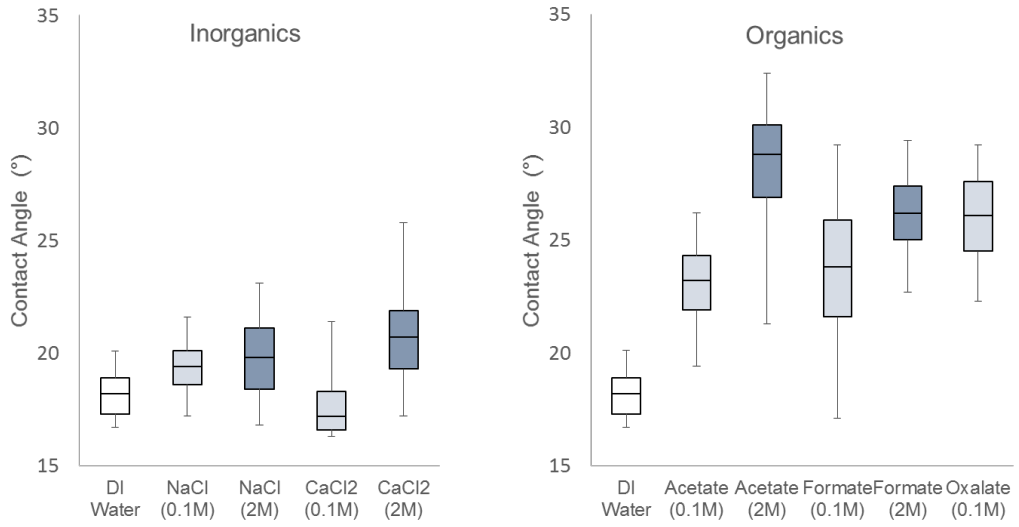

Figure 5.1. Static contact angle of CO_2/brine/quartz system with various brine chemistry: inorganic and organic effects

5.3.2 Dynamic contact angle measurements

Dynamic contact angle was measured under reservoir conditions by injecting and withdrawing a droplet from the mineral surface and measuring its contact angle as a function of size. These experiments were designed to understand the interplay between solution chemistry and the roughness of the mineral surface. The results, shown in Figure 5.3, show that on smooth surfaces, contact angle increases as a bubble shrinks and this behavior was consistent for solid surfaces in contact with DI water and with surfaces wetted by a 1M $CaCl_2$ solution. Very different behavior was observed for mineral surfaces with inherent roughness. As the bubbles shrink, (normalized diameter starts from 1 and then approaches 0.1-0.2), contact angle does not change in DI water, but increases from ~20 to ~ 50 degree in $CaCl_2$ solution. This suggests that a hysteretic stable water film many form on smoother surfaces in lower salinity conditions blocking the

evolution of the contact angle line via pinning and other processes [*Tokunaga*, 2012; *Wang et al.*, 2013a].

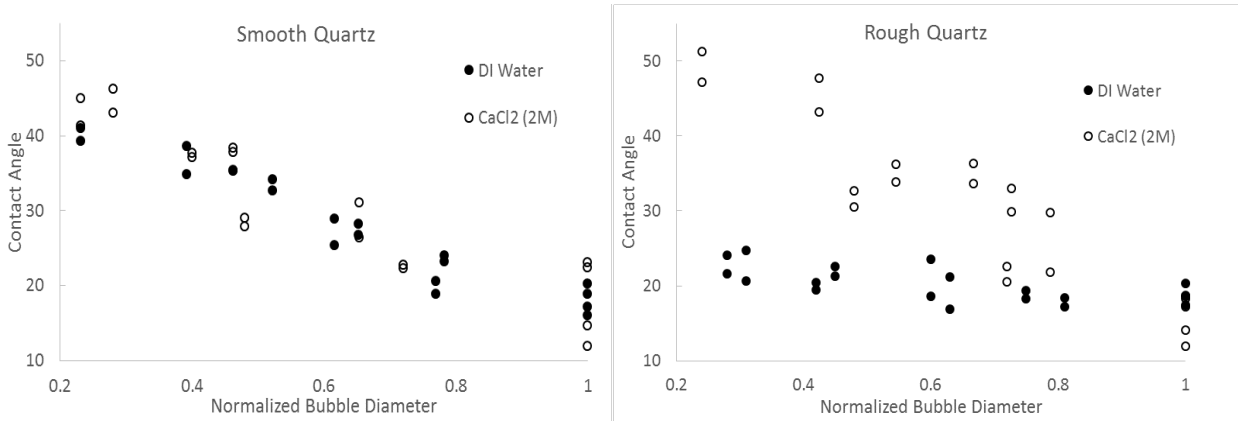

Figure 5.2. Contact angle change over time as bubble shrinks on rough quartz sample for smooth (left) and rough (right) mineral surfaces.

5.3.3 Wettability evolution

The roll of aging after prolonged exposure to CO_2 was measured and the results are presented in Figure 5.3. This plot presents static contact angle measurements for three different mineral surfaces exposed to CO_2 over the course of a seven days at 10MPa and 40º C using a 1M NaCl brine. Although the contact angle results do oscillate, there are no discernible trends in wettability shifts associated with CO_2 exposure. While other studies have suggested that mineral surfaces would have their wettability properties altered by CO_2 [*Farokhpoor et al.*, 2013; *Kaveh et al.*, 2014] I observed no difference, even for organic-rich minerals. Shale exhibits a higher average contact angle as a result of the higher organic content. This result is also consistent with other investigations [*Broseta et al.*, 2012; *Farokhpoor et al.*, 2013].

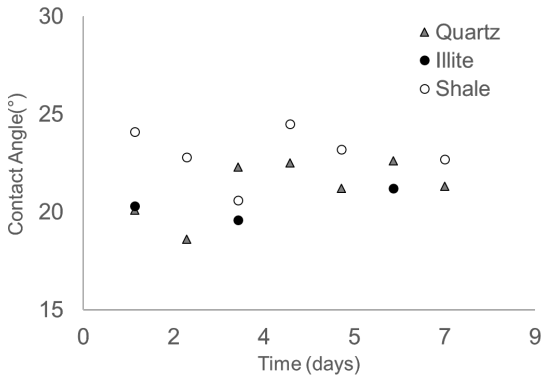

Figure 5.3. CO_2/brine contact angle over the 7-day period on three substrates: Quartz, Illite and Shale.

The results of Figure 5.3 suggest that ageing may not have a significant impact on wettability evolution on representative mineral surfaces but to better understand the impacts on hydrophobic mineral surfaces, we treated quartz surfaces with mineral oil to shift it from weakly water-wet to intermediate-wet, with contact angles ranging from 47 to 93 degrees. The sample was cleaned and aged in mineral oil, using the method developed by [Cuiec 1998] for two weeks, then put into the contact angel vessel with DI water and CO_2 under reservoir conditions. After two days of exposure to CO_2, the contact angle distribution was brought down to 35 - 64 degrees. This can be understood in terms of organic species partitioning from the solid into the CO_2 phase.

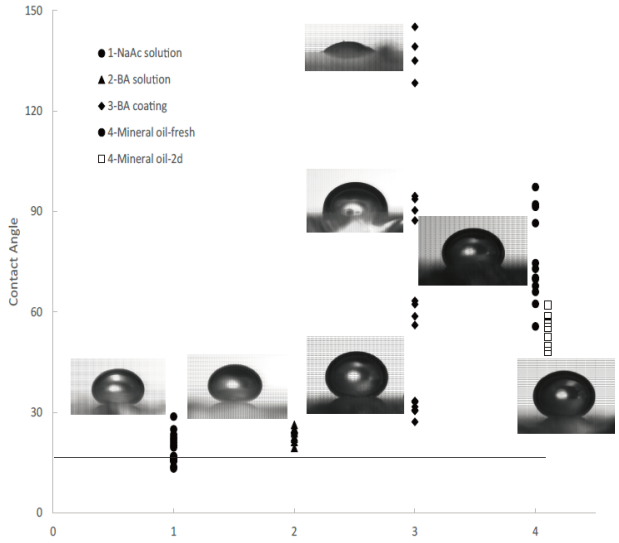

Figure 5.4. CO_2 wettability is impacted by various surface treatments: (1-3) Benzoic Acid coating used in the column study presented in Chapter 3; (4-5) the in-situ wettability restoration method developed by [Cuiec, 1998] involving Mineral oil and Toluene.

5.3.4 Putting these data into context and upscaling

To bring the wettability and roughness findings into the context of multiphase flow, we investigated their impact on the capillary pressure-saturation (Pc-S) curves, which are characteristic relationship used to describe the multiphase flow behavior in porous media. Mercury intrusion porosimetry (MIP) data was collected for a number of different synthetic rocks and then scaled to CO_2-water real fluid for modeling work.

Figure 5.5 provides the MIP results for four samples tested here all made using glass beads sintered together and then treated to create idealized porous media: untreated, different macroscale shape factor, different microscale roughness; and wettability treatment by Oxygen plasma. Untreated sample (U) and plasma treated sample (W1) have almost identical Pc-S characteristics,

suggesting that the wettability shift created by oxygen plasma is not captured in the mercury system, which is supported by theory. Comparing with untreated (U) sample, the roughness treated (R2) effectively shifted the average pore size by 5 um. As suggested by the SEM images, surface textures created by etching are less than 1 um thick, so these results indicate that roughness is a significant factor influencing Pc-S curves.

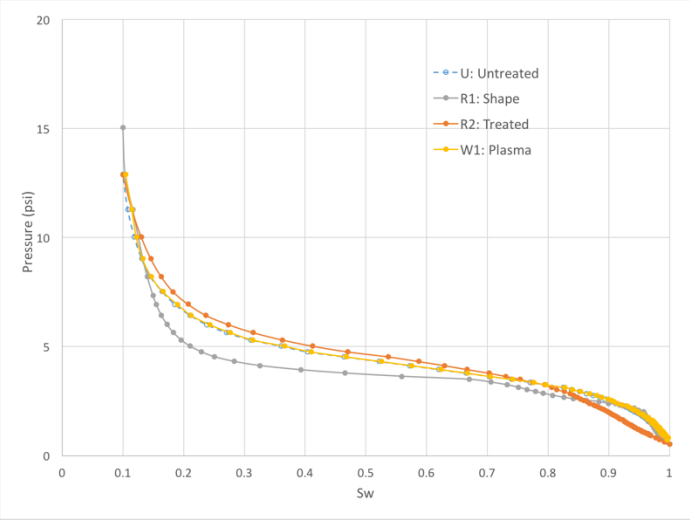

Figure 5.5. Capillary pressure - saturation (Pc-S) curve for U – untreated glass; R1- glass with different macroscale shape factor; R2 - glass with different microscale roughness; W1 – glass with wettability treatment by Oxygen plasma.

These results highlight the importance of surface roughness in controlling capillary pressure of a porous material. In Figure 5.6, the Pc-S curve for roughened porous media was scaled to match the untreated sample, resulting a contact angle change from 140 degrees to 144.5 degrees, with the Leverett J-function written as:

$$J(S_w) = \frac{1}{\sigma cos\theta}\sqrt{\frac{K}{\emptyset}}P_c(S_w)$$

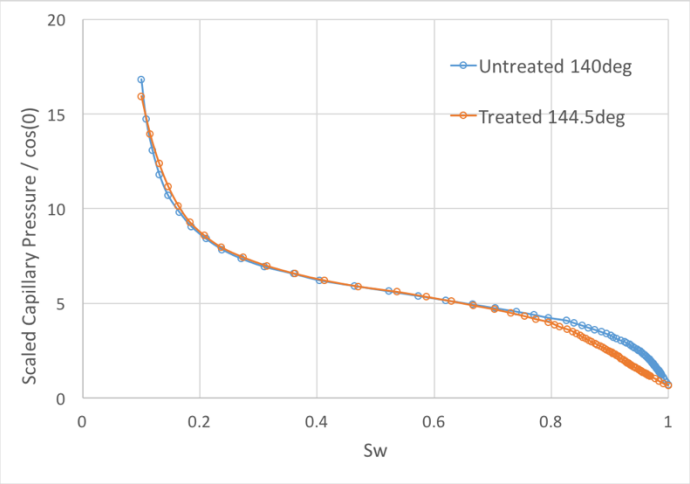

Figure 5.6. Capillary pressure - saturation (Pc-S) curve scaled by Leverett J-function.

The J-function is a characteristic function for a given porous material, from which we scale Pc from measures of interfacial tension and contact angle to high-pressure CO_2-water-rock system. This relationship allows us to further explore sensitivity for these chemical wettability and surface roughness. Most multiphase flow models to date does not take the effect of roughness into account when applying Pc-S curves, which could significantly misrepresent this important behavior.

5.3.5 Upscaling these effects using a continuum-scale model

Pc-S data collected from MIP are scaled using Leverett J-function, and then parameterized using the Van Genuchten empirical equation. MIP data is fitted to by Po (entry pressure) and λ (pore size distribution), providing key model parameters for each specific material. The fitting parameters for the three types of porous media are shown in Table 5.1. These three variables, together with ($S_{ws} = 1$), are model input parameters in TOUGH simulation.

Table 5.1. Van Genuchten fitting parameters for the glass beads media and sand pack used in Chapter 3.

	P_0	S_{wr}	λ
Glass	4.0	0.08	0.78
Sand 1	3.3	0.19	0.82
Sand 2	2.1	0.20	0.77

A 1-dimensional vertical modeling domain was created to model the role of buoyant flow in the subsurface. Pressure, temperature, flow rates and other physical parameters are all selected to reflect those used in the experiments reported in our column experiments. Figure 5.7 shows the preliminary results on the comparison between saturation results of the experiments and the simulated results. The simulation is able to effectively recreate the capillary trapping under the stratigraphic horizon, though the model underestimates the impact we observed in the lab. It also over predicts the saturation further down in the column, and after break-through, saturation does not reach a steady state.

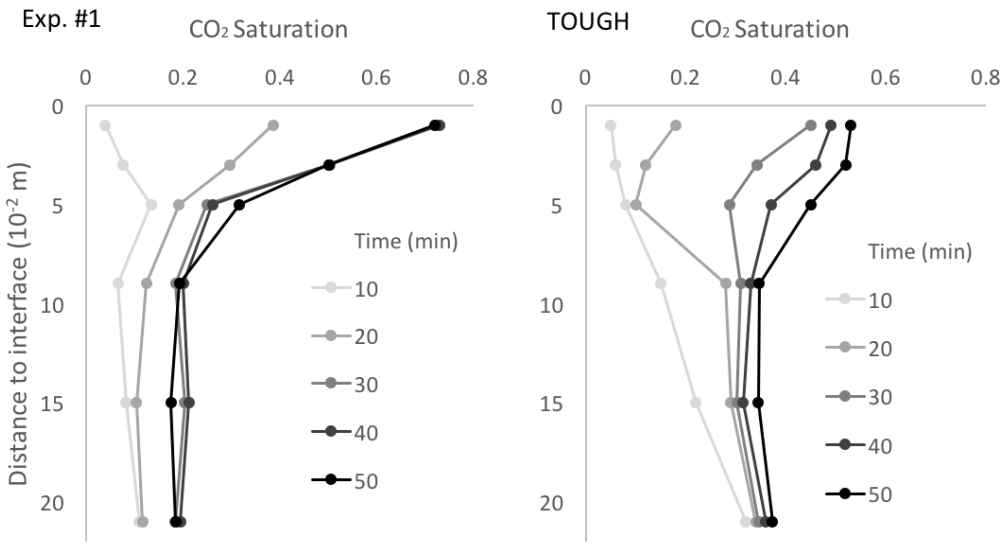

Figure 5.7. Saturation profiles of Exp. #1 in task 3.1, and the simulation results from TOUGH of the same system.

To further evaluate the strength of wettability and roughness on flow dynamics at the basin scale, a large 1-dimensional domain was selected to model multiple layers of heterogeneous porous media. The system contains 60 cylindrical grid blocks with thickness and radius of 1m, grid cells stacked together to form a 60 m long flow domain. There are 5m thick layers with modified properties, to reflect the change in Pc-S relationship caused by wettability and roughness, as well as permeability heterogeneity, as shown in dark area in Figure 5.8. Imbibition process is simulated with initial condition as a gas-saturated porous media (residual water saturation is reached), and water flow from the bottom of the domain with a volumetric flux of $1m^3$/day. Equilibrium CO_2 saturation profile is presented in Figure 5.8. Full drainage and imbibition cycle will be performed next to more accurately represent the real process of CO_2 leakage scenarios.

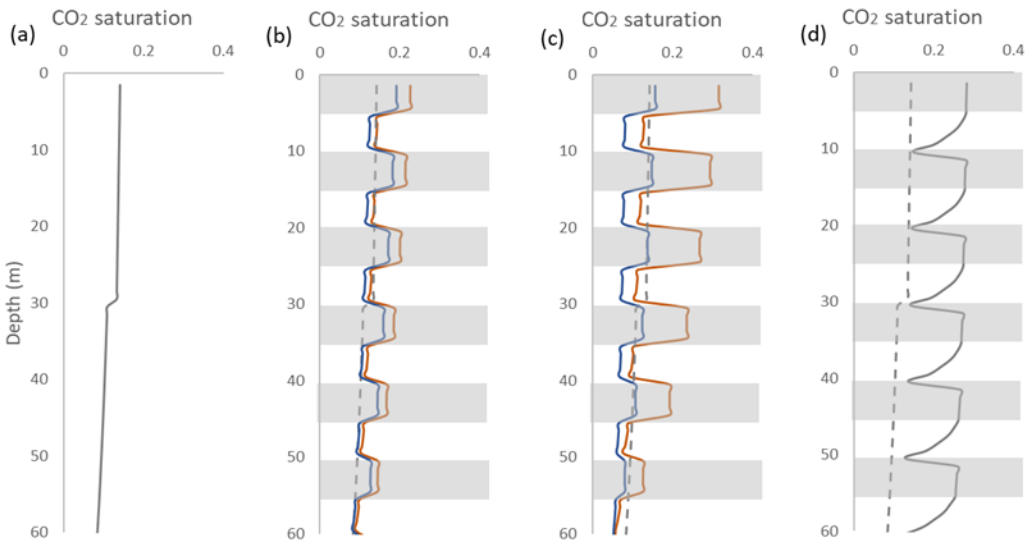

Figure 5.8. Residual CO_2 saturation for a large (60m) vertical domain, for three cases: (a) base, (b) wettability modification, (c) roughness modification and (d) permeability modification. Sensitivity are represented using two levels of effect strengths: blue (low) and orange (high).

The results, presented in Figure 5.8, show the effect of three test factors on capillary trapping within a subsurface formation. Figure 5.8a shows the background residual CO_2 saturation that would be expected in a homogeneous porous medium. The other 3 conditions include a layered domain, where the modified and unmodified area are 5m each. Figure 5.8b shows the residual trapping that would be expected in a layered formation where the orange line represents a high wettability case and blue represents a low wettability case and the dotted line is the baseline tapping from Figure 5.8a. These results show how CO_2 is trapped within the more highly CO_2 wetting layers and that over this 60m domain that represents an increase in 12-31% over baseline conditions. Figure 5.8b shows the effect of increasing roughness on the mineral surfaces, which impacts capillary trapping quite a bit more, ranging from 15-41%. Figure 5.8c shows the effect of decreasing the permeability of these horizontal interlayers. The effect of these permeability shifts

is significant as expected and most of the research to date has focused on studying its effect, which we quantify as 117%. These findings are important for prioritizing the impact these factors could have on CO_2 sequestration capacity, reducing the security risk associated with leakage.

Chapter 6

Conclusions and Future Work

6.1 Conclusions

This work provides a fundamental understanding of the ways in which fluid-rock interfacial properties impact the transport and trapping of CO_2 in porous media. Using a combination of experimental and modeling approaches, this work explores these connections at the pore (mm) to core (m) scale to provide new insight about fluid trapping and migration at the reservoir (km) scale where the security and efficacy of these injections will be determined.

In Chapter 4, results of capillary micro-model experiments were reported, in which spontaneous and forced imbibition experiments were carried out using glass micromodels with modified surface roughness and/or wettability. Two fluid pairs were tested with contrasting viscosities and interfacial tensions: water/Fluorinert and water/Dodecane. A modified 2^k factorial experimental design was used to test the effect of independent variables on interfacial dynamics

and flow. The results suggest that surface roughness, wettability and the presence of a water film are the most important factors in controlling dynamic contact angle effects. surface treatment and aqueous chemistry have a statistically significant impact on dynamic contact angle. Non-aqueous fluid type does show a statistically significant impact, but it doesn't interact with any other variables. Water film does not have a strong impact as a single variable, but its interaction effect with aqueous chemistry and surface feature is statistically significant. These results are used to propose a new empirical equation for predicting dynamic contact angle, using a modified empirical framework based on Joos equation that also incorporates elements of Wenzel's law to account for surface roughness. This newly proposed equation significantly improves the prediction accuracy of experiment data, by taking water film and aqueous chemistry into account. The RMSE of predicting experimental data is reduced up to 67.1%.

Column experiments presented in Chapter 4 assessed how sub-basin-scale horizons in porous media could impact the migration and trapping of a CO_2 plume. A high-pressure column packed with two layers of sand with different properties (e.g., grain size, wettability) was used to create a low-contrast stratigraphic horizon. CO_2 in supercritical or liquid phase was injected into the bottom of the column under various conditions (e.g., temperature, pressure, capillary number) and the transport of the resulting plume was recorded using electrical resistivity. The results show that CO_2 trapping were most strongly impacted by shifting the wettability balance to mixed wet conditions, particularly for residual saturation. A 16% increase in the cosine of the contact angle for a mixed wet sand resulted in nearly twice as much residual trapping. Permeability contrast, pressure, and temperature also impacted the residual saturation but to a lesser extent. Flow rate

affected the dynamics of saturation profile development, but the effect is transient, suggesting that the other effects observed here could apply to a broad range of leakage conditions.

To understand the impacts of these studies at the largest scales, Chapter 5 combines the previous results with new data on wettability and pore structure to inform a model of fluid transport. Capillary pressure and residual saturation curves were synthesized using a combination of previously published results and new experimental data to input into a two-phase flow simulations using the TOUGH suite of codes to understand how these interfacial phenomena influence fate and transport at the largest scales. The interfacial properties, and the spatial heterogeneity, have found to have significant impact on the CO_2 trapping.

two -phase flow simulations using the TOUGH suite of codes to understand how these interfacial phenomena influence fate and transport at the largest scales. The interfacial properties, and the spatial heterogeneity, have found to have significant impact on the CO2 trapping.

6.2 Future work

6.2.1 Full-scale 2D and 3D modeling on porous media with varying permeability and wettability

Building on this dissertation, further study on the role of heterogeneity in physical properties (e.g. permeability, k) and interfacial properties (e.g. wettability, resulting Pc) on vertical transport of CO_2 leakage could extend the understanding of this phenomenon in a larger scale. The hypotheses would be:

1. Wettability heterogeneity will enhance local trapping, thus increase storage efficiency, and reduce leakage rate.

2. This effect has a non-linear dependency on the distribution of wettability characteristics, and the correlation length.
3. Better understand and evaluate wettability characteristics could potentially optimize GCS and risk management.

In this section, large scale 2-dimensional simulation will be carried out to explore the effect of previously observed effects on CO_2 storage performances. These include heterogeneity in physical properties and interfacial properties. We simulate CO_2 injection into a vertical domain using TOUGH2/EOS7C framework, with heterogeneity in physical properties (e.g. permeability) and interfacial properties (e.g. wettability and surface roughness) in vertical transport of CO_2 leakage. The simulation field is a 20m wide by 100m long rectangular domain, consisting of 2000 square gridblocks (each has a 1m x 1m size), as shown in Figure 6.1. The heterogeneous field is generated by applying a log-normal distribution of P_0, with the spatial correlation controlled by the probability of having the same value with the previous block. The comparison between these factors at large scale provides better understanding and evaluation on how heterogeneity will enhance local trapping, thus increase storage efficiency, and reduce leakage risk.

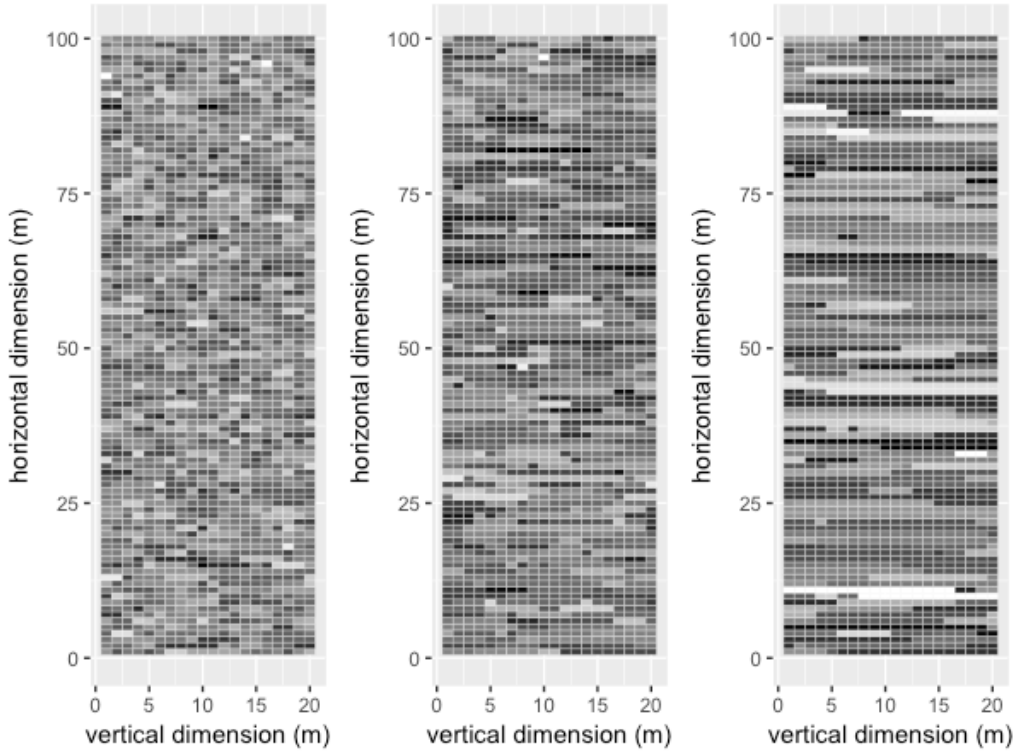

Fig 6.1. Capillary pressure distributions with same mean but increasing spatial correlation from left to right. It is realized by varying the P_0 value in Van Genuchten representation. Assuming the whole field has the same permeability, and capillary pressure only reflects interfacial properties.

There would be two major achievements for this work:

1. A more comprehensive comparison between TOUGH simulation and the column experiments shown in Chapter 3, to evaluate if the model predicts the experimental data, or if the data reveals something that the model does not capture.
2. Upscaling the Pc-S curves obtained in Chapter 5, using real-world geometries and physical properties of GCS sites, with variables of idealized Pc-S curves for different roughness and wettability.

6.2.2 Non-mechanistic methods that incorporates complex parameters to subsurface energy systems

"Big Data" is a relatively new concept to the traditional engineering applications. There are two major drawbacks of statistical method that limit its application in the geo-physical applications: (1) the heavy reliance on randomness of sampling, which is usually hard to achieve in the energy industry, and (2) the size of data requires limit number of parameters, where in reality, the problems in subsurface system usually have notoriously large numbers of parameters. However, with the advancement of computation speed and storage capacity, we are now at an age that sample is virtually the same as population. This greatly favors the advantage of data-based models in compared to physics-based models. Even though the oil and gas industry is among the slowest in adopting the "Big Data" concept, changes have already taken place, where the vast amount of data collected are used to build machine learning models to understand complex problems.

Based on the findings from this dissertation, interfacial properties are highly multi-dimensional and interactive. In the real world multiphase flow through porous media problems, it will be further coupled with other factors, e.g. geo-mechanical, geo-chemical and fluid dynamic properties. By applying "Big Data" approaches, we could take advantage of the size of data collected, and apply machine learning methods to achieve new objectives that traditional analysis are not able to, e.g. finding patterns and making predictions. Non-mechanistic method does not rely on establishing causal relationships between independent and dependent variables, but rather using simple mathematical models by leveraging the large amount of data. This provides a fundamentally different approach, that has the potential to drive value from all digital information, regardless the causality and mechanisms underlying these relationships, or how dis-connected the

information seem to be. Future work could extend this dissertation, by leveraging the knowledge gained from the mechanistic studies, with the computational power of big data, machine learning and artificial intelligence, to better understand carbon sequestration, other geo-physical applications, or any engineering systems.

References

Agbalaka, C., A. Y. Dandekar, S. L. Patil, S. Khataniar, and J. R. Hemsath (2008), The Effect of Wettability on Oil Recovery: A Review, *SPE Asia Pacific Oil Gas Conf. Exhib.*, 1–13, doi:10.2118/114496-MS.

Aggelopoulos, C. a., M. Robin, E. Perfetti, and O. Vizika (2010), $CO_2/CaCl_2$ solution interfacial tensions under CO2 geological storage conditions: Influence of cation valence on interfacial tension, *Adv. Water Resour.*, *33*(6), 691–697, doi:10.1016/j.advwatres.2010.04.006.

Al-Menhali, A., B. Niu, and S. Krevor (2015), Capillarity and wetting of carbon dioxide and brine during drainage in Berea sandstone at reservoir conditions, *Water Resour. Res.*, *51*, 7895–7914.

Al-menhali, A. S., and S. Krevor (2016), Capillary Trapping of CO_2 in Oil Reservoirs: Observations in a Mixed- Wet Carbonate Rock, , doi:10.1021/acs.est.5b05925.

Al-yaseri, A. Z., H. Roshan, M. Lebedev, A. Barifcani, and S. Iglauer (2016), Dependence of quartz wettability on fl uid density, , 1–6, doi:10.1002/2016GL068278.Received.

Al-Yaseri, A. Z., M. Lebedev, A. Barifcani, and S. Iglauer (2016), Receding and advancing (CO_2 + brine + quartz) contact angles as a function of pressure, temperature, surface roughness, salt type and salinity, *J. Chem. Thermodyn.*, *93*, 416–423, doi:10.1016/j.jct.2015.07.031.

Allred, T. P., J. A. Weibel, and S. V. Garimella (2017), A Wettability Metric for Characterization of Capillary Flow on Textured Superhydrophilic Surfaces, *Langmuir*, *33*(32), 7847–7853, doi:10.1021/acs.langmuir.7b01522.

Alvarado, V., and E. Manrique (2010), Enhanced oil recovery: An update review, *Energies*, *3*(9), 1529–1575, doi:10.3390/en3091529.

Ameri, a., N. S. Kaveh, E. S. J. Rudolph, K. Wolf, R. Farajzadeh, and J. Bruining (2013), Investigation on Interfacial Interactions among Crude Oil–Brine–Sandstone Rock– CO_2 by Contact Angle Measurements, *Energy & Fuels*, *27*(2), 1015–1025, doi:10.1021/ef3017915.

Anderson, W. G. (1987a), Wettabiility4 literature survery part 4- effects of wettability on capillary pressure, , 1283–1300.

Anderson, W. G. (1987b), Wettabiility literature survery part 5- the effects of wettability on relative permeability, , 1453–1468.

Andrew, M., B. Bijeljic, and M. J. Blunt (2014), Pore-by-pore capillary pressure measurements using X-ray microtomography at reservoir conditions: Curvature, snap-off, and remobilization of residual CO_2, *Water Resour. Res.*, *50*(11), 8760–8774, doi:10.1002/2014WR015970.

Bachu, S., and D. Brant Bennion (2009), Dependence of CO_2 -brine interfacial tension on aquifer pressure, temperature and water salinity, *Energy Procedia*, *1*(1), 3157–3164, doi:10.1016/j.egypro.2009.02.098.

Bandara, U. C., A. M. Tartakovsky, and B. J. Palmer (2011), Pore-scale study of capillary trapping mechanism during CO_2 injection in geological formations, *Int. J. Greenh. Gas Control*, *5*(6), 1566–1577, doi:10.1016/j.ijggc.2011.08.014.

Bandilla, K. W., M. A. Celia, J. T. Birkholzer, A. Cihan, and E. C. Leister (2015), Multiphase Modeling of Geologic Carbon Sequestration in Saline Aquifers, *Groundwater*, *53*(3), 362–377, doi:10.1111/gwat.12315.

Bateman, K., G. Turner, J. M. Pearce, D. J. Noy, D. Birchall, and C. A. Rochelle (2005), Large-scale column experiment: Study of CO_2, porewater, rock reactions and model test case, *Oil Gas Sci. Technol. L Inst. Fr. Du Pet.*, *60*(1), 161–175.

Bateman, K., C. Rochelle, A. Lacinska, and D. Wagner (2011), CO_2-porewater-rock reactions–Large-scale column experiment (Big Rig II), *Energy Procedia*, *4*(0), 4937–4944, doi:10.1016/j.egypro.2011.02.463.

Benson, S., and D. Cole (2008), CO_2 sequestration in deep sedimentary formations, *Elements*, *4*(5), 325–331.

Berg, S., S. Oedai, and H. Ott (2013), Displacement and mass transfer between saturated and unsaturated CO_2-brine systems in sandstone, *Int. J. Greenh. Gas Control*, *12*, 478–492, doi:10.1016/j.ijggc.2011.04.005.

Bikkina, P. K. (2011), Contact angle measurements of CO_2–water–quartz/calcite systems in the perspective of carbon sequestration, *Int. J. Greenh. Gas Control*, *5*(5), 1259–1271, doi:10.1016/j.ijggc.2011.07.001.

Blake, T. D. (2006), The physics of moving wetting lines, *J. Colloid Interface Sci.*, *299*(1), 1–13, doi:10.1016/j.jcis.2006.03.051.

Blake, T. D., and Y. D. Shikhmurzaev (2002), Dynamic Wetting by Liquids of Different Viscosity, *J. Colloid Interface Sci.*, *253*(1), 196–202, doi:https://doi.org/10.1006/jcis.2002.8513.

Botto, J., S. J. Fuchs, B. W. Fouke, A. F. Clarens, J. T. Freiburg, P. M. Berger, and C. J. Werth (2017), Effects of Mineral Surface Properties on Supercritical CO_2 Wettability in a Siliciclastic Reservoir, *Energy & Fuels*, *31*(5), 5275–5285, doi:10.1021/acs.energyfuels.6b03336.

Bourg, I. C., L. E. Beckingham, and D. J. Depaolo (2015), The Nanoscale Basis of CO_2 Trapping for Geologic Storage, *Environ. Sci. Technol.*, *49*(17), 10265–10284, doi:10.1021/acs.est.5b03003.

Bracke, M., F. Voeght, and P. Joos (1989), The kinetics of wetting: the dynamic contact angle, *Trends Colloid Interface Sci. III*, *149*, 142–149, doi:10.1007/BFb0116200.

Breen, S. J., C. R. Carrigan, D. J. LaBrecque, and R. L. Detwiler (2012), Bench-scale experiments to evaluate electrical resistivity tomography as a monitoring tool for geologic CO_2 sequestration, *Int. J. Greenh. Gas Control*, *9*, 484–494, doi:10.1016/j.ijggc.2012.04.009.

Brochard-Wyart, F., and P. G. De Gennes (1992), Dynamics of partial wetting, *Adv. Colloid Interface Sci.*, *39*, 1–11.

Broseta, D., N. Tonnet, and V. Shah (2012), Are rocks still water-wet in the presence of dense CO_2 or H_2S?, *Geofluids*, *12*(4), 280–294, doi:10.1111/j.1468-8123.2012.00369.x.

Bryant, S. L., S. Lakshminarasimhan, and G. A. Pope (2008), Buoyancy-Dominated Multiphase Flow and Its Effect on Geological Sequestration of CO_2, *SPE J.*, 447–454.

Burant, A., G. V. Lowry, and A. K. Karamalidis (2013), Partitioning behavior of organic contaminants in carbon storage environments: A critical review, *Environ. Sci. Technol.*, *47*(1), 37–54, doi:10.1021/es304262p.

Camarasa, E., C. Vial, S. Poncin, G. Wild, N. Midoux, and J. Bouillard (1999), Influence of coalescence behaviour of the liquid and of gas sparging on hydrodynamics and bubble characteristics in a bubble column, *Chem. Eng. Process. Process Intensif.*, *38*(4–6), 329–344, doi:10.1016/S0255-2701(99)00024-0.

Cassie, A. B. D., and S. Baxter (1945), Large Contact Angles of Plant and Animal Surfaces, *Nature*, *155*, 21.

Cavanagh, A. J., and R. S. Haszeldine (2014), The Sleipner storage site: Capillary flow modeling of a layered CO_2 plume requires fractured shale barriers within the Utsira Formation, *Int. J.*

Greenh. Gas Control, *21*, 101–112, doi:https://doi.org/10.1016/j.ijggc.2013.11.017.

Celia, M. A., S. Bachu, J. M. Nordbotten, and K. W. Bandilla (2015), Status of CO_2 storage in deep saline aquifers with emphasis on modeling approaches and practical simulations, *Water Resour. Res.*, *51*(9), 6846–6892, doi:10.1002/2015WR017609.

Chalbaud, C., M. Robin, J.-M. Lombard, F. Martin, P. Egermann, and H. Bertin (2009), Interfacial tension measurements and wettability evaluation for geological CO2 storage, *Adv. Water Resour.*, *32*(1), 98–109, doi:10.1016/j.advwatres.2008.10.012.

Chaudhary, K., M. Bayani Cardenas, W. W. Wolfe, J. a. Maisano, R. a. Ketcham, and P. C. Bennett (2013), Pore-scale trapping of supercritical CO_2 and the role of grain wettability and shape, *Geophys. Res. Lett.*, *40*(15), 3878–3882, doi:10.1002/grl.50658.

Chiquet, P., D. Broseta, and S. Thibeau (2007), Wettability alteration of caprock minerals by carbon dioxide, *Geofluids*, *7*(2), 112–122, doi:10.1111/j.1468-8123.2007.00168.x.

Clarkson, C. R., N. Solano, R. M. Bustin, A. M. M. Bustin, G. R. L. Chalmers, L. He, and Y. B. Melnichenko (2013), Pore structure characterization of North American shale gas reservoirs using USANS / SANS , gas adsorption , and mercury intrusion, , *103*, 606–616, doi:10.1016/j.fuel.2012.06.119.

Cottin, C., H. Bodiguel, and A. Colin (2010), Drainage in two-dimensional porous media: From capillary fingering to viscous flow, *Phys. Rev. E*, *82*(4), 46315, doi:10.1103/PhysRevE.82.046315.

Cox, R. G. (1986), The dynamics of the spreading of liquids on a solid surface. Part 1. Viscous flow, *J. Fluid Mech.*, *168*, 169–194, doi:DOI: 10.1017/S0022112086000332.

Deng, H., J. P. Fitts, D. Crandall, D. McIntyre, and C. A. Peters (2015), Alterations of Fractures in Carbonate Rocks by CO_2-Acidified Brines, *Environ. Sci. Technol.*, *49*(16), 10226–10234,

doi:10.1021/acs.est.5b01980.

Doughty, C., Æ. B. M. Freifeld, and R. C. Trautz (2008), Site characterization for CO_2 geologic storage and vice versa : the Frio brine pilot , Texas , USA as a case study, , 1635–1656, doi:10.1007/s00254-007-0942-0.

Du, X., and J. He (2012), Structurally colored surfaces with antireflective, self-cleaning, and antifogging properties, *J. Colloid Interface Sci.*, *381*(1), 189–197, doi:10.1016/j.jcis.2012.05.037.

El-Maghraby, R. M., and M. J. Blunt (2013), Residual CO_2 trapping in Indiana limestone., *Environ. Sci. Technol.*, *47*(1), 227–33, doi:10.1021/es304166u.

Ennis-King, J., and L. Paterson (2005), Role of Convective Mixing in the Long-Term Storage of Carbon Dioxide in Deep Saline Acquifer, *SPE J.*, *10*(3), 349–356.

Espinoza, D. N., and J. C. Santamarina (2010), Water- CO_2 -mineral systems: Interfacial tension, contact angle, and diffusion-Implications to CO_2 geological storage, *Water Resour. Res.*, *46*(7), n/a-n/a, doi:10.1029/2009WR008634.

Fagerlund, F., A. Niemi, and T. H. Illangasekare (2008), Modeling of nonaqueous phase liquid (NAPL) migration in heterogeneous saturated media: Effects of hysteresis and fluid immobility in constitutive relations, *Water Resour. Res.*, *44*(3), doi:10.1029/2007WR005974.

Farokhpoor, R., B. J. a. Bjørkvik, E. Lindeberg, and O. Torsæter (2013), Wettability behaviour of CO_2 at storage conditions, *Int. J. Greenh. Gas Control*, *12*, 18–25, doi:10.1016/j.ijggc.2012.11.003.

Geistlinger, H., and I. Ataei-dadavi (2015), Influence of the heterogeneous wettability on capillary trapping in glass-beads monolayers : Comparison between experiments and the

invasion percolation theory, *J. Colloid Interface Sci.*, *459*, 230–240, doi:10.1016/j.jcis.2015.07.074.

Geistlinger, H., I. Ataei-dadavi, and H.-J. Vogel (2016), Impact of Surface Roughness on Capillary Trapping Using 2D-Micromodel Visualization Experiments, *Transp. Porous Media*, *112*(1), 207–227, doi:10.1007/s11242-016-0641-y.

Georgiadis, A., G. Maitland, J. P. M. Trusler, and A. Bismarck (2010), Interfacial Tension Measurements of the (H_2O + CO_2) System at Elevated Pressures and Temperatures, *J. Chem. Eng. Data*, *55*(10), 4168–4175, doi:10.1021/je100198g.

Girardo, S., S. Palpacelli, A. De Maio, R. Cingolani, S. Succi, and D. Pisignano (2012a), Interplay between shape and roughness in early-stage microcapillary imbibition, *Langmuir*, *28*(5), 2596–2603, doi:10.1021/la2045724.

Girardo, S., S. Palpacelli, A. De Maio, R. Cingolani, S. Succi, and D. Pisignano (2012b), Interplay between shape and roughness in early-stage microcapillary imbibition, *Langmuir*, *28*(5), 2596–2603, doi:10.1021/la2045724.

Gozalpour, F., S. R. Ren, and B. Tohidi (2005), CO_2 EOR and storage in oil reservoirs, *Oil Gas Sci. Technol.*, *60*(3), 537–546, doi:10.2516/ogst:2005036.

Graue, A., B. G. Viksund, T. Eilertsen, and R. Moe (1999), Systematic wettability alteration by aging sandstone and carbonate rock in crude oil, *J. Pet. Sci. Eng.*, *24*(2–4), 85–97, doi:10.1016/S0920-4105(99)00033-9.

Guéguen, Y., and V. Palciauskas (1994), *Introduction to the Physics of Rocks*.

Hassanzadeh, H., M. Pooladi-darvish, and D. W. Keith (2007), Scaling Behavior of Convective Mixing , with Application to Geological Storage of CO_2, , *53*(5), 1121–1131, doi:10.1002/aic.

Heshmati, M., and M. Piri (2014), Experimental investigation of dynamic contact angle and capillary rise in tubes with circular and noncircular cross sections, *Langmuir*, *30*(47), 14151–14162, doi:10.1021/la501724y.

Holtzman, R., M. L. Szulczewski, and R. Juanes (2012), Capillary Fracturing in Granular Media, *Phys. Rev. Lett.*, *108*(26), doi:10.1103/PhysRevLett.108.264504.

Hu, Y., D. Devegowda, A. Striolo, A. T. Van Phan, and T. A. Ho (2015), Microscopic Dynamics of Water and Hydrocarbon in Shale-Kerogen Pores of Potentially Mixed Wettability, , (February).

Iglauer, S., M. a. Fernø, P. Shearing, and M. J. Blunt (2012), Comparison of residual oil cluster size distribution, morphology and saturation in oil-wet and water-wet sandstone, *J. Colloid Interface Sci.*, *375*(1), 187–192, doi:10.1016/j.jcis.2012.02.025.

Iglauer, S., A. Z. Al-yaseri, R. Rezaee, and M. Lebedev (2015a), CO_2 wettability of caprocks: Implications for structural storage capacity and containment security, , (Figure 1), 9279–9284, doi:10.1002/2015GL065787.Received.

Iglauer, S., C. Pentland, and A. Busch (2015b), CO_2 wettability of seal and reservoir rocks and the implications for carbon geo-sequestration, *Water Resour. Res.*, *51*(1), 729–774, doi:10.1002/2014WR015553.Received.

Jadhunandan, P. P., and N. R. Morrow (1995), Effect of Wettability on Waterflood Recovery for Crude-Oil/Brine/Rock Systems, *SPE Reserv. Eng.*, *10*(1), 40–46, doi:10.2118/22597-pa.

Jones, R., H. M. Pollock, J. A. S. Cleaver, and C. S. Hodges (2002), Adhesion Forces between Glass and Silicon Surfaces in Air Studied by AFM: Effects of Relative Humidity, Particle Size, Roughness, and Surface Treatment, *Langmuir*, *18*(21), 8045–8055, doi:10.1021/la0259196.

Joos, P., V. A. N. Remoortere, and M. Bracke (1990), The Kinetics of Wetting in a Capillary, *J. Colloid Interface Sci.*, *136*(1), 189–197.

Juanes, R., E. J. Spiteri, F. M. Orr, and M. J. Blunt (2006), Impact of relative permeability hysteresis on geological CO_2 storage, *Water Resour. Res.*, *42*(12), doi:Artn W12418Doi 10.1029/2005wr004806.

Jung, J., and J. Wan (2012), Supercritical CO_2 and Ionic Strength E ff ects on Wettability of Silica Surfaces : Equilibrium Contact Angle Measurements, *Energy & Fuels*, *26*, 6053–6059, doi:10.1021/ef300913t.

Kang, K. H. (2002), How Electrostatic Fields Change Contact Angle in Electrowetting, *Langmuir*, *18*(26), 10318–10322, doi:10.1021/la0263615.

Karadimitriou, N. K., V. Joekar-Niasar, S. M. Hassanizadeh, P. J. Kleingeld, and L. J. Pyrak-Nolte (2012), A novel deep reactive ion etched (DRIE) glass micro-model for two-phase flow experiments., *Lab Chip*, *12*(18), 3413–3418, doi:10.1039/c2lc40530j.

Kaveh, N. S., and A. B. Delft (2015), Study of Shale Wettability for CO_2 Storage, , (June), 1–4.

Kaveh, N. S., E. S. J. Rudolph, P. van Hemert, W. R. Rossen, and K.-H. Wolf (2014), Wettability Evaluation of a CO_2/Water/Bentheimer Sandstone System: Contact Angle, Dissolution, and Bubble Size, *Energy & Fuels*, *28*(6), 4002–4020, doi:10.1021/ef500034j.

Kent, M. E. (2011), Examining Supercritical CO_2 Dissolution Kinetics during Carbon Sequestration through Column Experiments, *Geol. Sci.*, *Master*.

Kharaka, Y. K., J. J. Thordsen, S. D. Hovorka, H. S. Nance, D. R. Cole, T. J. Phelps, and K. G. Knauss (2009), Applied Geochemistry Potential environmental issues of CO_2 storage in deep saline aquifers : Geochemical results from the Frio-I Brine Pilot test , Texas , USA, *Appl. Geochemistry*, *24*(6), 1106–1112, doi:10.1016/j.apgeochem.2009.02.010.

Kibbey, T. C. G. (2013), The configuration of water on rough natural surfaces: Implications for understanding air-water interfacial area, film thickness, and imaging resolution, *Water Resour. Res.*, *49*(8), 4765–4774, doi:10.1002/wrcr.20383.

Kim, T. W., T. K. Tokunaga, J. R. Bargar, M. J. Latimer, and S. M. Webb (2013), Brine film thicknesses on mica surfaces under geologic CO_2 sequestration conditions and controlled capillary pressures, *Water Resour. Res.*, *49*(8), 5071–5076, doi:10.1002/wrcr.20404.

Kim, Y., J. Wan, T. J. Kneafsey, and T. K. Tokunaga (2012), Dewetting of silica surfaces upon reactions with supercritical CO_2 and brine: pore-scale studies in micromodels., *Environ. Sci. Technol.*, *46*(7), 4228–35, doi:10.1021/es204096w.

Kowalewski, E., T. Boassen, and O. Torsaeter (2003), Wettability alterations due to aging in crude oil; wettability and Cryo-ESEM analyses, *J. Pet. Sci. Eng.*, *39*(3–4), 377–388, doi:10.1016/S0920-4105(03)00076-7.

Krevor, S. C. M., R. Pini, B. Li, and S. M. Benson (2011), Capillary heterogeneity trapping of CO_2 in a sandstone rock at reservoir conditions, *Geophys. Res. Lett.*, *38*(15), n/a-n/a, doi:10.1029/2011GL048239.

Krevor, S. C. M., R. Pini, L. Zuo, and S. M. Benson (2012), Relative permeability and trapping of CO_2 and water in sandstone rocks at reservoir conditions, *Water Resour. Res.*, *48*(2), n/a-n/a, doi:10.1029/2011WR010859.

Kunz, P., I. M. Zarikos, N. K. Karadimitriou, M. Huber, U. Nieken, and S. M. Hassanizadeh (2015), Study of Multi-phase Flow in Porous Media: Comparison of SPH Simulations with Micro-model Experiments, *Transp. Porous Media*, 1–20, doi:10.1007/s11242-015-0599-1.

Lamert, H. et al. (2012), Feasibility of geoelectrical monitoring and multiphase modeling for process understanding of gaseous CO_2 injection into a shallow aquifer, *Environ. Earth Sci.*,

67(2), 447–462, doi:10.1007/s12665-012-1669-0.

Land, C. S. (1968), Calculation of Imbibition Relative Permeability for Two- and Three-Phase Flow From Rock Properties, *Soc. Pet. Eng.*, *8*(9), doi:10.2118/1942-PA.

Lassen, R. N., M. Plampin, T. Sakaki, T. H. Illangasekare, J. Gudbjerg, T. O. Sonnenborg, and K. H. Jensen (2015), International Journal of Greenhouse Gas Control Effects of geologic heterogeneity on migration of gaseous CO_2 using laboratory and modeling investigations, *Int. J. Greenh. Gas Control*, *43*, 213–224, doi:10.1016/j.ijggc.2015.10.015.

Legens, C., H. Toulhoat, L. Cuiec, F. Villieras, and T. Palermo (1999), Wettability Change Related to Adsorption of Organic Acids on Calcite: Experimental and Ab Initio Computational Studies, *SPE J.*, *4*(4), 328–333, doi:10.2118/57721-PA.

Levine, J. S., J. M. Matter, D. S. Goldberg, K. S. Lackner, M. G. Supp, and T. S. Ramakrishnan (2011), Two phase brine- CO_2flow experiments in synthetic and natural media, *Energy Procedia*, *4*(0), 4347–4353, doi:10.1016/j.egypro.2011.02.386.

Lewicki, J. L., J. Birkholzer, and C. F. Tsang (2007), Natural and industrial analogues for leakage of $CO_2$from storage reservoirs: Identification of features, events, and processes and lessons learned, *Environ. Geol.*, *52*(3), 457–467, doi:10.1007/s00254-006-0479-7.

Li, X., E. Boek, G. C. Maitland, and J. P. M. Trusler (2012), Interfacial tension of (Brines + CO_2): (0.864 NaCl + 0.136 KCl) at temperatures between (298 and 448) K, pressures between (2 and 50) MPa, and total molalities of (1 to 5) mol·kg -1, *J. Chem. Eng. Data*, *57*(4), 1078–1088, doi:10.1021/je201062r.

Li, X., X. Fan, A. Askounis, K. Wu, K. Sefiane, and V. Koutsos (2013), An experimental study on dynamic pore wettability, *Chem. Eng. Sci.*, *104*, 988–997, doi:10.1016/j.ces.2013.10.026.

Lovoll, G., Y. Meheust, K. Jorgen Maloy, E. Aker, and J. Schmittbuhl (2005), Competition of gravity , capillary and viscous forces during drainage in a two-dimensional porous medium , a pore scale study, *Energy*, *30*, 861–872, doi:10.1016/j.energy.2004.03.100.

Lu, C., and P. C. Lichtner (2007), High resolution numerical investigation on the effect of convective instability on long term CO_2 storage in saline aquifers, *J. Phys. Conf. Ser.*, *78*, 12042, doi:10.1088/1742-6596/78/1/012042.

Luhmann, A. J., X.-Z. Kong, B. M. Tutolo, K. Ding, M. O. Saar, and W. E. Seyfried (2013), Permeability reduction produced by grain reorganization and accumulation of exsolved CO_2 during geologic carbon sequestration: a new CO_2 trapping mechanism., *Environ. Sci. Technol.*, *47*(1), 242–51, doi:10.1021/es3031209.

Manceau, J. C., J. Ma, R. Li, P. Audigane, P. X. Jiang, R. N. Xu, J. Tremosa, and C. Lerouge (2015), Two-phase flow properties of a sandstone rock for the CO_2/water system: Core-flooding experiments, and focus on impacts of mineralogical changes, *Water Resour. Res.*, *51*(4), 2885–2900, doi:10.1002/2014WR015725.

Mazurczyk, R., G. El Khoury, V. Dugas, B. Hannes, E. Laurenceau, M. Cabrera, S. Krawczyk, E. Souteyrand, J. P. Cloarec, and Y. Chevolot (2008), Low-cost, fast prototyping method of fabrication of the microreactor devices in soda-lime glass, *Sensors Actuators, B Chem.*, *128*(2), 552–559, doi:10.1016/j.snb.2007.07.033.

McCaughan, J., S. Iglauer, and F. Bresme (2013), Molecular Dynamics Simulation of Water/ CO_2-quartz Interfacial Properties: Application to Subsurface Gas Injection, *Energy Procedia*, *37*, 5387–5402, doi:10.1016/j.egypro.2013.06.457.

METZ, B. eds (2007), Special report on carbon dioxide capture and storage, *http://www.ipcc.ch/pub/reports.htm*.

Michael, K., a. Golab, V. Shulakova, J. Ennis-King, G. Allinson, S. Sharma, and T. Aiken (2010), Geological storage of CO_2 in saline aquifers—A review of the experience from existing storage operations, *Int. J. Greenh. Gas Control*, *4*(4), 659–667, doi:10.1016/j.ijggc.2009.12.011.

Mikami, Y., Y. Deguchi, and T. Suekane (2014), Effect of Heterogeneity of Porous Media on Gas Permeation and Entrapment *, *J. Flow Control. Meas. Vis.*, *2*(July), 110–119.

Miller, Q. R. S., J. P. Kaszuba, H. T. Schaef, C. J. Thompson, L. Qiu, M. E. Bowden, V. A. Glezakou, and B. P. Mcgrail (2014), Experimental study of organic ligand transport in supercritical CO_2 fluids and impacts to silicate reactivity, *Energy Procedia*, *63*(209), 3225–3233, doi:10.1016/j.egypro.2014.11.349.

Mirchi, V., S. Saraji, L. Goual, and M. Piri (2015), Dynamic interfacial tension and wettability of shale in the presence of surfactants at reservoir conditions, *FUEL*, *148*, 127–138, doi:10.1016/j.fuel.2015.01.077.

Mohammed, M., and T. Babadagli (2015), Wettability alteration : A comprehensive review of materials / methods and testing the selected ones on heavy-oil containing oil-wet systems, *Adv. Colloid Interface Sci.*, *220*, 54–77, doi:10.1016/j.cis.2015.02.006.

Mori, H., T. Sakaki, and T. H. Illangasekare (2015), Laboratory study of geological carbon sequestration using surrogate fluids: Dielectric measurement and scaling of capillary pressure-saturation relationships, *Int. J. Greenh. Gas Control*, *37*, 146–157, doi:10.1016/j.ijggc.2015.01.023.

Mouche, E., M. Hayek, and C. Mügler (2010), Upscaling of CO_2 vertical migration through a periodic layered porous medium: The capillary-free and capillary-dominant cases, *Adv. Water Resour.*, *33*(9), 1164–1175, doi:10.1016/j.advwatres.2010.07.005.

Murakami, D., H. Jinnai, and A. Takahara (2014), Wetting Transition from the Cassie − Baxter State to the Wenzel State on Textured Polymer Surfaces,

Nakatsuka, Y., Z. Xue, Y. Yamada, and T. Matsuoka (2009), Experimental study on monitoring and quantifying of injected CO_2 from resistivity measurement in saline aquifer storage, *Energy Procedia*, *1*(1), 2211–2218.

Nakatsuka, Y., Z. Q. Xue, H. Garcia, and T. Matsuoka (2010), Experimental study on CO_2 monitoring and quantification of stored CO(2) in saline formations using resistivity measurements, *Int. J. Greenh. Gas Control*, *4*(2), 209–216, doi:Doi 10.1016/J.Ijggc.2010.01.001.

Nicot, J.-P., C. M. Oldenburg, S. L. Bryant, and S. D. Hovorka (2009), Pressure perturbations from geologic carbon sequestration: Area-of-review boundaries and borehole leakage driving forces, *Energy Procedia*, *1*(1), 47–54, doi:10.1016/j.egypro.2009.01.009.

Nielsen, L. C., I. C. Bourg, and G. Sposito (2012), Predicting CO_2–water interfacial tension under pressure and temperature conditions of geologic CO_2 storage, *Geochim. Cosmochim. Acta*, *81*, 28–38, doi:10.1016/j.gca.2011.12.018.

Niu, B., A. Al-Menhali, and S. C. Krevor (2015), The impact of reservoir conditions on the residual trapping of carbon dioxide in Berea sandstone, *Water Resour. Res.*, *51*(4), 2009–2029, doi:10.1002/2014WR016441.

Nordbotten, J. M., M. A. Celia, S. Bachu, and H. K. Dahle (2005), Semianalytical Solution for CO2 Leakage through an Abandoned Well, *Environ. Sci. Technol.*, *39*(2), 602–611, doi:10.1021/es035338i.

Nordbotten, J. M., D. Kavetski, M. a Celia, and S. Bachu (2009), Model for CO_2 leakage including multiple geological layers and multiple leaky wells., *Environ. Sci. Technol.*,

43(3), 743–9.

Oldenburg, C. M. (2011), Buoyancy Effects on Upward Brine Displacement Caused by CO_2 Injection, *Transp. Porous Media*, (2/87(2011)), doi:10.1007/s11242-010-9699-0.

Oldenburg, C. M., and J. L. Lewicki (2006), On leakage and seepage of CO_2 from geologic storage sites into surface water, *Environ. Geol.*, *50*(5), 691–705, doi:Doi 10.1007/S00254-006-0242-0.

Oruganti, Y., and S. L. Bryant (2009), Pressure build-up during CO_2 storage in partially confined aquifers, *Energy Procedia*, *1*(1), 3315–3322, doi:10.1016/j.egypro.2009.02.118.

Oughanem, R., S. Youssef, D. Bauer, Y. Peysson, E. Maire, and O. Vizika (2015), A Multi-Scale Investigation of Pore Structure Impact on the Mobilization of Trapped Oil by Surfactant Injection, *Transp. Porous Media*, *109*(3), 673–692, doi:10.1007/s11242-015-0542-5.

Palamara, D. R., T. Neeman, A. N. Golab, and A. Sheppard (2015), International Journal of Greenhouse Gas Control A statistical analysis of the effects of pressure , temperature and salinity on contact angles in CO_2 – brine – quartz systems, *Int. J. Greenh. Gas Control*, *42*, 516–524, doi:10.1016/j.ijggc.2015.09.007.

Pentland, C. H., R. El-Maghraby, a. Georgiadis, S. Iglauer, and M. J. Blunt (2011), Immiscible Displacements and Capillary Trapping in CO_2 Storage, *Energy Procedia*, *4*, 4969–4976, doi:10.1016/j.egypro.2011.02.467.

Pinder, G. F., and W. G. Gray (2008), *Essentials of multiphase flow and transport in porous media*.

Pini, R., S. C. M. Krevor, and S. M. Benson (2012), Capillary pressure and heterogeneity for the CO_2/water system in sandstone rocks at reservoir conditions, *Adv. Water Resour.*, *38*, 48–59, doi:10.1016/j.advwatres.2011.12.007.

Plampin, M., T. Illangasekare, T. Sakaki, and R. Pawar (2014a), Experimental study of gas evolution in heterogeneous shallow subsurface formations during leakage of stored CO_2, *Int. J. Greenh. Gas Control*, *22*, 47–62, doi:10.1016/j.ijggc.2013.12.020.

Plampin, M. R., R. N. Lassen, T. Sakaki, M. L. Porter, R. J. Pawar, K. H. Jensen, and T. H. Illangasekare (2014b), Heterogeneity-enhanced gas phase formation in shallow aquifers during leakage of CO_2-saturated water from geologic sequestration sites, *Water Resour. Res.*, *50*(12), 9251–9266, doi:10.1002/2014WR015715.

Plug, W.-J., and J. Bruining (2007), Capillary pressure for the sand– CO_2–water system under various pressure conditions. Application to CO_2 sequestration, *Adv. Water Resour.*, *30*(11), 2339–2353, doi:10.1016/j.advwatres.2007.05.010.

Polak, S., Y. Cinar, T. Holt, and O. Torsæter (2011), An experimental investigation of the balance between capillary, viscous, and gravitational forces during CO_2 injection into saline aquifers, *Energy Procedia*, *4*, 4395–4402, doi:10.1016/j.egypro.2011.02.392.

Pollak, M. F., J. M. Bielicki, J. a. Dammel, E. J. Wilson, J. P. Fitts, and C. a. Peters (2013), The Leakage Impact Valuation (LIV) Method for Leakage from Geologic CO_2 Storage Reservoirs, *Energy Procedia*, *37*(Liv), 2819–2827, doi:10.1016/j.egypro.2013.06.167.

Popescu, M. N., J. Ralston, and R. Sedev (2008), Capillary rise with velocity-dependent dynamic contact angle., *Langmuir*, *24*(21), 12710–12716, doi:10.1021/la801753t.

Prather, C. A., J. M. Bray, J. D. Seymour, and S. L. Codd (2016), NMR study comparing capillary trapping in Berea sandstone of air, carbon dioxide, and supercritical carbon dioxide after imbibition of water, *Water Resour. Res.*, *52*(2), 713–724, doi:10.1002/2015WR017547.

Pruess, K. (2008), On CO_2 fluid flow and heat transfer behavior in the subsurface, following

leakage from a geologic storage reservoir, *Environ. Geol.*, *54*(8), 1677–1686, doi:10.1007/s00254-007-0945-x.

Quéré, D. (2008a), Wetting and Roughness, *Annu. Rev. Mater. Res.*, *38*(1), 71–99, doi:10.1146/annurev.matsci.38.060407.132434.

Quéré, D. (2008b), Wetting and Roughness, *Annu. Rev. Mater. Res.*, *38*(1), 71–99, doi:10.1146/annurev.matsci.38.060407.132434.

Raeesi, B., N. R. Morrow, and G. Mason (2013), Effect of surface roughness on wettability and displacement curvature in tubes of uniform cross-section, *Colloids Surfaces A Physicochem. Eng. Asp.*, *436*, 392–401, doi:10.1016/j.colsurfa.2013.06.034.

Rahman, T., M. Lebedev, A. Barifcani, and S. Iglauer (2016), Residual trapping of supercritical CO_2 in oil-wet sandstone, *J. Colloid Interface Sci.*, *469*, 63–68, doi:10.1016/j.jcis.2016.02.020.

Ross, D. J. K., and R. M. Bustin (2009), The importance of shale composition and pore structure upon gas storage potential of shale gas reservoirs, *Mar. Pet. Geol.*, *26*(6), 916–927, doi:10.1016/j.marpetgeo.2008.06.004.

Saadatpoor, E., S. L. Bryant, and K. Sepehrnoori (2010), New Trapping Mechanism in Carbon Sequestration, *Transp. Porous Media*, *82*(1), 3–17, doi:10.1007/s11242-009-9446-6.

Saraji, S., L. Goual, M. Piri, and H. Plancher (2013), Wettability of Supercritical Carbon Dioxide/Water/Quartz Systems: Simultaneous Measurement of Contact Angle and Interfacial Tension at Reservoir Conditions, *Langmuir*, *29*(23), 6856–6866, doi:10.1021/la3050863.

Saraji, S., M. Piri, and L. Goual (2014), The effects of SO_2 contamination, brine salinity, pressure, and temperature on dynamic contact angles and interfacial tension of supercritical

CO2/brine/quartz systems, *Int. J. Greenh. Gas Control*, *28*, 147–155, doi:10.1016/j.ijggc.2014.06.024.

Scherf, A., C. Zetzl, I. Smirnova, and M. Zettlitzer (2011), Energy Procedia Mobilisation of organic compounds from reservoir rocks through the injection of CO_2 – Comparison of baseline characterization and laboratory experiments, , *4*, 4524–4531, doi:10.1016/j.egypro.2011.02.409.

Schnaar, G., and M. L. Brusseau (2006), Characterizing Pore-Scale Configuration of Organic Immiscible Liquid in Multiphase Systems With Synchrotron X-Ray Microtomography, *Vadose Zo. J.*, *5*(2), 641, doi:10.2136/vzj2005.0063.

Sheng, J. J. (2014), Critical review of low-salinity waterflooding, *J. Pet. Sci. Eng.*, *120*, 216–224, doi:10.1016/j.petrol.2014.05.026.

Sheng, P., and M. Zhou (1992), Immiscible-fluid displacement: Contact-line dynamics and the velocity-dependent capillary pressure, *Phys. Rev. A*, *45*(8), 5694–5708, doi:10.1103/PhysRevA.45.5694.

Shojai Kaveh, N., K.-H. Wolf, S. N. Ashrafizadeh, and E. S. J. Rudolph (2012), Effect of coal petrology and pressure on wetting properties of wet coal for CO_2 and flue gas storage, *Int. J. Greenh. Gas Control*, *11*, S91–S101, doi:10.1016/j.ijggc.2012.09.009.

Silin, D., T. Patzek, and S. M. Benson (2008), A Model of Buoyancy-Driven Two-Phase Countercurrent Fluid Flow, *Transp. Porous Media*, *76*(3), 449–469, doi:10.1007/s11242-008-9257-1.

Singh, K., H. Menke, M. Andrew, Q. Lin, C. Rau, M. J. Blunt, and B. Bijeljic (2017), Dynamics of snap-off and pore-filling events during two-phase fluid flow in permeable media, *Sci. Rep.*, *7*(1), 5192, doi:10.1038/s41598-017-05204-4.

Skurtveit, E., E. Aker, M. Soldal, M. Angeli, and Z. Wang (2015), Experimental investigation of CO_2 breakthrough and flow mechanisms in shale, , *18*, 3–15, doi:10.1144/1354-079311-016.1354-0793/12/.

Spiteri, E. J., C. Energy, T. Company, and R. Juanes (2008), A New Model of Trapping and Relative Permeability Hysteresis for All Wettability Characteristics, , (September).

Steefel, C. I., S. Molins, and D. Trebotich (2013), Pore Scale Processes Associated with Subsurface CO_2 Injection and Sequestration, , *77*, 259–303.

Steitz, R., W. Jaeger, and R. v. Klitzing (2001), Influence of Charge Density and Ionic Strength on the Multilayer Formation of Strong Polyelectrolytes, *Langmuir*, *17*(15), 4471–4474, doi:10.1021/la010168d.

Strandli, C. W., and S. M. Benson (2013), Identifying diagnostics for reservoir structure and CO_2 plume migration from multilevel pressure measurements, *Water Resour. Res.*, *49*(6), 3462–3475, doi:10.1002/wrcr.20285.

Survey, Y. K. K. U. S. G., M. Rd, M. Park, K. G. K. Lawrence, and L. National (2006), Gas-water-rock interactions in Frio Formation following CO_2 injection : Implications for the storage of greenhouse gases in sedimentary basins, , (7), 577–580, doi:10.1130/G22357.1.

Sutjiadi-Sia, Y., P. Jaeger, and R. Eggers (2008), Interfacial phenomena of aqueous systems in dense carbon dioxide, *J. Supercrit. Fluids*, *46*(3), 272–279, doi:10.1016/j.supflu.2008.06.001.

Tanino, Y., and M. J. Blunt (2012), Capillary trapping in sandstones and carbonates: Dependence on pore structure, *Water Resour. Res.*, *48*(8), doi:10.1029/2011WR011712.

Tokunaga, T. K. (2012), DLVO-Based Estimates of Adsorbed Water Film Thicknesses in Geologic CO_2 Reservoirs,

Tokunaga, T. K., J. Wan, J.-W. Jung, T. W. Kim, Y. Kim, and W. Dong (2013), Capillary pressure and saturation relations for supercritical CO_2 and brine in sand: High-pressure Pc (Sw) controller/meter measurements and capillary scaling predictions, *Water Resour. Res.*, *49*(8), 4566–4579, doi:10.1002/wrcr.20316.

Trevisan, L., A. Cihan, F. Fagerlund, E. Agartan, H. Mori, J. T. Birkholzer, Q. Zhou, and T. H. Illangasekare (2014), Investigation of mechanisms of supercritical CO_2 trapping in deep saline reservoirs using surrogate fluids at ambient laboratory conditions, *Int. J. Greenh. Gas Control*, *29*, 35–49, doi:10.1016/j.ijggc.2014.07.012.

Trevisan, L., R. Pini, A. Cihan, J. T. Birkholzer, Q. Zhou, and T. H. CO_2 *Res.*, *50*, 8791–8805, doi:10.1002/2014WR016259.

Wan, J., Y. Kim, and T. K. Tokunaga (2014), Contact angle measurement ambiguity in supercritical CO_2–water–mineral systems: Mica as an example, *Int. J. Greenh. Gas Control*, *31*, 128–137, doi:10.1016/j.ijggc.2014.09.029.

Wang, H., Y. Liu, Y. Song, Y. Zhao, J. Zhao, and D. Wang (2012), Fractal analysis and its impact factors on pore structure of artificial cores based on the images obtained using magnetic resonance imaging, *J. Appl. Geophys.*, *86*, 70–81, doi:https://doi.org/10.1016/j.jappgeo.2012.07.015.

Wang, S., and T. K. Tokunaga (2015), Capillary Pressure-Saturation Relations for Supercritical CO_2 and Brine in Limestone/Dolomite Sands: Implications for Geologic Carbon Sequestration in Carbonate Reservoirs, *Environ. Sci. Technol.*, *49*(12), 7208–7217, doi:10.1021/acs.est.5b00826.

Wang, S., Z. Tao, S. M. Persily, A. F. Clarens, E. Engineering, T. Hall, and M. Road (2013a), CO_2 Adhesion on Hydrated Mineral Surfaces,

Wang, S., I. M. Edwards, and A. F. Clarens (2013b), Wettability phenomena at the CO_2-brine-mineral interface: implications for geologic carbon sequestration., *Environ. Sci. Technol.*, *47*(1), 234–41, doi:10.1021/es301297z.

Wang, S., T. K. Tokunaga, J. Wan, W. Dong, and Y. Kim (2016), Capillary pressure-saturation relations in quartz and carbonate sands: Limitations for correlating capillary and wettability influences on air, oil, and supercritical CO_2 trapping, *Water Resour. Res.*, *52*(8), 6671–6690, doi:10.1002/2016WR018816.Received.

Wang, Y., C. Zhang, N. Wei, M. Oostrom, T. W. Wietsma, X. Li, and A. Bonneville (2013c), Experimental study of crossover from capillary to viscous fingering for supercritical CO_2-water displacement in a homogeneous pore network., *Environ. Sci. Technol.*, *47*(1), 212–8, doi:10.1021/es3014503.

Wang, Y., C. Bryan, T. Dewers, J. E. Heath, and C. Jove-Colon (2013d), Ganglion dynamics and its implications to geologic carbon dioxide storage., *Environ. Sci. Technol.*, *47*(1), 219–26, doi:10.1021/es301208k.

Washburn, E. W. (1921), The dynamics of capillary flow, *Phys. Rev.*, *17*(3), 273–283, doi:10.1103/PhysRev.17.273.

Wenzel, R. N. (1936), Resistance of solid surfaces to wetting by water, *Ind. Eng. Chem.*, *28*(8), 988–994, doi:10.1021/ie50320a024.

White, C. M., B. R. Strazisar, E. J. Granite, J. S. Hoffman, W. Pennline, and H. W. Pennline (2003), Separation and Capture of CO_2 from Large Stationary Sources and Sequestration in Geological Formations — Coalbeds and Deep Saline Aquifers, *J. Air Waste Manage. Assoc.*, *53*(6), 645–715.

Wigand, M., J. W. Carey, H. Schütt, E. Spangenberg, and J. Erzinger (2008), Geochemical

effects of CO_2 sequestration in sandstones under simulated in situ conditions of deep saline aquifers, *Appl. Geochemistry*, *23*(9), 2735–2745, doi:10.1016/j.apgeochem.2008.06.006.

Xiong, J., S. N. Das, J. P. Kar, J.-H. Choi, and J.-M. Myoung (2010), A multifunctional nanoporous layer created on glass through a simple alkali corrosion process, *J. Mater. Chem.*, *20*(45), 10246, doi:10.1039/c0jm01695k.

Yadali Jamaloei, B., and R. Kharrat (2009), Fundamental study of pore morphology effect in low tension polymer flooding or polymer-assisted dilute surfactant flooding, *Transp. Porous Media*, *76*(2), 199–218, doi:10.1007/s11242-008-9243-7.

Yadali Jamaloei, B., R. Kharrat, K. Asghari, and F. Torabi (2011), The influence of pore wettability on the microstructure of residual oil in surfactant-enhanced water flooding in heavy oil reservoirs: Implications for pore-scale flow characterization, *J. Pet. Sci. Eng.*, *77*(1), 121–134, doi:10.1016/j.petrol.2011.02.013.

Yao, L., and J. He (2014), Recent progress in antireflection and self-cleaning technology - From surface engineering to functional surfaces, *Prog. Mater. Sci.*, *61*, 94–143, doi:10.1016/j.pmatsci.2013.12.003.

Zhang, C., M. Oostrom, T. W. Wietsma, J. W. Grate, and M. G. Warner (2011), Influence of Viscous and Capillary Forces on Immiscible Fluid Displacement: Pore-Scale Experimental Study in a Water-Wet Micromodel Demonstrating Viscous and Capillary Fingering, *Energy & Fuels*, *25*(8), 3493–3505, doi:10.1021/ef101732k.

Zhao, B., C. W. MacMinn, M. L. Szulczewski, J. a. Neufeld, H. E. Huppert, and R. Juanes (2013), Interface pinning of immiscible gravity-exchange flows in porous media, *Phys. Rev. E*, *87*(2), 23015, doi:10.1103/PhysRevE.87.023015.

Zhao, B., C. W. MacMinn, and R. Juanes (2016), Wettability control on multiphase flow in

patterned microfluidics, *Proc. Natl. Acad. Sci.*, *113*(37), 10251–10256, doi:10.1073/pnas.1603387113.

Zhao, C., B. E. Hobbs, and A. Ord (2010), Theoretical analyses of nonaqueous phase liquid dissolution-induced instability in two-dimensional fluid-saturated porous media, , (December 2009), 1767–1796, doi:10.1002/nag.

Zhou, D., F. J. Fayers, and F M Orr (1994), Scaling of Multiphase Flow in Simple Heterogeneous Porous Media, , (April), 559–569.

Zhou, Y., J. O. Helland, and D. G. Hatzignatiou (2013), A Dimensionless Capillary Pressure Function for Imbibition Derived From Pore-Scale Modeling in Mixed-Wet-Rock Images, *SPE J.*, *18*(2), 296–308.